Synthesis of mixed ligand metal-organic frameworks for sorption studies

BY

MAHWASANE ROLIVHUWA

.

A dissertation submitted in the fulfilment of the requirements of the Master of Science in the

Department of Chemistry

Faculty of Mathematical and Natural Sciences

University of Venda

Supervisor: Dr Eustina Batisai

Co-supervisor: Dr Clive Oliver

April 2021

DECLARATION

I Mahwasane Rolivhuwa of student number 14004622 hereby declare that this mini-thesis entitled “Synthesis of mixed ligand metal-organic frameworks for sorption studies” submitted by me to the department of chemistry at the University of Venda, and a mini-thesis of the same topic as mine has not been previously submitted at the University of Venda or any other institution and that is my own work design and information derived from literature has been truly acknowledged in text and a list of references provided.

Signature……. Date…….

ABSTRACT

Metal-organic frameworks (MOFs) are a class of crystal engineered materials consisting of organic and inorganic units. They are made up of metal ions connected by bridging ligands to form three dimensional (3D) networks. MOFs have attracted widespread interest owing to their diverse applications in gas storage and separation, luminescence, catalysis, non-linear optics as well as magnetism. The first part of this study describes the synthesis and characterisation of five pyridyl N-donor diimide ligands namely; *N,N′*-bis(pyridin-3-ylmethyl)naphthalene diimide (L1), *N,N′*-bis(pyridin-4-ylmethyl) naphthalene diimide (L2), 2,2′-bis(pyridin-2-ylmethyl)-[5,5′-biisoindoline]-1,1′-3,3′-tetraone (L3), 2,2′-bis(pyridin-4-ylmethyl)-[5,5′-biisoindoline]-1,1′-3,3′-tetraone (L4) and 5,5′-carbonylbis(2-(pyridin-3-ylmethyl) isoindoline-1,3′-dione) (L5). The second part of this study describes the synthesis of seven (7) new MOFs namely; $\{[Zn(DCT)(L1)_{0.5}]\cdot(DMF)\}_n$ **(RMMOF 1)**, $\{[Zn(DCT)(L2)_{0.5}]\cdot(DMF)\cdot(H_2O)\}_n$ **(RMMOF 2)**, $\{[Co(DCT)(L2)_{0.5}]\cdot(DMF)\}_n$ **(RMMOF 3)**, $\{[Zn_5(OBZ)_3(DMF)_2]\cdot(DMF)_4\}_n$ **(RMMOF 4)**, $\{[Cd(NDC)(L4)_2]\cdot(DMF)_3\}_n$ **(RMMOF 5)**, $\{[Zn_{0.5}(NDC)_{0.5}(L4)_{0.5}]\cdot(DMF)_2\}_n$ **(RMMOF 6)** and $\{[Cu(NDC)(L5)_{0.5}](DMF)_3\}_n$ **(RMMOF 7)**. The MOFs were synthesized from the reactions of the pyridyl N-donor diimide ligands, carboxylate O-donor co-ligands (6,6′-dithiodinicotinic acid (DCT), 4,4′-oxybis benzoic acid (OBZ) and 2,6-naphthalene dicarboxylic acid (NDC)) and transition metal salts. The MOFs were characterized using single crystal X-ray diffraction (SCXRD), thermogravimetric analysis (TGA), powder X-ray diffraction (PXRD) and Brunauer-Emmet-Teller (BET). SCXRD revealed that the MOFs are three dimensional and possess voids that are occupied by solvent molecules. The nature of the voids as well as the void volumes were determined using the Mercury program. **RMMOF 7** possesses the largest void space (~33%) compared to the other MOFs. The sorption capacities were determined for **RMMOF 4**, **RMMOF 5**, **RMMOF 6** and **RMMOF 7** using carbon dioxide gas at 195 K and 273 K. **RMMOF 7** adsorbs the largest amount of CO_2 at 195 K compared to the other MOFs.

ACKNOWLEDGEMENTS

I would like to give thanks to God for protection and ability to do work.

My special and heartily thanks to my supervisor Dr E Batisai for her support, guidance, encouragement and never-ending patience throughout the course of this study and in the preparation of this thesis. I thank her for what she taught me in the field of supramolecular chemistry and science in general.

I would also like to thank my co-supervisor Dr Oliver Clive for his constant support mostly during the analysis of my results.

I am grateful to the NRF/Sasol Inzalo Foundation for funding my research project.
I am also thankful to the University of Cape Town (UCT) and Stellenbosch University for single crystal X-ray diffraction (SCXRD), thermogravimetric analysis (TGA), Powder X-ray diffraction (PXRD), Brunauer-Emmet-Teller (BET) and gas sorption analysis.

I am so grateful for department of chemistry at the University of Venda for allowing me to study masters here.

Lastly, I would like to thank my parents and sisters who encouraged me and prayed for me throughout the time of my research. I am especially grateful to my mother who always believed in me and wanted the best for me. May God bless you.

DEDICATION

This study is wholeheartedly dedicated to Almighty God, thank you for the guidance, strength and power of mind. My beloved parents, who have been my source of inspiration and gave me strength when I thought of giving up, who continually provide their moral and support. To my sisters, friends and classmates who shared their words of advice and encouragement to finish this study.

TABLE OF CONTENTS

LIST OF FIGURES

LIST OF TABLES

LIST OF SCHEMES

ABBREVIATIONS

1-dimensional – **1D**

2-dimensional – **2D**

3-dimensional – **3D**

Ligand – **L**

Metal – **M**

Asymmetric unit– **ASU**

Dimethylformamide – **DMF**

6,6′-dithiodinicotinic acid – **DCT**

2,6′-naphthalenedicarboxylic acid – **NDC**

4,4′-oxybis(benzoic acid) – **OBZ**

Single crystal X-ray diffraction – **SCXRD**

Thermogravimetric analysis – **TGA**

Powder X-ray diffraction – **PXRD**

Brunauer-Emmet-Teller– **BET**

Hot stage microscopy– **HSM**

Nuclear magnetic resonance spectroscopy - **NMR**

Metal-organic frameworks – **MOFs**

Post-synthetic modification – **PSM**

Deuterated dimethylsulfoxide – **DMSO-d6**

Deuterated chloroform – **$CDCl_3$**

Crystallographic Information File – **CIF**

N,N′-bis(pyridin-3-ylmethyl) naphthalene diimide – **L1**

N,N′-bis(pyridine-4-ylmethyl) naphthalene diimide – **L2**

2,2′-bis(pyridin-2-ylmethyl)-[5,5′-biisoindoline]-1,1′-3,3′-tetraone– **L3**

2,2′-bis(pyridin-4-ylmethyl)-[5,5′-biisoindoline]-1,1′-3,3′-tetraone – **L4**

5,5′-carbonylbis (2-(pyridin-3-ylmethyl) isoindoline- 1,3′- dione) – **L5**

CHAPTER 1

INTRODUCTION

1.1 SUPRAMOLECULAR CHEMISTRY

Supramolecular chemistry is the study of molecular ensembles and non-covalent interactions.[1] The field of supramolecular chemistry is expanding at an extraordinary pace since it was first introduced by Jean-Marie Lehn in 1978. The term 'supramolecular' is derived from Latin where 'supra' means above or beyond. Therefore, supramolecular chemistry can also be defined as "chemistry beyond molecules".[2]

Supramolecular chemistry plays an important role in the formation of host-guest complexes in which a host molecule interacts with a certain guest and selectively binds to it.[3,4] A host can be defined as a large molecule that accommodates a guest within channels.[5] A guest is a small molecule that occupies the pores of a host molecule.[6] The guest may be a simple molecule such as an organic molecule or a more sophisticated molecule such as a hormone, pheromone or neurotransmitter.[7] Supramolecular synthesis differs from molecular synthesis in that it results in 'supermolecules' which contain molecules held together by non-covalent bonds.[7] Molecular synthesis involves synthesis of molecules made up of atoms connected by covalent bonds.[7]

1.2 INTERMOLECULAR INTERACTIONS

The communication network between two or more molecules is called intermolecular interactions.[8] Types of intermolecular interactions include hydrogen bonds, coordinate bonds, π···π interactions and van der Waals interactions. The overall packing of molecules in a crystal lattice depends on these interactions. Intermolecular interactions can be classified into long-range forces or medium range forces.[9] Long range forces are responsible for strong attractions and repulsions between ions or molecules. They are electrostatic in nature and are directional.[10] Long range forces mostly occur in the heteroatoms which include N, S or O atoms.[10] Types of long range forces include hydrogen bonds and coordination bonds. Medium range forces are relatively weak dispersion forces and are anisotropic in nature; these forces influence the molecular shape, size and close packing.[9]

C···H, C···C and H···H interactions are some examples of medium range forces. These medium range forces involve van der Waals interactions as well as π···π interactions.

1.2.1 Hydrogen bonds

The hydrogen bond is the most important and most utilized type of interaction in crystal engineering due to its strength and directionality.[11] According to G. R. Desiraju ''the strong hydrogen bond is the master key of molecular recognition and full control of this interaction will lead to mastery of supramolecular chemistry in general''.[12]

The hydrogen bond has directional character, it is much weaker than both the covalent bond and ionic bond but stronger than a van der Waals interaction.[13] Hydrogen bonds can be divided into three categories namely: strong, medium and weak, based on their strengths and directionality (Table 1.1).[14] The strength of hydrogen bonds ranges from 14 Kcal mol^{-1} to 40 Kcal mol^{-1} (strong), 4 Kcal mol^{-1} to 14 Kcal mol^{-1} (medium) and 1 to 4 Kcal mol^{-1} (weak)[14].

In 1960 Pimentel and McClellan conducted a study which involved analysis of hydrogen bond geometries of more than 200 000 published organic and organometallic crystals structures.[15] From this study it was found that the shape and the arrangement of the hydrogen bond between a donor atom (A) and an acceptor atom (B) are related by the angle θ. The angle between these two atoms is greater than 120°.[16] Using this criterion, the hydrogen bond geometry can be defined as A—H···B, where the A—H group represents the donor group and H···B represents the acceptor group. The hydrogen bond interaction is represented by three dots (Fig 1.1a). In most cases hydrogen bond occurs between one donor group and one acceptor group. However, due to the long-range nature, one donor group may interact with two or three acceptors at the same time. When this happens, the hydrogen bond is termed bifurcated and trifurcated, respectively (Fig 1.1 b and Fig 1.1 c).[17]

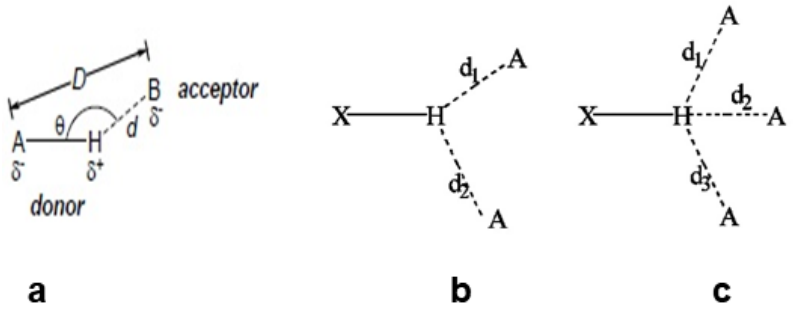

Fig 1. 1 (a) The hydrogen bond represented by dotted line, (b) bifurcated and (c) trifurcated hydrogen bonds.[14,20]

Table 1. 1 Some properties of strong, medium and weak hydrogen bonds. From "An introduction to hydrogen bonding".[14]

	Strong	**Medium**	**Weak**
Energy (Kcal mol^{-1})	14 to 40	4 to 14	<4
Interaction type	Mostly covalent	Mostly electrostatic	Electrostatic
Bond lengths (Å)	A—H = H··· B	A—H < H···B	A—H << H···B
A···B	2.2 to 2.5	2.5 to 3.2	3.2 to 4.0
H···B	1.2 to 1.5	1.5 to 2.2	2.2 to 3.2
Bond angle (º)	175 to 180	130 to 180	90 to 150
Reduction in IR stretch frequency	25%	10-25%	<10%
Examples	Proton-sponges,HF complexes, hydrated protons	Carboxylic acids, alcohols, biomolecules	C—H···O/N O/N—H···π

1.2.2 Coordinate bond

A coordinate bond refers to a chemical bond between two atoms whereby one of the atoms provides a pair of electrons. This bond occurs when a ligand donates a pair of electrons to an empty metal orbital. This bond is basically a covalent bond with the difference that the shared pair is provided by one atom. The coordinate bond plays an important role in the formation of coordination polymers. The strength of the coordinate bond ranges from 20 Kcal mol^{-1} to 45 Kcal mol^{-1}.[18] It is therefore considered to be the strongest among all the intermolecular interactions. The coordinate bond offers greater directionality and stability than other intermolecular interactions.[19]

1.2.3 π···π interactions

π···π interactions are non-covalent interactions occurring between aromatic compounds.[20] The aromatic moieties can be arranged either in a sandwich or displaced stacking manner (Fig 1.2). These interactions are mainly caused by the overlap of *p*-orbitals occurring in π conjugated systems.[20] The strength of π···π interactions ranges from 2 Kcal mol^{-1} to 10 Kcal

mol^{-1}.[21] Their strength increases with an increase in the number of π electrons. π···π interactions are the primary non-covalent interactions that influence base stacking in DNA and RNA.[21]

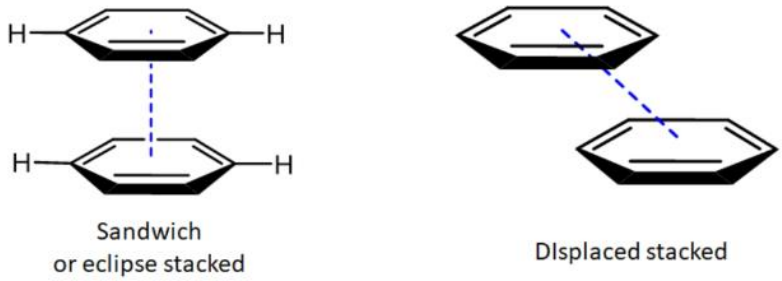

Fig 1. 2 Two types of π···π stacking interactions between aromatic rings; (a) sandwich or eclipse stacked and (b) displaced stacked. [22]

1.2.4 Van der Waals interactions

Van der Waals interactions are defined as the attractive interactions between molecules that collide with or pass very close to each other. These interactions are the weakest of all interactions and their strength ranges from 0.1 Kcal mol^{-1} to 1 Kcal mol^{-1} (Table 1.2). In 1873 Johannes Diderik van der Waals postulated that these intermolecular forces account for real gas properties.[23] Van der Waals interactions also play an important role in numerous applications, such as in metal-organic frameworks (MOFs) whereby they dominate the interactions between small guest molecules and the walls of the MOFs.[24]

Table 1. 2 Strength of hydrogen bonds, π-π interactions, coordination bonds and Van der Waals interactions. [25, 18]

Type of interactions	**Strength (Kcal mol^{-1})**
Hydrogen bond	2-40
Pi-pi interactions	0-10
Van der Waals	0.1-1
Coordination bond	20-45

1.3 CRYSTAL ENGINEERING

Crystal engineering is “the understanding of intermolecular interactions in the context of crystal packing and in the utilization of such understanding in the design and synthesis of new solids with desired physical and chemical properties”.[26] Crystal engineering relies on intermolecular interactions and uses supramolecular synthons as a design strategy.[27] A supramolecular

synthon is a recognised recurring pattern often occurring between the same functional groups in the solid state.[27] Crystal engineering is a worldwide interest and has therefore attracted researchers from a diversity of disciplines including materials science, pharmaceutics, organic chemistry and inorganic chemistry. The main purpose of crystal engineering is to design and synthesize materials with desired properties.[28]

1.4 METAL-ORGANIC FRAMEWORKS

Metal-organic frameworks are porous crystalline materials consisting of organic ligands and metal ions or clusters (Fig 1.3). MOFs can be 1, 2 or 3-dimensional (1D, 2D or 3D) respectively in nature. In 1D MOFs, the coordinate bonds propagate the polymer in one direction.[29] In 2D, the single type layers are superimposed through either the edge-to-edge or staggered type of stacking, where weak interactions exist between the layers.[29] In 3D MOFs, the framework is stable and highly porous due to the coordinate bonds that propagate the polymer in three directions.[29]

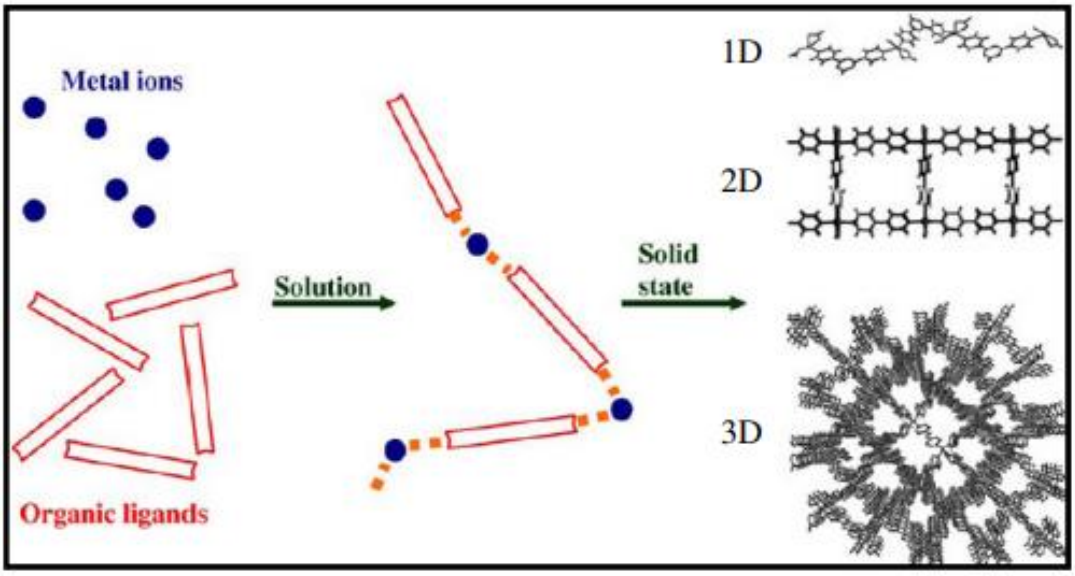

Fig 1. 3 A schematic representation for the formation of MOF from solution by self-assembly of organic ligands and metal ions. [30]

MOFs have attracted widespread interest owing to their diverse applications in gas storage and separation,[31] luminescence,[32] catalysis,[33] non-linear optics[34] as well as magnetism.[35] Much of the interest in MOFs is motivated by their unique properties such as high surface areas extending beyond 6000 m^2 g^{-1}, ultrahigh porosities (up to 90% free volume), tunable pore sizes and low framework densities.[36,37,38]

1.4.1 Synthesis and characterization of MOFs

MOFs can be synthesized using different methods such as solvothermal, solvent evaporation and mechanochemical methods. In general, MOFs synthesis involves reacting a metal salt and an organic ligand in a suitable solvent. Transition metal salts are the most commonly utilized metal salts in the synthesis of MOFs. Organic ligands used include carboxylate, pyridyl and imidazoyl ligands. Factors such as nature of solvents, pH, molar ratio of reactants and temperature are some of the parameters that affect the formation of MOFs.[39] During the formation of the MOFs solvent molecules are included in the pores of the 3D framework. The as-synthesized guest (DMF, ethanol, coordinated water and any other solvent molecules) can be removed and a new guest molecules introduced without the collapse of the framework.

1.4.2 Post-synthetic modification (PSM) of MOFs

Post-synthetic modification of MOFs can be defined as the transformation of an original MOF to a new MOF with new physical and chemical properties that are absent in the original MOF.[40] This can be achieved via a chemical reaction, adsorption and ligand or metal exchange. Post-synthetic modification can be used to prepare functional MOFs by systematic modification of their cavities. This approach was first proposed by the Cohen group in 2007 wherein they reacted IRMOF-3 with acetic anhydride to yield a framework containing a newly formed amide group.[40] To achieve PSM, it is important that the framework of the original MOF maintains structural integrity and crystallinity. Post-synthetic modification can be divided into three methods; covalent PSM, dative PSM and post-synthetic deprotection (PSD) (Fig 1.4).

Covalent post-synthetic modification is regarded as the most well-developed type of PSM. It involves covalent modification of the coordinated ligand.[42] Dative PSM involves coordination of metal centre to a coordinated linker.[42] Dative PSM has become a mainstream approach for tuning the pore functionality of MOFs.[43] In 2011, Hupp and co-workers reported systematic studies on dative PSM using a Zn(II) paddlewheel-derived MOF.[43] Recently, post-synthetic deprotection is starting to gain attention as a post-synthetic functionalization method. Post-synthetic deprotection involves introducing a protected functional group onto an organic linker before the protecting group is removed post-synthetically.[41] Example of post-synthetic deprotection involves the use of thermally-induced deprotection with *tert*-butylcarbamate (Boc) protecting group and was demonstrated by Kitagawa and co-workers in 2010.[44]

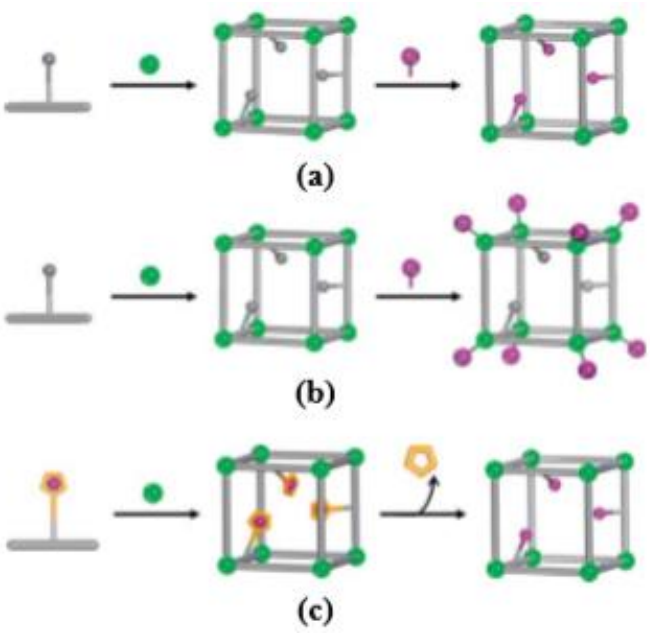

Fig 1. 4 Three examples of post-synthetic modification; (a) covalent PSM, (b) dative PSM and (c) post-synthetic deprotection. [41]

1.5 ADSORPTION ISOTHERMS

An adsorption isotherm is a graph that represents the variation in the amount of adsorbate adsorbed on the surface of the adsorbent with the change in pressure at a constant temperature (Fig 1.5).[45] Six types of adsorption isotherms were originally proposed by Brunauer and co-workers.[46]

Type I isotherm is observed during the adsorption on a microporous solid. It represents an adsorption process with a low affinity for the adsorbate and the plateau indicates monolayer coverage.[47] This type is typical for chemisorption.

Type II isotherms are usually observed in physical adsorption. They are mostly encountered when adsorption occurs on non-porous or macroporous powders. The point B is called the inflection point or the knee of the isotherm.[48]

Type III isotherms indicate weak adsorbate-adsorbent interactions and are observed in non-porous or macroporous solids. These weak interactions cause a small uptake at first but once the molecule has been adsorbed, the adsorbate-adsorbate forces will promote the adsorption of molecules.[47]

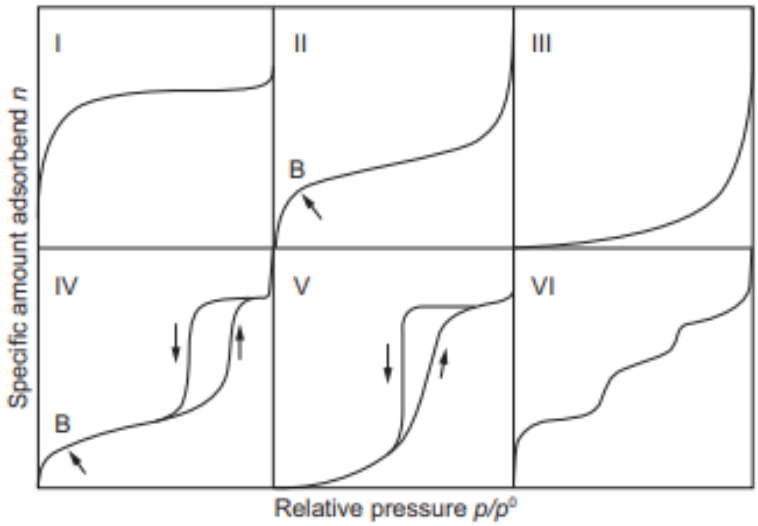

Fig 1. 5 The six types of adsorption isotherms according to the classification of Brunauer. [47]

Type IV and V isotherms are characteristic of vapour adsorption by capillary condensation into small adsorbent pores. The adsorption reaches an asymptotic value as the saturation pressure is approached. Adsorption of organic vapours on activated carbon is typically type IV, whereas adsorption of water vapour on activated carbon is type V.[49] The shape of the adsorption isotherm of a solute from solution depends on the competitive adsorption of the solvent and other components. In both adsorption curves a hysteresis loop is observed. On type IV isotherm a hysteresis is associated with the presence of mesoporosity while in type V it occurs in multimolecular adsorption regions.[47]

Type VI isotherms are typically rare and are associated with layer-by-layer adsorption on a highly uniform surface. The sharpness of the steps is dependent on the system.[50]

1.6 LITERATURE REVIEW

Numerous articles on the topic of MOFs have been written, indicating the important aspects of this exciting research area. The field of MOFs is developing at an extraordinary pace as shown by the increase in the number of published papers and review articles.

The interest in MOFs is motivated by their unique properties such as exceptionally high surface areas, low framework densities, high pore volumes and tunable pore sizes and functionalities.[51] These properties make them ideal candidates for gas storage, catalysis, sensing and separation of small molecules.[42] Over the past years, tremendous efforts have been directed towards the design and synthesis of MOFs for storage of gases such as hydrogen, carbon dioxide, methane and nitrogen. Some of the synthesized MOFs include

MOF-210 with surface area of over 6200 m^2 g^{-1}, MOF-5 with surface area of 4400 m^2 g^{-1} and NU-100 with surface area of 6143 m^2 g^{-1}.[53]

In 2003, the first example of hydrogen storage in MOFs (MOF-5) was investigated and reported by Yaghi *et al*.[52] The synthesized MOF-5 was found to have the highest hydrogen uptake record of 0.076 kg kg^{-1} at saturation with the surface area of 4400 m^2 g^{-1}.[54] This remains the highest uptake followed by UMCM-2 with 0.0069 kg kg^{-1} and MIL-101 with 0.061 kg kg^{-1}.[55] Some of the synthesized MOFs with high surface areas include NOTT-112, NU-100/PCN-610 and NU-111 with BET surface areas of 3800, 6143 and 4930 m^2 g^{-1}, respectively.[56] These MOFs have total gravimetric hydrogen uptake (77 K, 70 bar) of 10.0, 16.4 and 13.6% respectively. In 2010, Furukawa *et al*. reported MOF-210 at 77 K and 80 bar having a surface area of over 6200 m^2 g^{-1} exhibiting a total gravimetric hydrogen uptake of 17.6 wt%.[57]

In 1997, Kitagawa and Yaghi were the first scientists to report the uptake of methane by porous MOFs.[58] In 2013, six MOFs were investigated (HKUST-1, NiMOF-74, PCN-14, UTSA-20, NU-111, and NU-125)[53] for their ability to adsorb methane gas using a standard measurement protocol made by Peng and co-workers.[59] Amongst all the above-mentioned MOFs, NU-111 has the highest gravimetric uptake of 0.36 g g^{-1} with a BET surface area of 4930 m^2 g^{-1}.[53] Similar structures of copper tetracarboxylate (NOTT-100, NOTT-101, NOTT-102, NOTT-103 and NOTT-109) were also investigated for their ability to adsorb methane by He and co-workers.[60] Their excess gravimetric methane uptakes were found to increase with an increase in their porosity.

Adsorption of carbon dioxide has been one of the promising applications of MOFs.[61] MOF-177 was successfully synthesized by Yaghi *et al.* for carbon capture. The MOF has an adsorption capacity of up to 33.5 mmol g^{-1}.[61] In the past few years, there has been an increase in the synthesis of MOFs for gas storage.

1.7 MOTIVATION OF THE STUDY

MOFs have been recognised as promising adsorbents for gas storage due to their permanent porosities.[53] To date several MOFs have been synthesized and utilized in carbon dioxide capture and sequestration. The field of MOFs is an active area of research which presents possibilities in solving the problems currently faced in climate change. The aim of this work is to synthesize porous MOFs for carbon dioxide sorption.

The project will firstly involve the synthesis and characterization of five (5) pyridyl N-donor ligands namely; *N,N′*-bis(pyridin-3-ylmethyl)naphthalene diimide (L1), *N,N′*-bis(pyridin-4-ylmethyl) naphthalene diimide (L2), 2,2′-bis(pyridin-2-ylmethyl)-[5,5′-biisoindoline]-1,1′-3,3′-

tetraone (L3), 2,2′-bis(pyridin-4-ylmethyl)-[5,5′-biisoindoline]-1,1′-3,3′-tetraone (L4) and 5,5′-carbonylbis(2-(pyridin-3-ylmethyl) isoindoline- 1,3′- dione) (L5) (Scheme 1.1). A Cambridge Structural Database (CSD) search revealed that ligands L1, L2 and L4 have been previously investigated in the synthesis of MOFs while ligands L3 and L5 have not been used. Ligand L1 was used in the synthesis of nine (9) MOFs with different metal salts. However, in all reported MOFs containing ligand L1, carboxylate co-ligands were not used. Ligand L2 was used to synthesize thirty-three (33) MOFs with different metal salts. Among these, only twelve (12) MOFs contain ligand L2 in combination with aromatic carboxylate co-ligands. Ligand L4 has been used to synthesize only two MOFs with different metal salts.

In the second part of the project, ligands L1 to L5 will each be reacted with a variety of transition metal salts in the presence of a carboxylate co-ligand (Scheme 1.2) to generate 3D porous MOFs. The mixed-ligand strategy is the preferred method of synthesis for MOFs as it enhances stability of the MOF. In the third part of the project the activated MOFs will be tested for their ability to adsorb carbon dioxide.

1.8 AIMS AND OBJECTIVES

The aim of this project is to synthesize and characterize MOFs for carbon dioxide sorption. The objectives are:

(i) To synthesize pyridine N-donor diimide ligands.

(ii) To synthesize metal-organic frameworks by reacting a metal salt, pyridyl N-donor ligand and a carboxylate O-donor co-ligand.

(iii) To characterize the synthesized MOFs using thermogravimetric analysis (TGA), single crystal X-ray diffraction (SCXRD), powder X-ray diffraction (PXRD) and Brunauer-Emmett-Teller (BET).

(iv) To test the sorption capacity of the MOF using carbon dioxide gas.

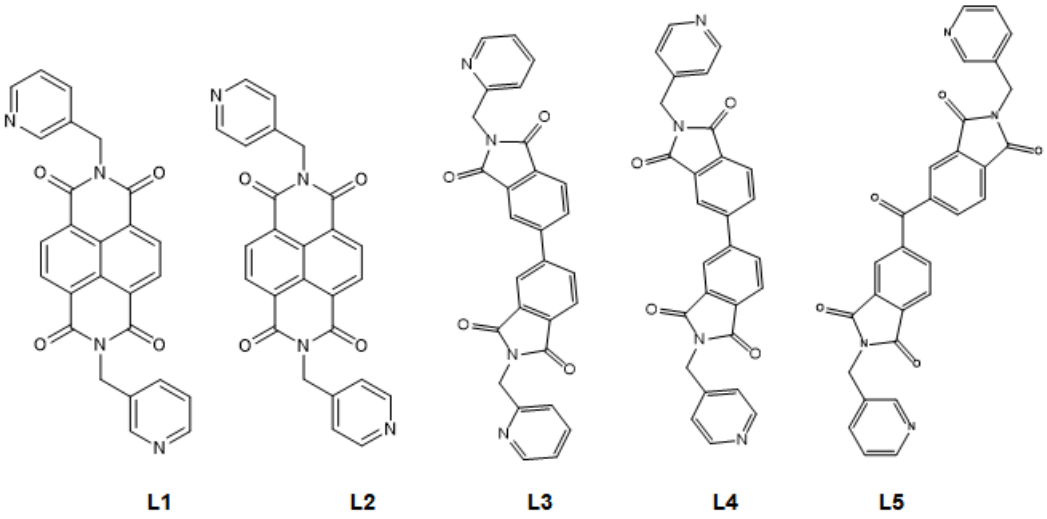

Scheme 1. 1 Chemical structures of the ligands used in this study.

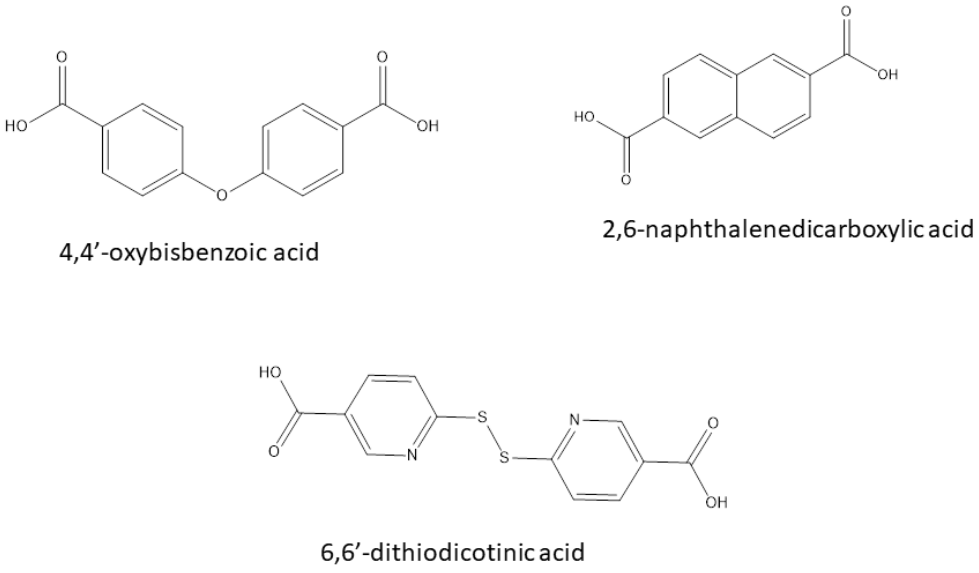

Scheme 1. 2 Chemical structures of co-ligands used in this study.

1.9 THESIS OUTLINE

Chapter 2 describes the synthesis of the ligands and the metal-organic frameworks (MOFs), as well as the characterization techniques used.

Chapter 3 discusses the analysis of the MOFs using SCXRD, PXRD, TGA and BET. The gas sorption experiments are also discussed.

Chapter 4 gives a short summary of the outcomes of this work as well as suggestions for future work.

CHAPTER 2

EXPERIMENTAL

This chapter describes the synthesis and characterization of organic ligands and metal-organic frameworks.

2.1 SYNTHESIS AND CHARACTERIZATION OF LIGANDS

2.1.1 Synthesis of N,N′-Bis(pyridin-3-ylmethyl) naphthalene diimide (L1).[62]

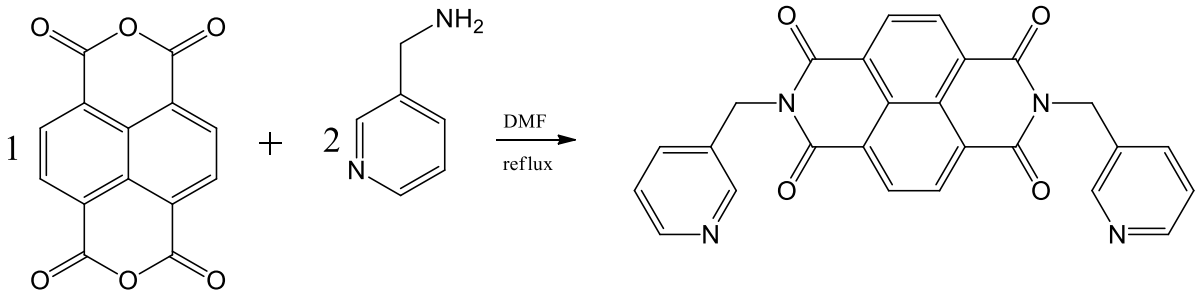

Scheme 2.1 Synthesis of N,N′-bis(pyridin-3-ylmethyl) naphthalene diimide (L1).

L1 was synthesized by refluxing a mixture of 1,4,5,8-naphthalenetetracarboxylic dianhydride (1.0 g, 3.73 mmol) and 3-(aminomethyl) pyridine (1.0 g, 7.46 mmol) in DMF (30 mL) for 12 hours at 160 °C. On cooling, the black solution was filtered and the crude solid was collected and recrystallized from DMF. L1 was characterized using proton and carbon NMR (Fig 2.1 and 2.2). Yield: 51%. ^{1}H-NMR ($CDCl_3$, 400 MHz): δ 8.779 (s, H_{py}, 2H), δ 8.719 (s, H_{nat}, 4H), δ 8.468 (d, H_{py}, 2H), δ 7.866 (d, H_{py}, 2H), δ 7.223 (m, H_{py}, 2H), δ 5.333 (s, CH_2, 4H). ^{13}C-NMR ($CDCl_3$, 100 MHz): δ 162.69 (Cx4), δ 150.49 (CHx2), δ 148.99 (CHx2), δ 137.43 (CHx4), δ 132.34 (Cx4), δ 131.37 (CHx2), δ 126.76 (Cx2), δ 126.59 (Cx2), δ 123.61 (CHx2), δ 41.56 (CH_2x2).

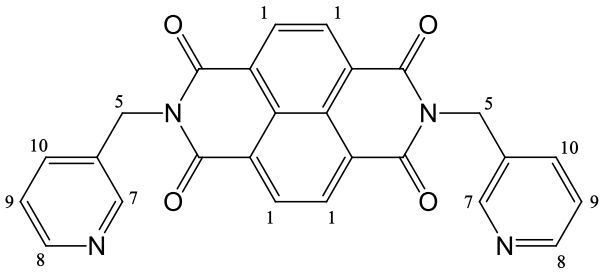

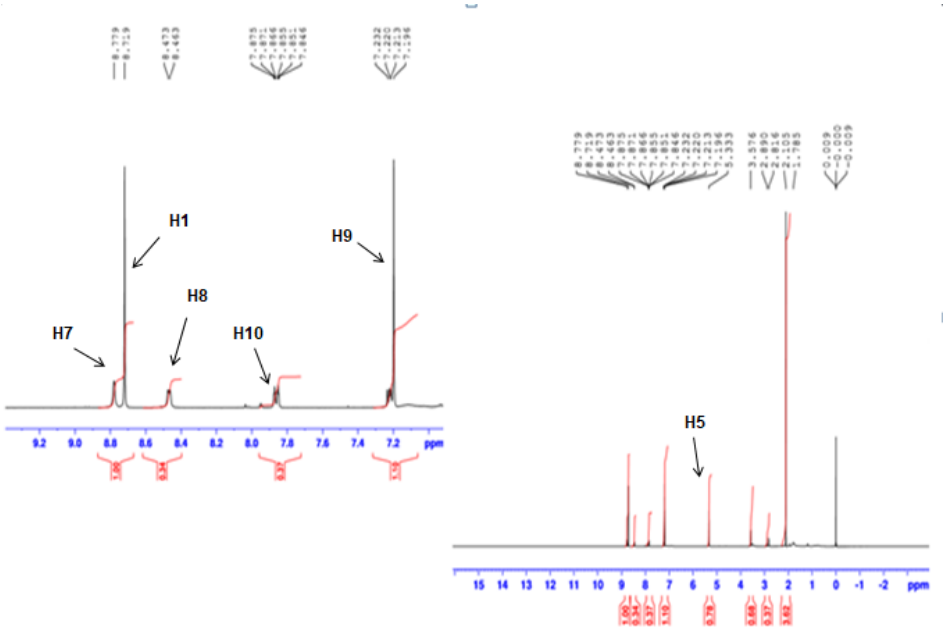

Fig 2. 1 Proton NMR spectra of L1.

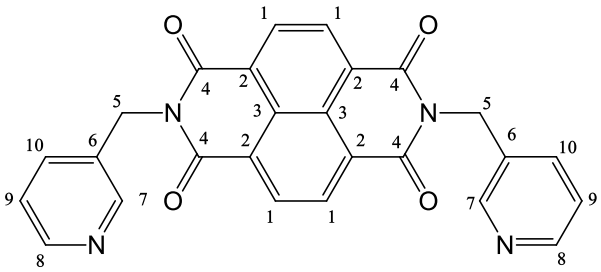

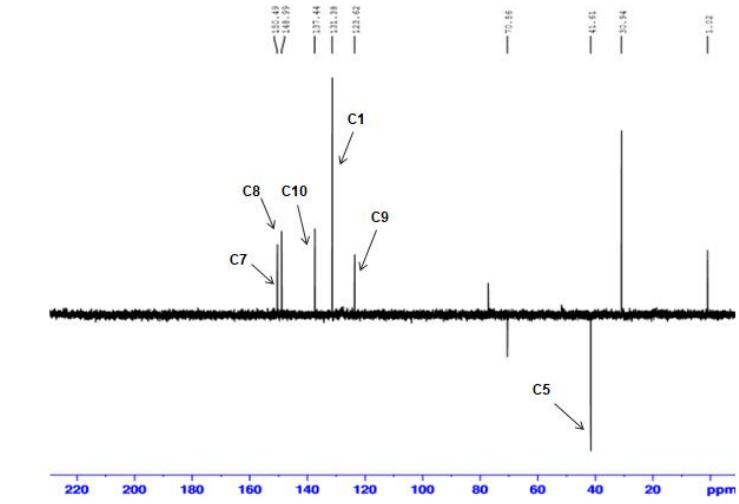

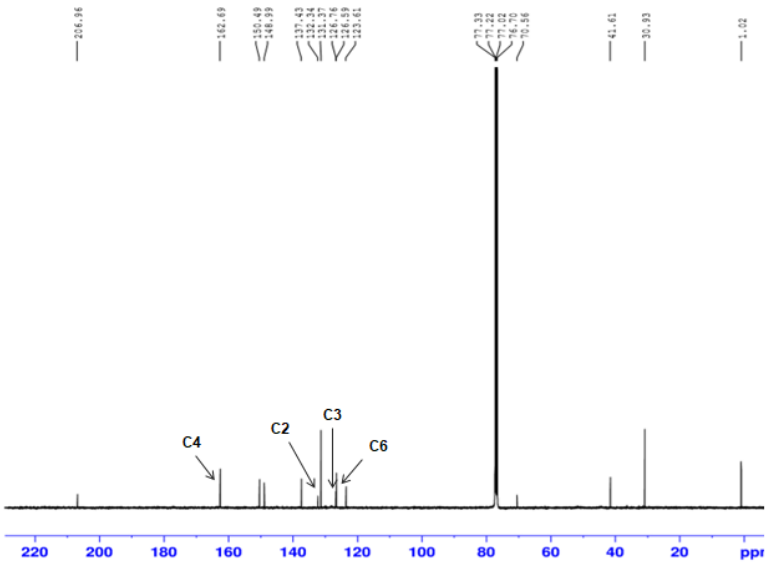

Fig 2. 2 Carbon NMR spectra of L1.

2.1.2 Synthesis of *N,N′*-bis(pyridin-4-ylmethyl) naphthalene diimide (L2).[62]

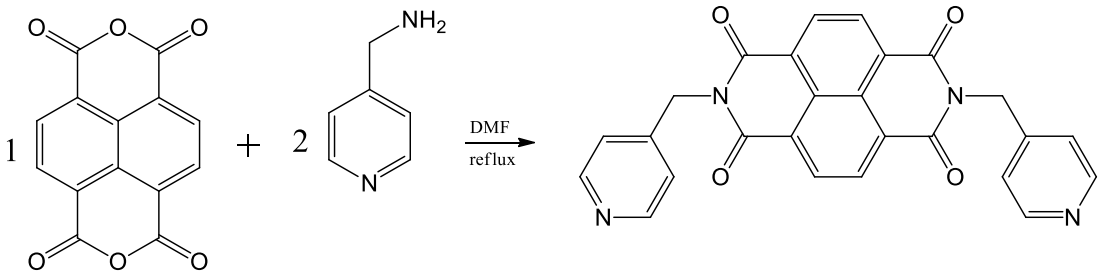

Scheme 2. 2 Synthesis of N,N′-bis(pyridin-4-ylmethyl) naphthalene diimide (L2).

L2 was synthesized by refluxing a mixture of 1,4,5,8-napthalenetetracarboxylic dianhydride (1.0 g, 3.73 mmol) and 4-(aminomethyl) pyridine (1.0 g, 7.46 mmol) in DMF (30 mL) for 12 hours at 160 °C. On cooling, the black solution was filtered and the crude solid was recrystallized from DMF. L2 was characterized using proton and carbon NMR (Fig 2.3 and 2.4). Yield: 52%.^{1}H-NMR ($CDCl_3$, 400 MHz): δ 8.832 (s, H_{nat} 4H), δ 8.602 (d, H_{py}, 4H), δ 7.434 (d, H_{py}, 4H), δ 5.414 (s, CH_2, 4H). ^{13}C-NMR ($CDCl_3$, 100 MHz): δ 162.66 (Cx4), δ 150.03 (Cx4), δ 145.17 (Cx2), δ 131.50 (CHx4), δ 126.87 (Cx4), δ 126.55 (Cx2), δ 123.51 (CHx4), δ 43.08 (CH_2x2).

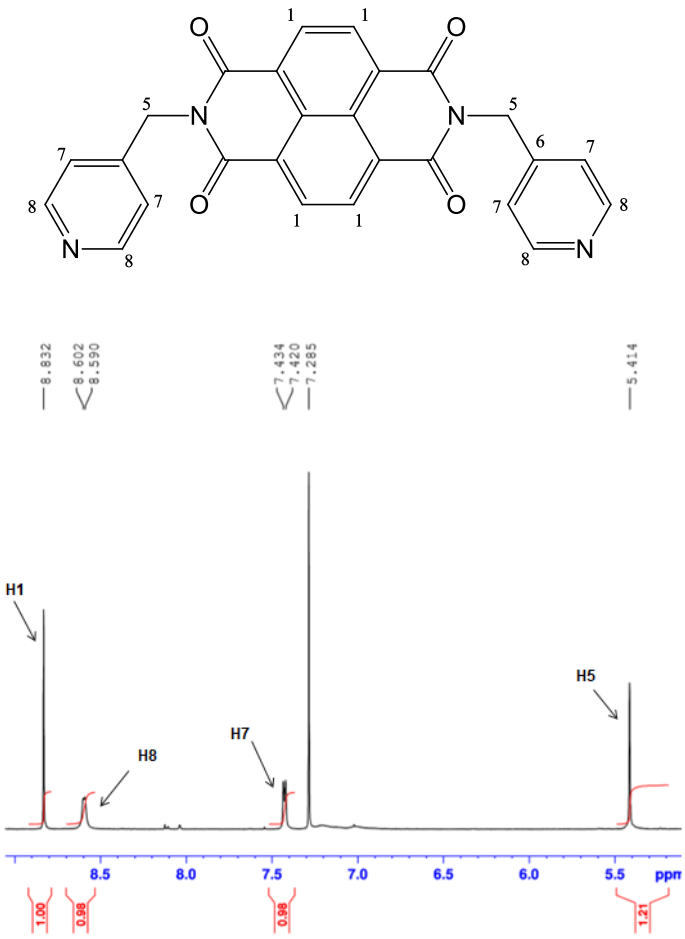

Fig 2. 3 Proton NMR spectra of L2.

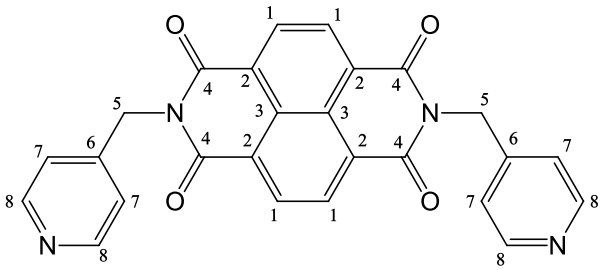

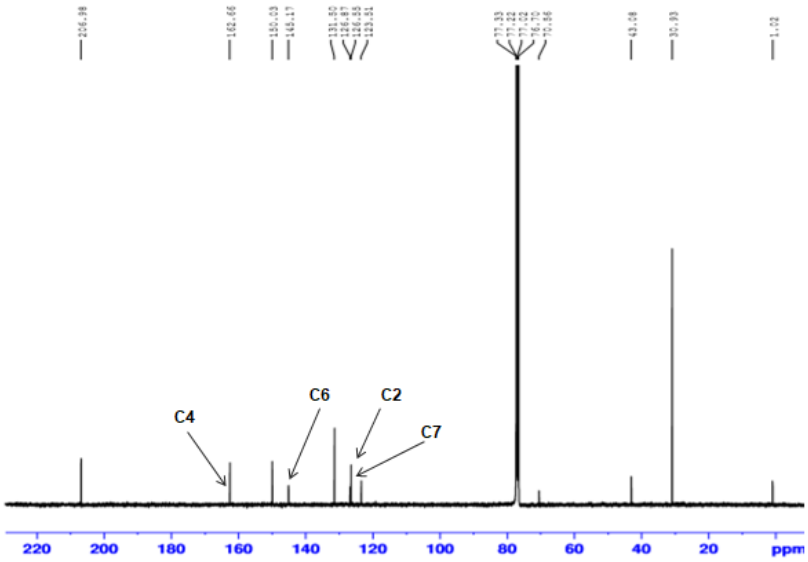

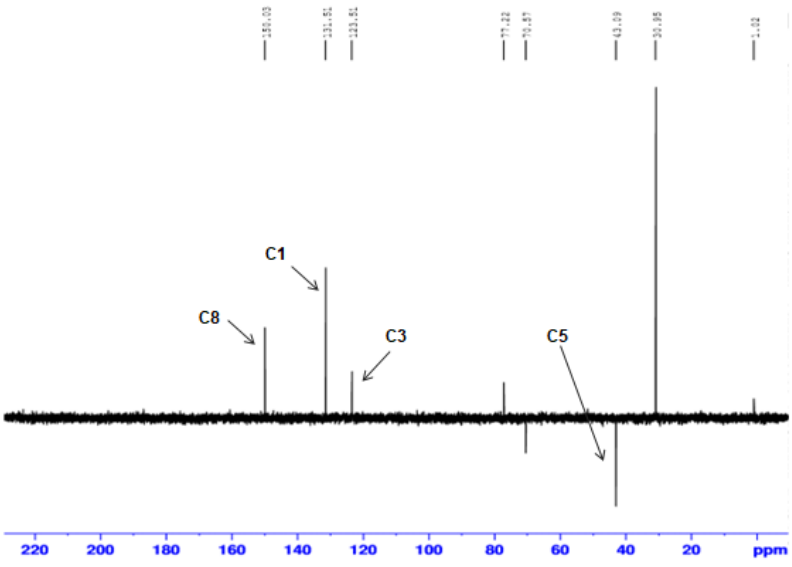

Fig 2. 4 Carbon NMR spectra of L2.

2.1.3 Synthesis of 2,2′-bis(pyridin-2-ylmethyl)-[5,5′-biisoindoline]-1,1′-3,3′-tetraone (L3).

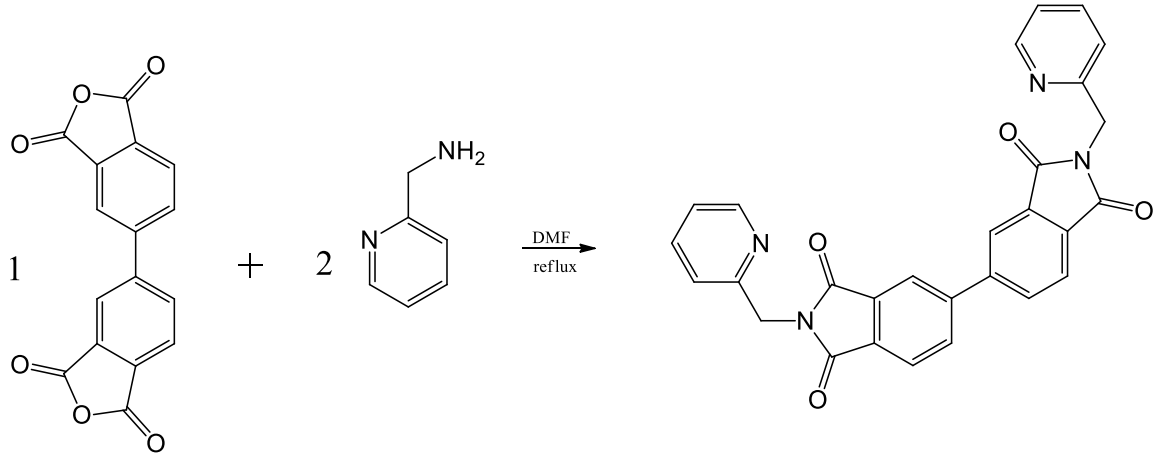

Scheme 2. 3 Synthesis of 2,2′-bis(pyridin-2-ylmethyl)-[5,5′-biisoindoline]-1,1′-3,3′-tetraone (L3).

L3 was synthesized by refluxing a mixture of 3,3′,4,4′-biphenyltetracarboxylic dianhydride (1.0 g, 3.34 mmol) and 2-picolyamine (0.74 g, 6.80 mmol) in DMF (20 mL) for 12 hours at 160 °C. On cooling, the yellow solution was filtered and the crude solid was collected and recrystallized from DMF. L3 was characterized using proton and carbon NMR (Fig 2.5 and 2.6). Yield: 58 %. ^{1}H-NMR (DMSO-d6, 400 MHz): δ 8.442 (d, H_{Ar}, 2H), δ 8.352 (m, H_{py}, 4H), δ 8.064 (d, H_{Ar}, 2H), δ 7.812 (t, H_{Ar}, 2H), δ 7.449 (d, H_{py}, 2H), δ 7.303 (m, H_{py}, 2H), δ 4.958 (s, CH_2, 4H). ^{13}C-NMR ($CDCl_3$, 100 MHz): δ 167.87 (Cx4), δ 155.44 (Cx2), δ 149.56 (Cx2), δ 144.92 (Cx2), δ 137.44 (CHx2), δ 134.17 (CHx2), δ 133.25 (Cx2), δ 131.95 (Cx2), δ 124.49 (CHx2), δ 123.08 (CHx2), δ 122.71 (CHx2), δ 121.81 (CHx2), δ 31.14 (CH_2x2).

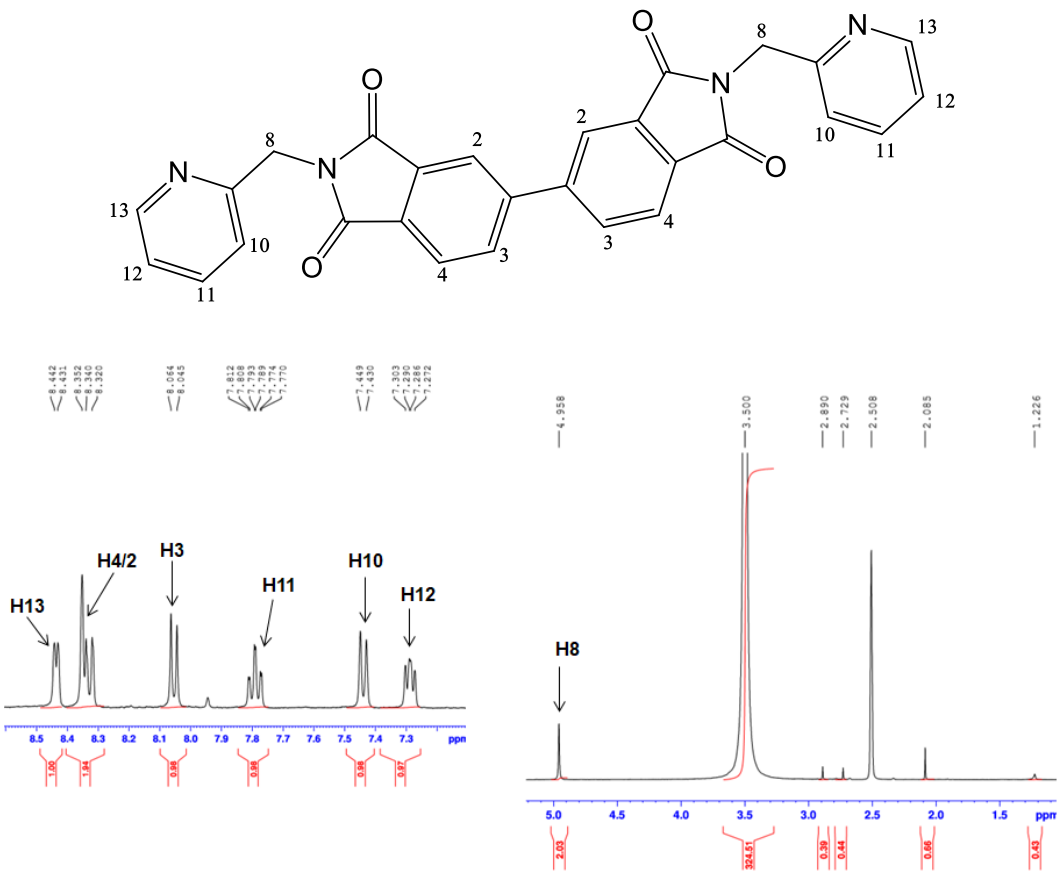

Fig 2. 5 Proton NMR spectra of L3.

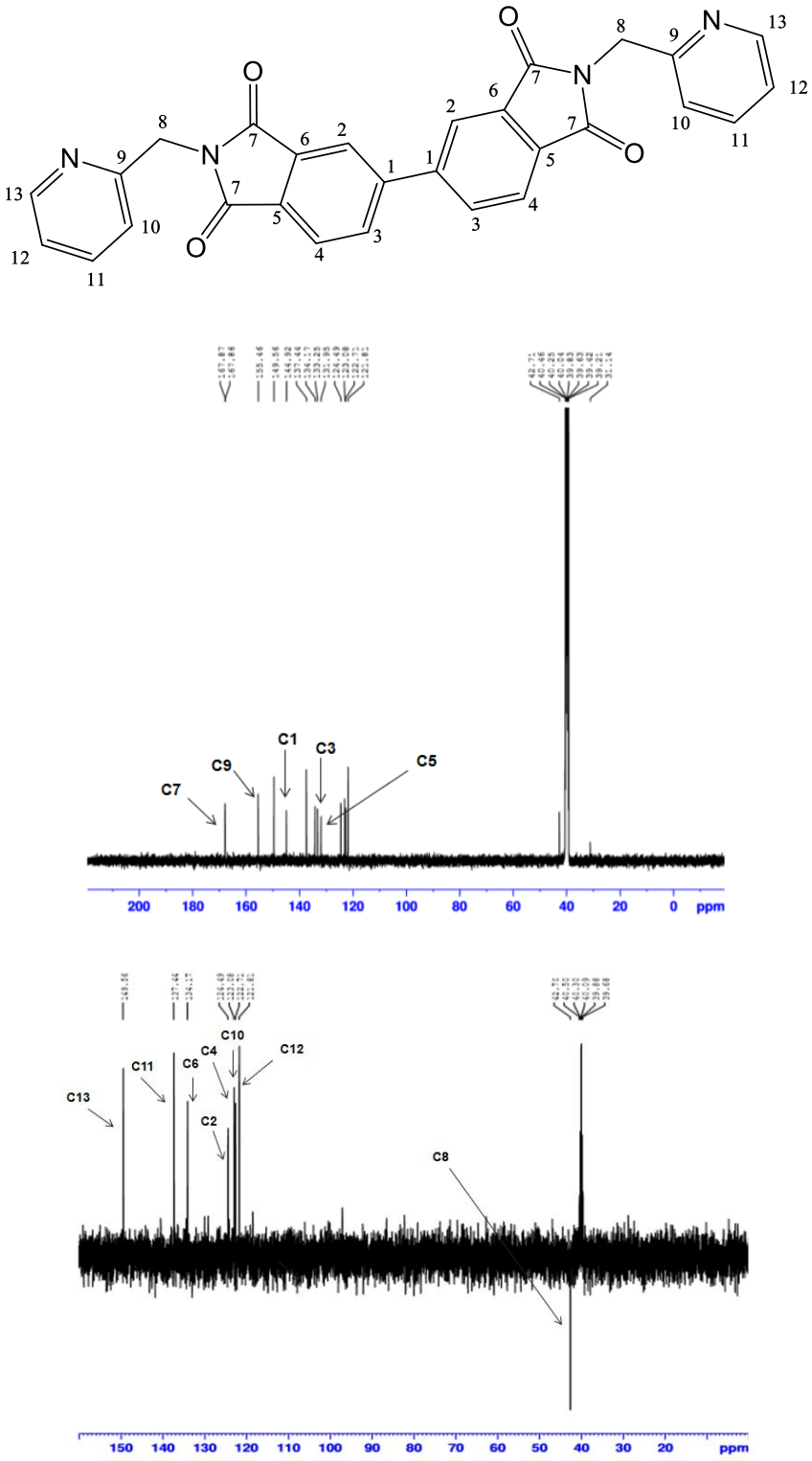

Fig 2. 6 Carbon NMR spectra of L3.

2.1.4 Synthesis of 2,2′-bis(pyridin-4-ylmethyl)-[5,5′-biisoindoline]-1,1′-3,3′-tetraone (L4)

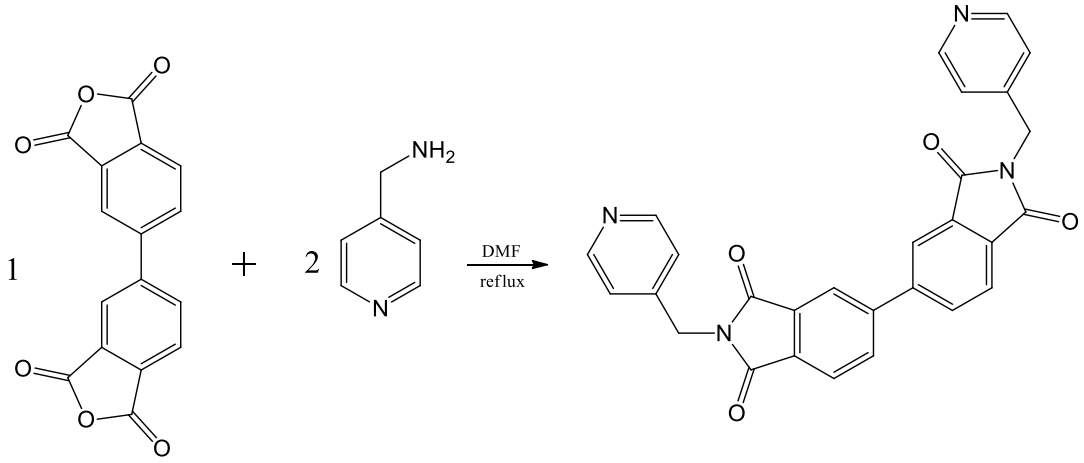

Scheme 2. 4 Synthesis of 2,2′-bis(pyridin-4-ylmethyl)-[5,5′-biisoindoline]-1,1′-3,3′-tetraone (L4).

L4 was synthesized by refluxing a mixture of 3,3′,4,4′-biphenyltetracarboxylic dianhydride (1.0 g, 3.34 mmol) and 4-aminomethyl pyridine (0.74 g, 6.80 mmol) in DMF (20 mL) for 12 hours at 160 °C. On cooling, the white solution was filtered and the crude solid was recrystallized from DMF. L4 was characterized using proton and carbon NMR (Fig 2.7 and 2.8). Yield: 66%**.** ^{1}H-NMR (DMSO-d6, 400 MHz): δ 8.532 (d, H_{py}, 4H), δ 8.360 (m, H_{Ar}, 4H), δ 8.063 (d, H_{Ar}, 2H), δ 7.353 (d, H_{py}, 4H), δ 4.860 (s, CH_2, 4H). ^{13}C-NMR (DMSO-d6, 100 MHz): δ 167.76 (Cx4), δ 150.27 (CHx4), δ 145.86 (Cx2), δ 144.82 (Cx2), δ 134.11 (CHx2), δ 133.21 (Cx2), δ 131.91 (Cx2), δ 124.56 (CHx2), δ 122.72 (CHx2), δ 122.51 (CHx2), δ 31.15 (CH_2x2).

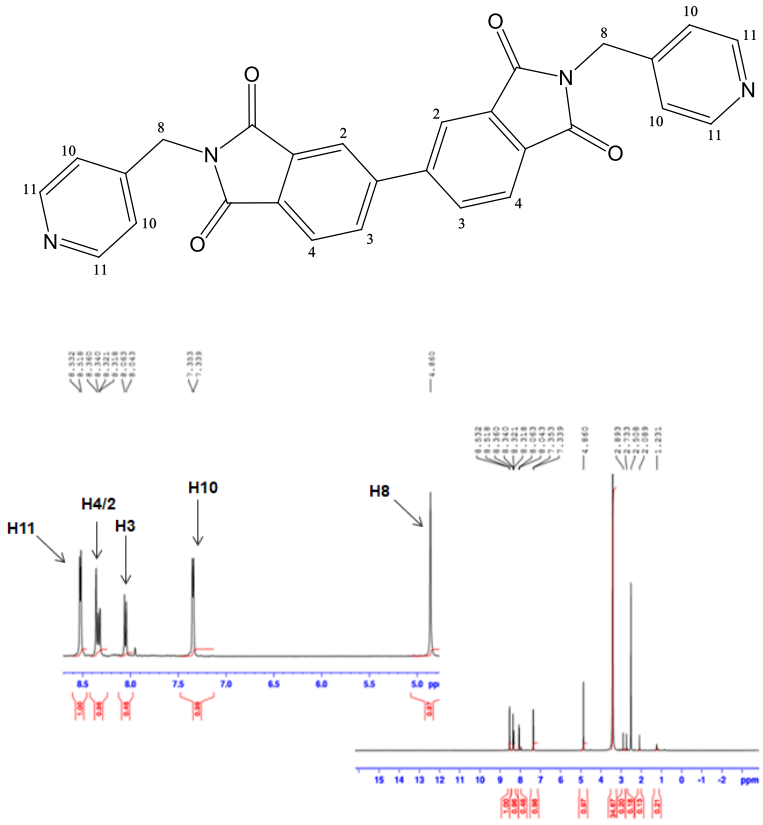

Fig 2. 7 Proton NMR spectra of L4.

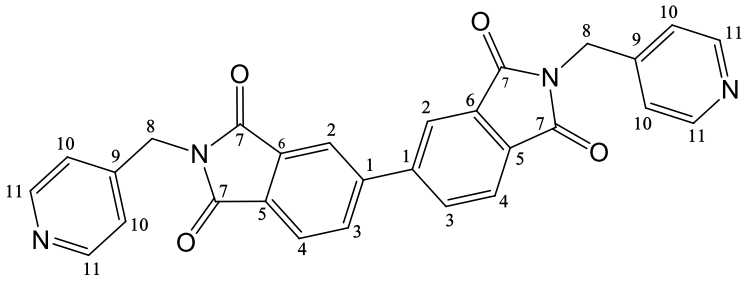

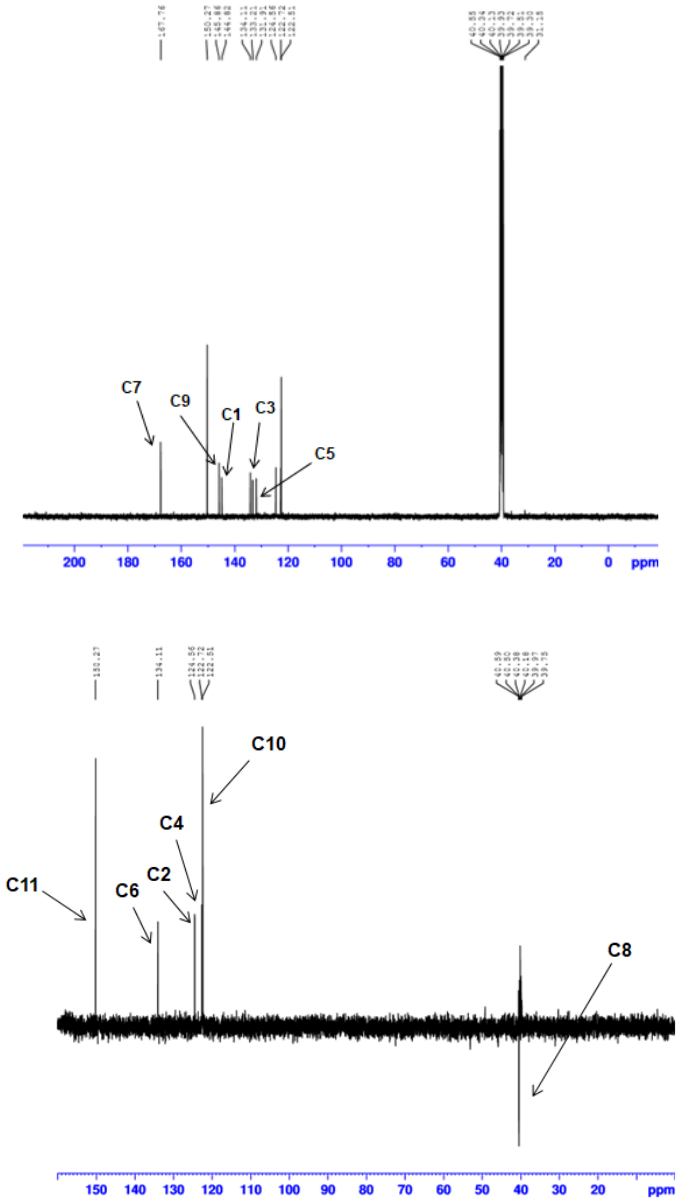

Fig 2. 8 Carbon NMR spectra of L4.

2.1.5 Synthesis of 5,5′-carbonylbis(2-(pyridin-3-ylmethyl) isoindoline-1,3′-dione) (L5)

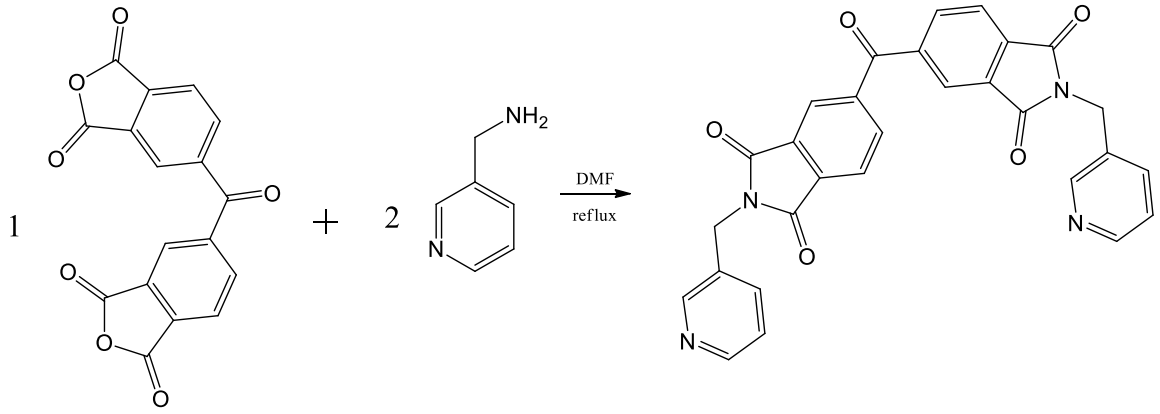

Scheme 2. 5 Synthesis of 5,5′-carbonylbis (2-(pyridin-3-ylmethyl) isoindoline-1,3′- dione) (L5).

L5 was synthesized by refluxing a mixture of benzophenone-3,3′,4,4′-tetracarboxylic dianhydride (1 g, 3.10 mmol) and 3-aminomethyl pyridine (0.67 g, 6.21 mmol) in DMF (20 mL) for 12 hours at 160 °C. On cooling, the yellow solution was filtered and the crude solid was collected and recrystallized from DMF. L5 was characterized using proton and carbon NMR (Fig 2.9 and 2.10). Yield: 73%. ^{1}H-NMR (DMSO-d6, 400 MHz): δ 8.613 (s, H_{py}, 2H), δ 8.503 (s, H_{py}, 2H), δ 8.199 (d, H_{Ar}, 2H), δ 8.107 (m, H_{Ar}, 4H), δ 7.776 (d, H_{py}, 2H), δ 7.393 (t, H_{py}, 2H), δ 4.862 (s, CH_2, 4H). ^{13}C-NMR ($CDCl_3$, 100 MHz): δ 193.89 (C), δ 167.40 (Cx4), δ 162.76 (Cx2), δ 149.44 (CHx2), δ 149.21 (CHx2), δ 141.94 (Cx2), δ 136.17 (CHx2), δ 135.92 (CHx2), δ 135.30 (Cx2), δ 132.54 (Cx2), δ 132.46 (Cx2), δ 124.19 (CHx2), δ 124.14 (CHx2), δ 39.81 (CH_2x2)

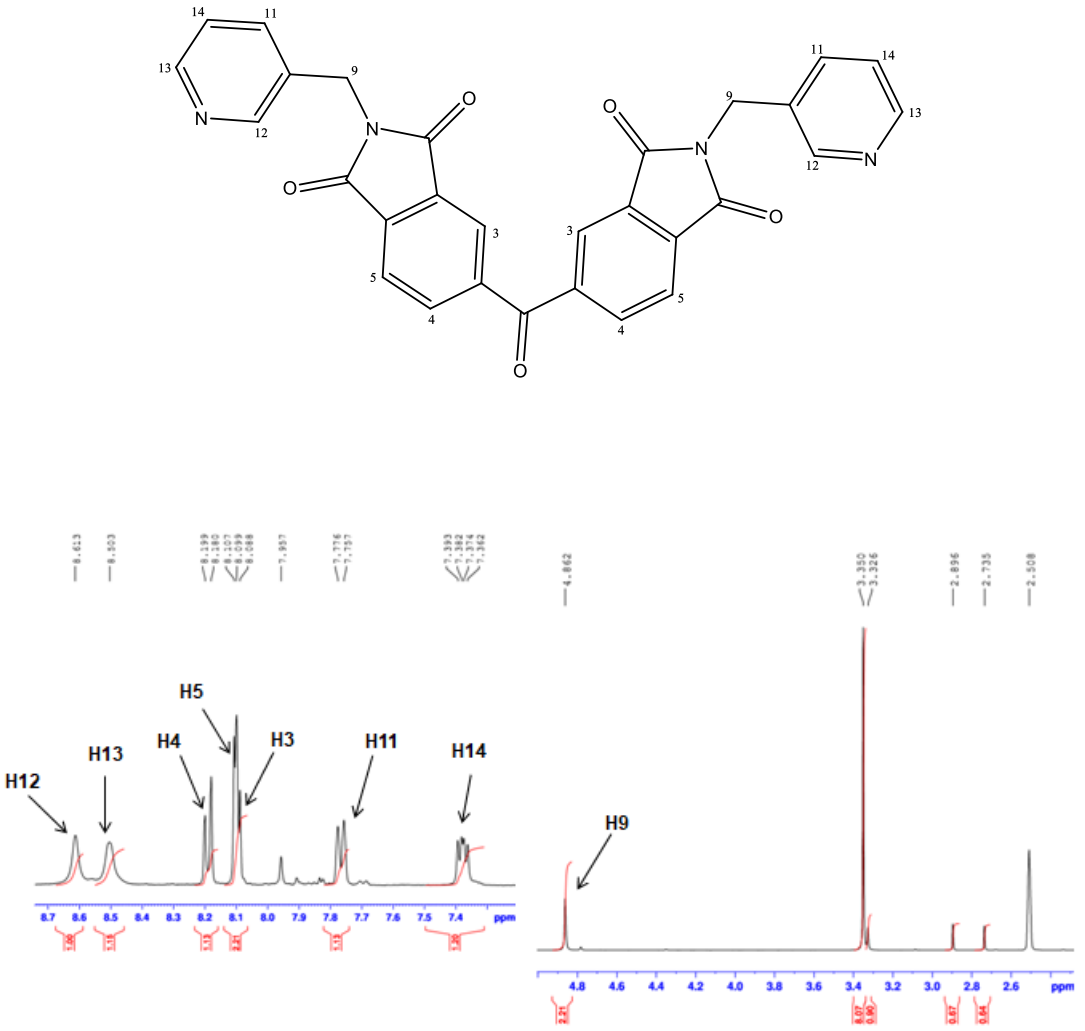

Fig 2. 9 Carbon NMR spectra of L5.

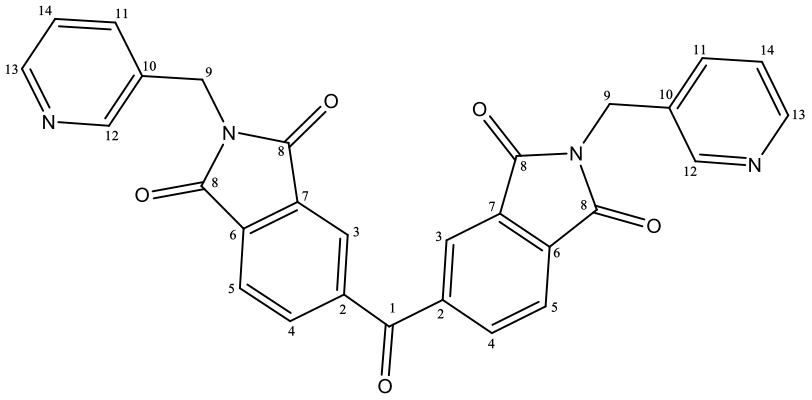

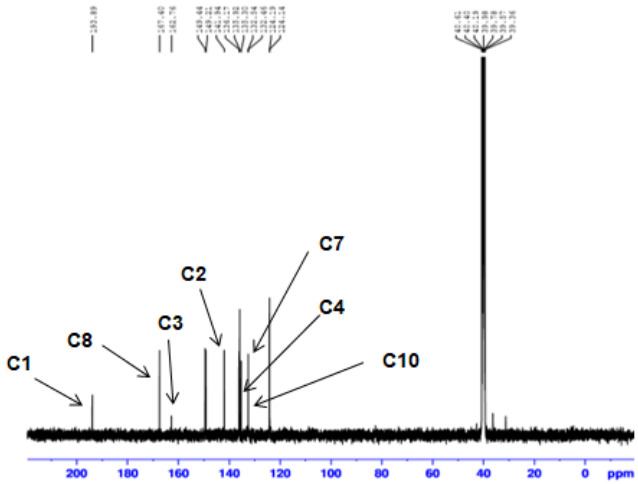

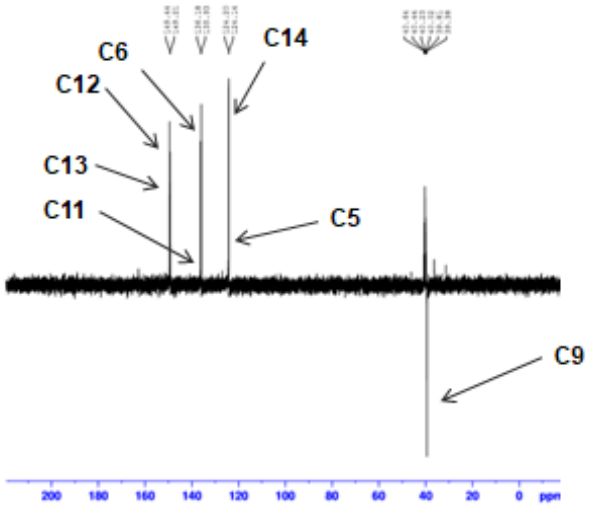

Fig 2. 10 Carbon NMR spectra of L5.

2.2 SYNTHESIS OF METAL-ORGANIC FRAMEWORKS (MOFs)

Several methods are used in the synthesis of MOFs and these include solvothermal, solvent evaporation and mechanochemical synthesis. For this study MOFs were synthesized using the solvothermal method. Each of the synthesized ligands and the co-ligand were reacted with metal salts in either DMF or a DMF ethanol mixture. The mixture was heated in an oven at 100 °C (Scheme 2.6). After the formation of crystals, the reaction was stopped and the crystals were washed with DMF. The crystals were then analysed using thermogravimetric analysis (TGA), single crystal X-ray diffraction (SCXRD) and powder X-ray diffraction (PXRD). The as-synthesized MOFs were then desolvated at 100 °C under vacuum and characterized using TGA, PXRD and Brunauer-Emmet-Teller (BET) surface area analysis. All the metal salts, co-ligands and some of reactions carried out in the synthesis of MOFs for this study are shown in Table 2.1.

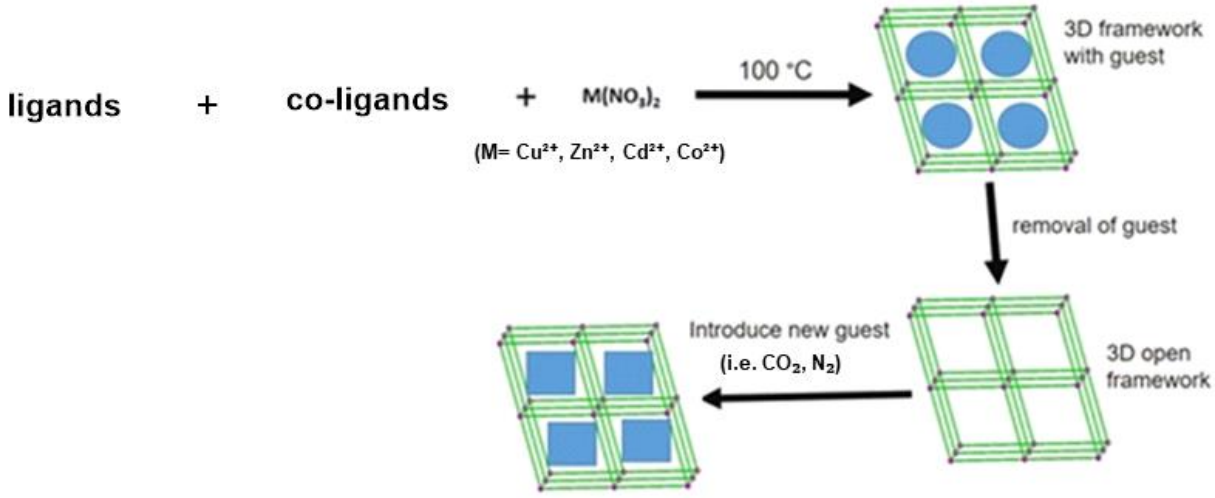

Scheme 2. 6 A reaction scheme for the synthesis and desolvation of a mixed ligand MOFs.

2.2.1 Synthesis of RMMOF 1

RMMOF 1 was synthesized by reacting 6,6′-dithiodinicotinic acid (20 mg, 0.06 mmol), *N,N′*-bis(pyridin-3-ylmethyl) naphthalene diimide (L1) (29.07 mg, 0.06 mmol) and zinc(II) nitrate hexahydrate (12.31 mg, 0.06 mmol) in DMF:ethanol (5 mL:2 mL). The mixture was heated in oven at 100 °C for 72 hours. The crystals were then analysed using SCXRD, TGA, PXRD and BET analysis.

2.2.2 Synthesis of RMMOF 2

RMMOF 2 was synthesized by reacting 6,6′-dithiodinicotinic acid (13.87 mg, 0.04 mmol), *N,N′*-bis(pyridin-4-ylmethyl) naphthalene diimide (L2) (20 mg, 0.04 mmol) and zinc(II) nitrate hexahydrate (17.04 mg, 0.08 mmol) DMF:ethanol (5 mL:2 mL) under solvothermal conditions

(100 °C, 72 hours). The crystals were then analysed using SCXRD, TGA, PXRD and BET analysis.

2.2.3 Synthesis of RMMOF 3

RMMOF 3 was synthesized by reacting 6,6′-dithiodinicotinic acid (13.87 mg, 0.04 mmol), *N,N′*-bis(pyridin-4-ylmethyl) naphthalene diimide (L2) (20 mg, 0.04 mmol) and cobalt(II) nitrate hexahydrate (14.64 mg, 0.08 mmol) in 1:1:2 molar ratio in DMF:ethanol (5 mL:2 mL) and was heated in oven at 100 °C for 72 hours. The crystals were then analysed using SCXRD, TGA and PXRD.

Table 2. 1 Reactions carried out in the synthesis of MOFs.

Ligands	**Co-ligand**	**Metal ion** $M(NO_3)_2.XH_2O$	**Product**	**Structure**
N,N′-bis(pyridin-3-ylmethyl) naphthalene diimide **(L1)**	6,6′-Dithiodinicotinic acid	$Zn(NO_3)_2{\cdot}6H_2O$	Good quality crystals	**RMMOF 1**
N,N′-bis(pyridin-4-ylmethyl) naphthalene diimide **(L2)**	6,6′-Dithiodinicotinic acid	$Zn(NO_3)_2{\cdot}6H_2O$ $Co(NO_3)_2{\cdot}6H_2O$	Good quality crystals Good quality crystals	**RMMOF 2** **RMMOF 3**
2,2′-bis(pyridin-2-ylmethyl)-[5,5'-biisoindoline]-1,1',3,3'-tetraone **(L3)**	4,4′-oxybis(benzoic acid)	$Zn(NO_3)_2{\cdot}6H_2O$	Good quality crystals	**RMMOF 4**
2,2′-bis(pyridin-4-ylmethyl)-[5,5'-biisoindoline]-1,1',3,3'-tetraone **(L4)**	2,6-naphthalene dicarboxylic acid	$Cd(NO_3)_2{\cdot}4H_2O$ $Zn(NO_3)_2{\cdot}6H_2O$	Good quality crystals	**RMMOF 5** **RMMOF 6**
5,5′-carbonylbis(2-(pyridin-3-ylmethyl) isoindoline- 1,3- dione) **(L5)**	2,6-naphthalene. dicarboxylic acid	$CuCl_2$	Good quality crystals	**RMMOF 7**

2.2.4 Synthesis of RMMOF 4

RMMOF 4 was synthesized by the solvothermal reaction (100 °C, 7 days) of 4,4′-oxybis(benzoic acid) (12.91 mg, 0.05 mmol), 2,2′-bis(pyridin-2-ylmethyl)-[5,5′-biisoindoline]-1,1′-3,3′-tetraone (L3) (24 mg, 0.05 mmol) and zinc(II) nitrate hexahydrate (30 mg, 0.1 mmol)

in DMF (10 mL). The crystals were then analysed using SCXRD, TGA, PXRD and BET analysis.

2.2.5 Synthesis of RMMOF 5

RMMOF 5 was synthesized by reacting 2,6-naphthalenedicarboxylic acid (22 mg, 0.1 mmol), 2,2′-bis(pyridin-4-ylmethyl)-[5,5′-biisoindoline]-1,1′-3,3′-tetraone (L4) (24 mg, 0.05 mmol) and cadmium(II) nitrate tetrahydrate (31 mg, 0.1 mmol) in DMF:ethanol (5 mL:2 mL) under solvothermal conditions (100 °C, 48 hours). The crystals were then analysed using SCXRD, TGA, PXRD and BET analysis.

2.2.6 Synthesis of RMMOF 6

RMMOF 6 was synthesized by reacting 2,6-naphthalenedicarboxylic acid (22 mg, 0.1 mg), 2,2′-bis(pyridin-4-ylmethyl)-[5,5′-biisoindoline]-1,1′,3,3′-tetraone (L4) (24 mg, 0.05 mmol) and zinc(II) nitrate hexahydrate (30 mg, 0.1 mmol) in DMF:ethanol (5 mL:2 mL) at 100 °C for 48 hours. The crystals were then analysed using SCXRD, TGA, PXRD and BET analysis.

2.2.7 Synthesis of RMMOF 7

RMMOF 7 was synthesized by reacting 2,6-naphthalenedicarboxylic acid (22 mg, 0.1 mmol), 5,5′-carbonyl bis(2-(pyridin-3-ylmethyl) isoindoline-1,3-dione) (L5) (25 mg, 0.05 mmol) and copper(II) chloride anhydrous (13 mg, 0.1 mmol) in DMF:ethanol (5 mL:2 mL) at 100 °C for 72 hours. The crystals were then analysed using SCXRD, TGA, PXRD and BET analysis.

2.2.8 Synthesis of RMMOF 1-Cu and RMMOF 2-Cu

RMMOF 1-Cu and **RMMOF 2-Cu** was synthesized by adding copper(II) chloride (32.70 mg, 0.2 mmol) into 5 mL of DMF solvent. The desolvated phase **RMMOF 1** and **RMMOF 2** was soaked into DMF solution of copper chloride at room temperature for 3 weeks and the mixture was heated at 100 °C for 24 hours. The crystals were then analysed using TGA, PXRD and BET analysis.

2.3 INSTRUMENTATION AND COMPUTER PACKAGES

2.3.1 Single crystal X-ray diffraction (SCXRD)

Crystals suitable for single crystal X-ray diffraction were selected and placed on a glass slide under paratone N oil.[63] Intensity data for **RMMOF 1**, **RMMOF 2**, **RMMOF 3**, **RMMOF 4**, **RMMOF 5**, **RMMOF 6** and **RMMOF 7** were collected at 100 K on a Bruker D8 VENTURE diffractometer equipped with an Oxford Cryostream 800 and Mo (λ = 0.71073 Å) radiation

generated at 50 kV and 1.4 mA through a Bruker K430 generator.[64] Data collection and cell refinement were carried out using SAINT-Plus.[65] Data were corrected for absorption effects using the Multi-Scan method (SADABS).[66] Space groups were then determined from systematic absences using XPREP. The crystal structures were solved and refined within the X-Seed[67] graphical user interface using SHELXS-97[68] and SHELXL-97, respectively.[69] Non-hydrogen atoms (except for disordered atoms) were refined anisotropically. All C-H hydrogen atoms were placed at calculated positions using the riding model and were refined isotropically. Images were generated using Mercury and POV-RAY.[70]

2.3.2 Thermogravimetric analysis (TGA)

TGA was used to determine the percentage weight loss of guest molecules and the temperature at which the framework decomposes. TGA data were obtained using a TA-Q500 thermogravimetric analyser. The samples were heated at a flow rate of 60 mL min^{-1} under nitrogen gas from 10 °C to 600 °C.

2.3.3 Powder X-ray diffraction (PXRD)

Samples were analysed using both powder X-ray diffraction (PXRD) and variable-temperature powder X-ray diffraction (VT-PXRD). The samples were first dried using filter paper followed by grinding until finely powdered. Ground powders were placed on a zero-background sample holder. X-ray intensity data were collected on a Bruker D8 advance X-ray diffractometer equipped with copper radiation (Cu Kα, λ = 1.5406 Å) produced at 30 kV and 40 mA. Each of the samples was scanned between 4 and 40° 2θ using a step size of 0.02° s^{-1}. VT-PXRD data were recorded at different temperatures to determine any changes in the crystalline patterns as the temperature was varied. VT-PXRD reveals any changes in the crystal structure when the included solvent is removed. It is also used to check the crystallinity of a compound as well as its stability at different temperatures during heating and cooling. During the collection of PXRD data collection the stage was rotated to correct for preferred orientations effects, however this was not possible for the VT-PXRD data collections due to the stage settings.

2.3.4 Nuclear Magnetic Resonance (NMR)

Carbon and proton spectra were recorded using Varian Unity INOVA (400MHz). Samples were dissolved in deuterated dimethylsulfoxide (DMSO-d6) and in deuterated chloroform ($CDCl_3$). Ligands L1 and L2 were dissolved in $CDCl_3$ and ligands L3, L4 and L5 were dissolved in DMSO-d6.

2.3.5 Brunauer-Emmett-Teller (BET) analysis

BET was used to determine the surface areas of **RMMOF 1, RMMOF 2, RMMOF 1-Cu** and **RMMOF 2-Cu**. BET measurements were performed at 77 K using a Micromeritics (USA) TRISTAR II 3020. The samples were degassed at 150 °C for 2 hours prior to analysis.

2.3.6 Hot Stage Microscopy (HSM)

Thermal behaviour of compounds **RMMOF 6** and **RMMOF 7** was studied using hot stage microscopy (HSM). Data were collected using Nikon SMZ-10 stereoscopic microscope equipped with Linkam THMS600 hot stage as well as Linkam TP92 control unit. Samples were heated at 10 °C min^{-1}. Images were captured after every 10 °C min^{-1} using Sony Digital Hyper HAD colour camera and were generated using the soft imaging system program analysis.[71]

2.3.7 Gas sorption

The carbon dioxide sorption capacities of **RMMOF 4, RMMOF 5, RMMOF 6** and **RMMOF 7** were determined using a Micrometrics 3Flex surface area analyser. Before analysis, samples were first washed with ethanol and dried on a filter paper and, evacuated under a high vacuum (less than 10^{-5} torr) at 60 °C to 150 °C overnight. The samples were weighed before and after the evacuation process to ensure complete removal of included solvents. Carbon dioxide sorption experiments were performed at 195 K and 273 K using a dry ice / acetone slurry and a water bath, respectively.

2.3.8 Cambridge Structural Database (CSD)

The CSD[72] was used as a search tool for reported organic and inorganic structures related to this project. The CSD is curated hosting published or unpublished crystal structures determined from X-ray and neutron diffraction data.

CHAPTER 3

RESULTS AND DISCUSSION

This chapter discusses characterization and structural analysis of the following metal- organic frameworks namely: $\{[Zn(DCT)(L1)_{0.5}]\cdot(DMF)\}_n$ **(RMMOF 1)**, $\{[Zn(DCT)(L2)_{0.5}]\cdot(DMF)\cdot(H_2O)\}_n$ **(RMMOF 2)**, $\{[Co(DCT)(L2)_{0.5}]\cdot(DMF)\}_n$ **(RMMOF 3)**, $\{[Zn_5(OBZ)_3(DMF)_2]\cdot(DMF)_4\}_n$ **(RMMOF 4)**, $\{[Cd(NDC)(L4)_2]\cdot(DMF)_3\}_n$ **(RMMOF 5)**, $\{[Zn_{0.5}(NDC)_{0.5}(L4)_{0.5}]\cdot(DMF)_2\}_n$ **(RMMOF 6)** and $\{[Cu(NDC)(L5)_{0.5}](DMF)_3\}_n$ **(RMMOF 7)**. Solvent accessible volumes of the MOFs were estimated using the Mercury program (0.18 Å grid spacing, 1.4 Å probe radius). Crystallographic data are given on pages 66 to 67.

3.1 RMMOF 1

3.1.1 Single crystal X-ray diffraction (SCXRD)

RMMOF 1 was synthesized by reacting 6,6'-dithiodinicotinic acid (DCT), *N,N*'-bis(pyridin-3-ylmethyl) naphthalene diimide (L1) and zinc(II) nitrate hexahydrate in DMF:ethanol (5 mL:2 mL) under solvothermal conditions (100 °C, 72 hours). **RMMOF 1** crystallizes in the triclinic space group $P\bar{1}$ with one deprotonated DCT, one zinc(II) cation, an uncoordinated DMF molecule and half a molecule of L1 in the asymmetric unit (ASU) (Fig 3.1). The Zn(II) center is six-coordinate, exhibiting a zinc paddle wheel coordination environment composed of two nitrogen atoms and four oxygen atoms. The packing diagram, viewed in the *ac* plane shows continuous channels running along the *b* axis (Fig 3.2). The DMF molecules are located in these channels occupying a potential solvent accessible volume of 14% (Fig 3.3). The neighboring aromatic rings of L1 and DCT interact *via* π-π interactions with a centroid – centroid distance of 3.549 Å.

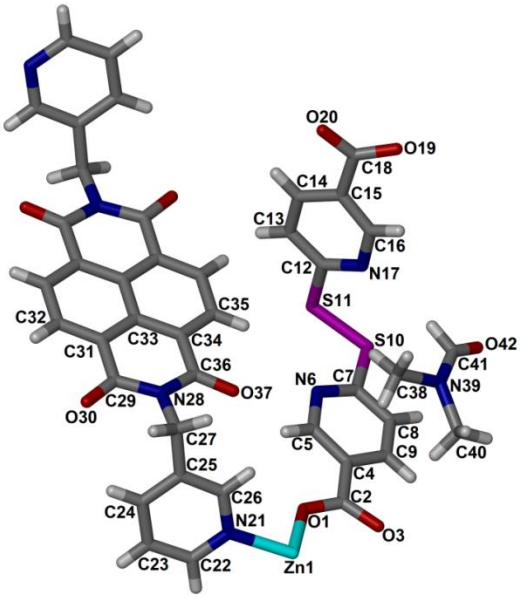

Fig 3. 1 The molecular structure of **RMMOF 1** showing the crystallographic labelling scheme for the asymmetric unit.

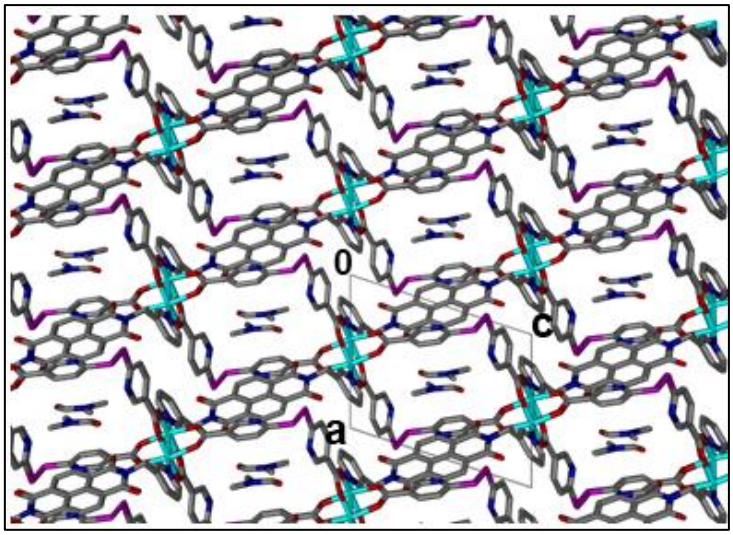

Fig 3. 2 The packing diagram of **RMMOF 1** viewed in the ac plane. The DMF molecules are located in channels running along the *b* axis.

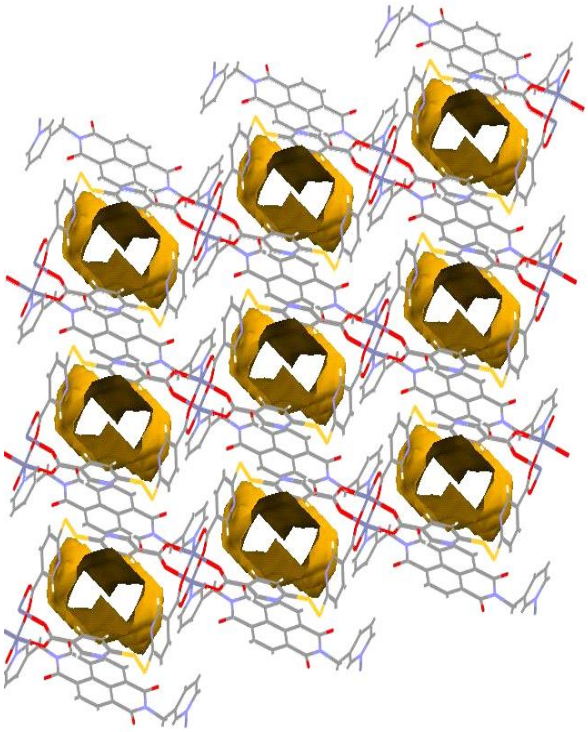

Fig 3. 3 A plot of solvent accessible volume in **RMMOF 1** generated using the Mercury program. The structure contains 1D channels along the *b* axis.

3.1.2. Thermogravimetric analysis (TGA)

The thermal profile of **RMMOF 1** was determined using TGA (Fig 3.4)**. RMMOF 1** shows a weight loss of 8.58% between 50 °C and 220 °C which is attributed to the loss of one DMF molecule (calculated 9.20%). From 220–292 °C, no further significant weight losses are observed and decomposition commences at 292 °C. Desolvated **RMMOF 1** was prepared by heating the as-synthesized crystals at 100 °C for 24 hours under vacuum. The TGA profile of the desolvated phase shows no weight loss from 20 °C to 292 °C which confirms successful desolvation. The framework decomposes at 292 °C. To determine the porosity of **RMMOF 1,** the as-synthesized **RMMOF 1** was immersed in ethanol for one week and analyzed using TGA. The TGA trace of **RMMOF 1** ethanol-exchange (Fig 3.4) shows a weight loss of 6.48% (calculated 7.10%) indicating the removal of ethanol between 20 °C and 200 °C. Decomposition of the framework commences at 292 °C.

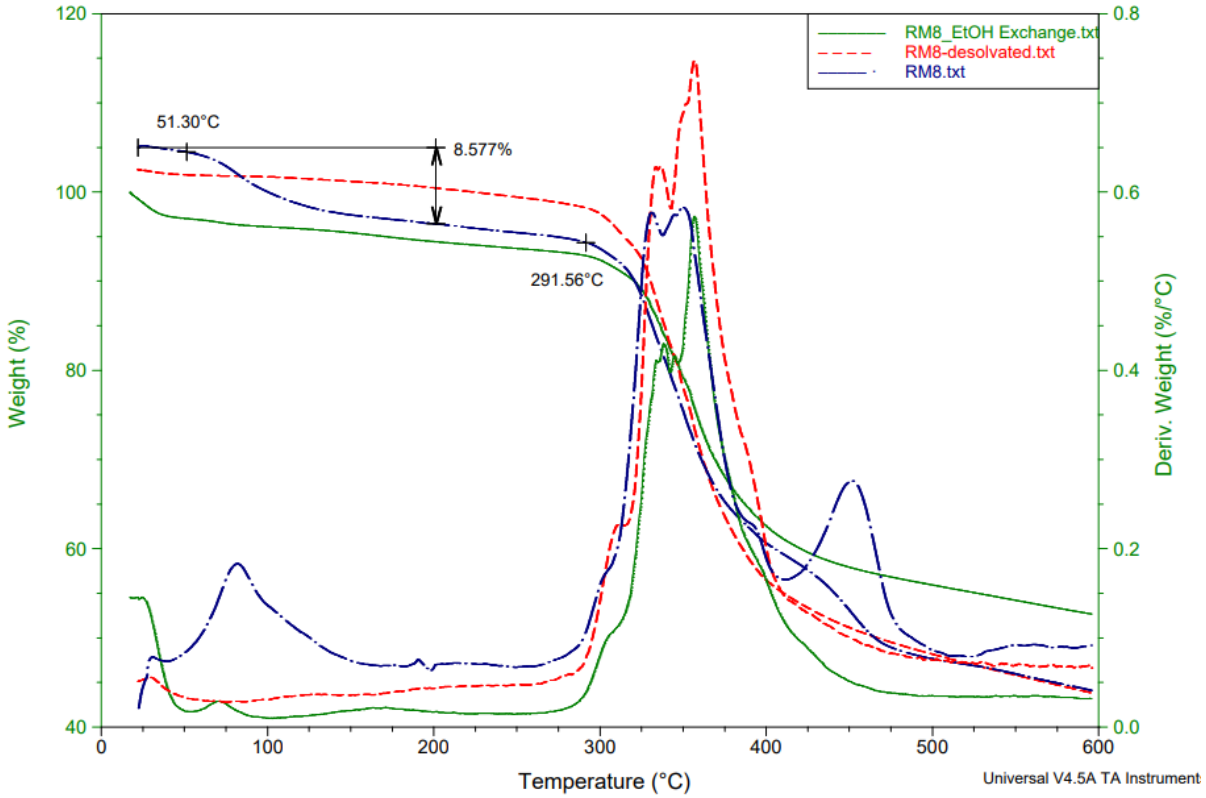

Fig 3. 4 TGA profiles of as-synthesized **RMMOF 1** (dashed blue), desolvated **RMMOF 1** (dashed red), and ethanol-exchange **RMMOF 1** (solid green) as well as the first derivatives of the weight %; as-synthesized (dashed blue), desolvated (dashed red) and ethanol-exchange.

3.1.3 Powder X-ray diffraction (PXRD)

PXRD was used to confirm the bulk phase purity of **RMMOF 1.** The PXRD pattern of the as-synthesized **RMMOF 1** matches the simulated pattern (Fig 3.5) indicating that the crystal selected for SCXRD has the same structure as the bulk sample. The PXRD of desolvated **RMMOF 1** matches the as-synthesized **RMMOF 1** pattern indicating that the framework maintains structural integrity and crystallinity after the desolvation process. The PXRD patterns of the as-synthesized and that of the ethanol-exchange **RMMOF 1** are very similar which indicates that there was no structural change during guest exchange.

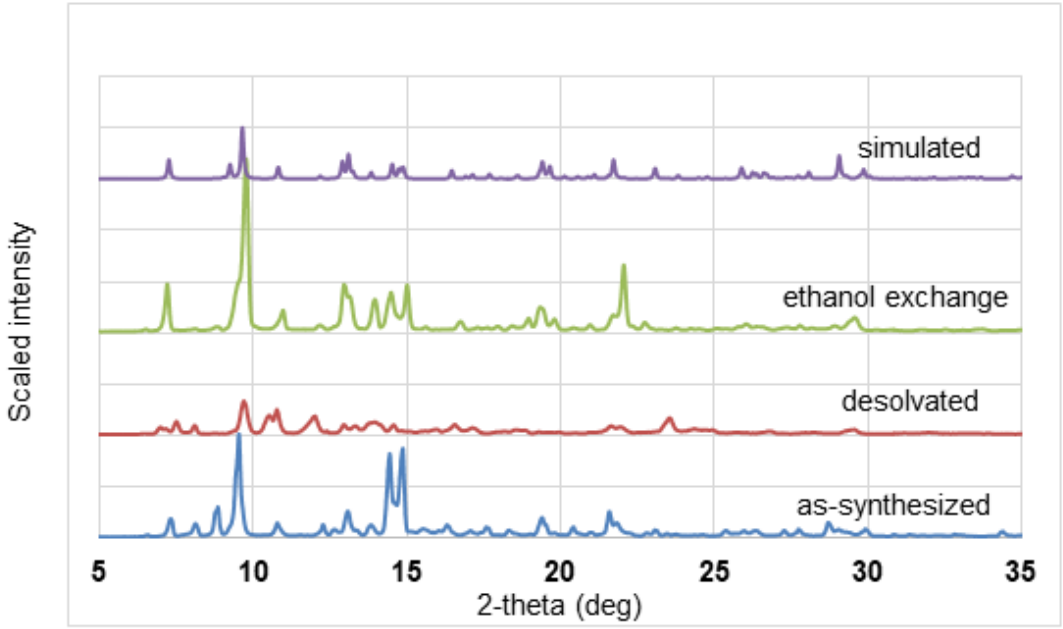

Fig 3. 5 PXRD patterns of as-synthesized **RMMOF 1** (blue), desolvated **RMMOF 1** (red), ethanol-exchange **RMMOF 1** (green) and simulated **RMMOF 1** (purple).

3.1.4 Post-synthetic modification (PSM) of RMMOF 1

RMMOF 1 consists of free donor atoms (N6 and N17) which can coordinate to metal ions post-synthetically. Post-synthetic coordination of the free donor atoms to the metal ions could potentially result in unsaturated metal centre which can offer additional adsorption sites for gases such as hydrogen. Desolvated **RMMOF 1** was soaked in a DMF solution of $CuCl_2$ at room temperature for three (3) weeks. The resulting green powder was isolated by filtration and washed with DMF to remove any unreacted metal and dried in an oven at 100 °C for 24 hours. The thermal profile of the desolvated **RMMOF 1** as well as **RMMOF 1-Cu** is shown in Fig 3.6. **RMMOF 1-Cu** decomposes at 300 °C. The PXRD pattern (Fig 3.7) of **RMMOF 1-Cu** shows that **RMMOF 1** maintains crystallinity during the PSM process.

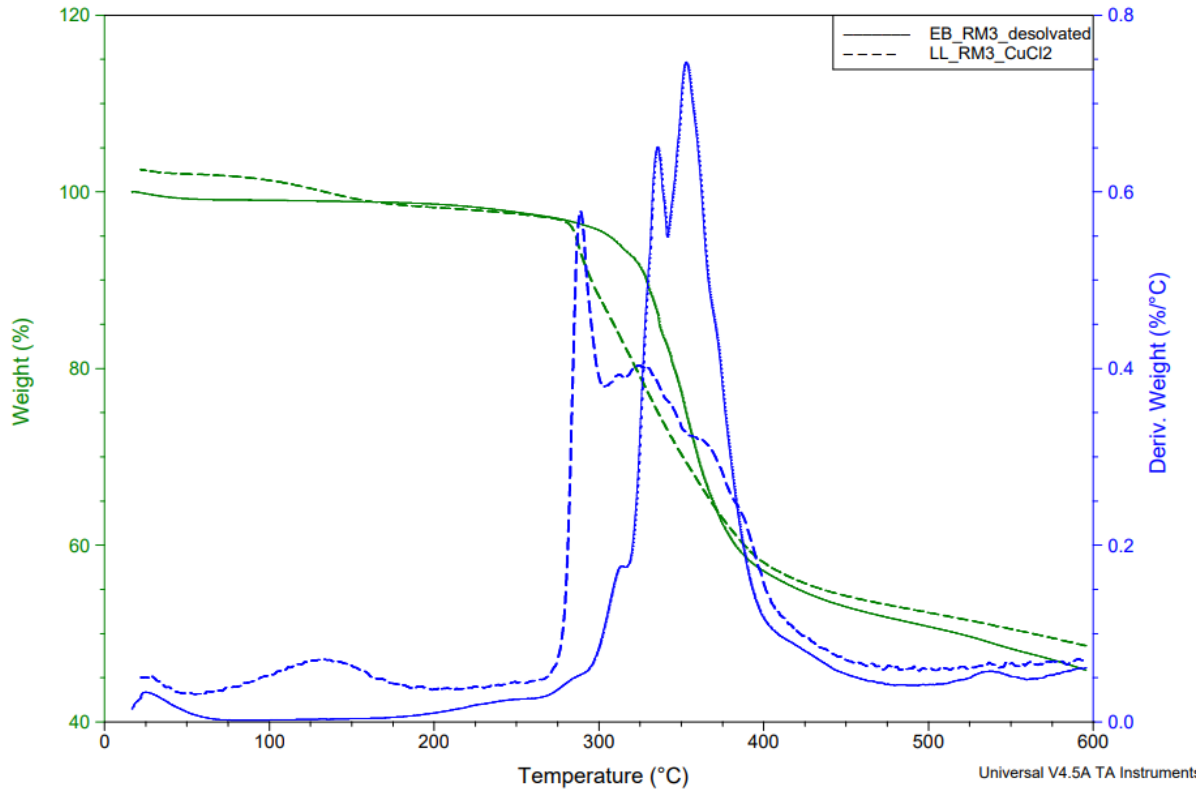

Fig 3. 6 TGA profiles of desolvated **RMMOF 1** (solid green) and desolvated **RMMOF 1**-Cu (dashed green) as well as the first derivatives; desolvated **RMMOF 1** (solid blue) and desolvated **RMMOF 1**-Cu (dashed blue).

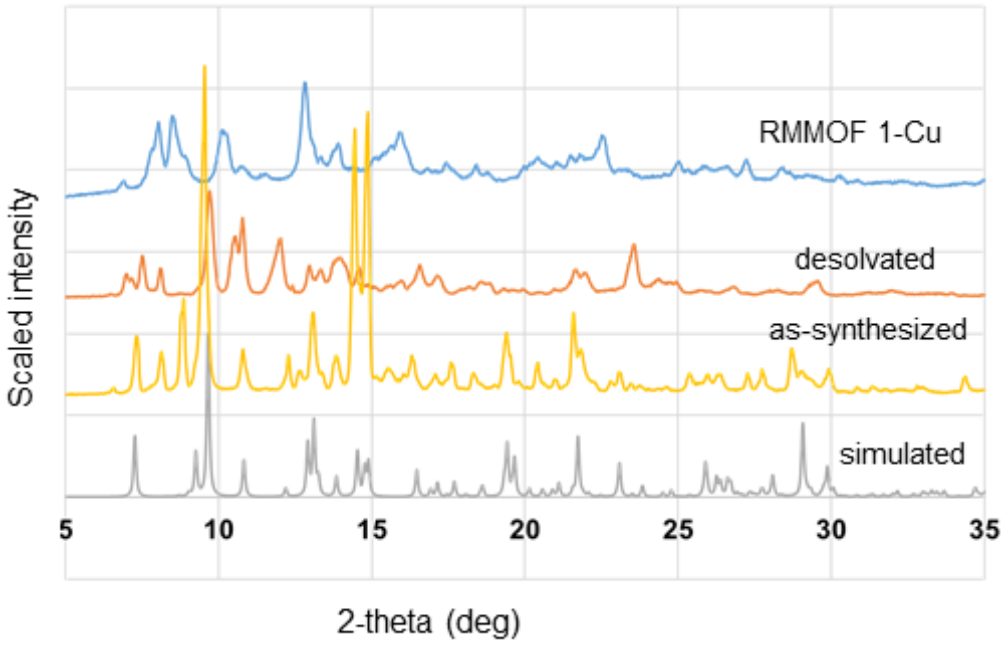

Fig 3. 7 PXRD patterns of simulated **RMMOF 1** (purple), as-synthesized **RMMOF 1** (yellow), desolvated **RMMOF 1** (orange) and **RMMOF 1**-Cu (blue).

3.1.5 Brunauer-Emmet-Teller (BET) analysis

BET measurements for **RMMOF 1** and **RMMOF 1-Cu** were performed using N_2 at 77 K (Fig 3.8). The BET surface area of **RMMOF 1** and **RMMOF 1-Cu** were 2.6814 $m^2\ g^{-1}$ and 16.3475 $m^2\ g^{-1}$ respectively. The quantity of gas adsorbed by pure **RMMOF 1** was found to be 6.19 $cm^3\ g^{-1}$ (STP) and the amount adsorbed by **RMMOF 1**-Cu was found to be 22.59 $cm^3\ g^{-1}$ (STP).

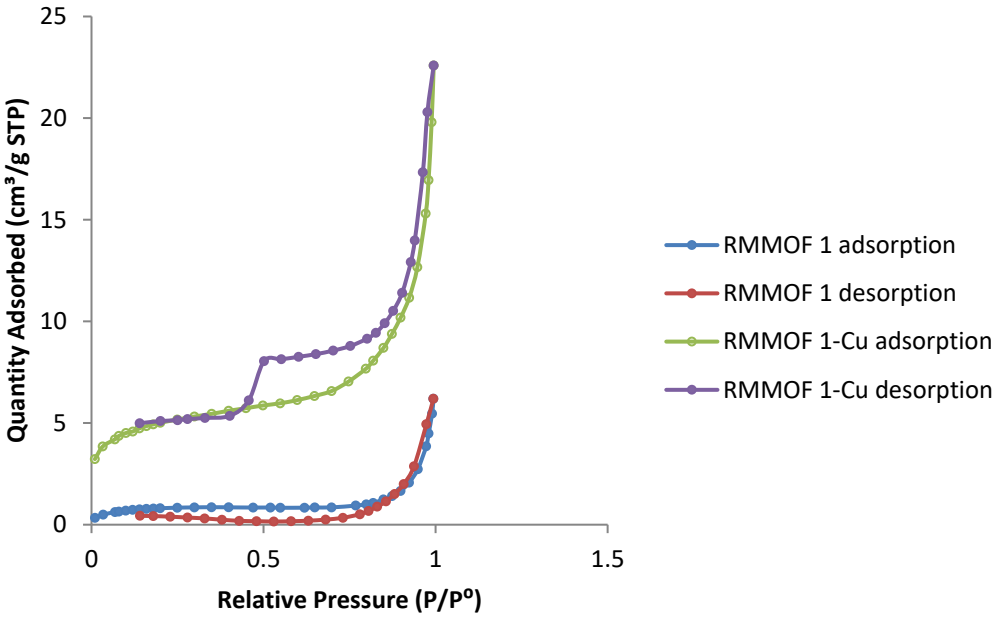

Fig 3. 8 BET measurements for pure **RMMOF 1** and **RMMOF 1**-Cu at 77 K.

3.2 RMMOF 2 and RMMOF 3

3.2.1 Single crystal X-ray diffraction (SCXRD)

RMMOF 2 was synthesized by heating a mixture of 6,6'-dithiodinicotinic acid (DCT), *N,N*'-bis(pyridin-4-ylmethyl) naphthalene diimide (L2) and zinc(II) nitrate hexahydrate in an oven at 100 °C for 72 hours. **RMMOF 3** was synthesized using the same procedure as **RMMOF 2** except that cobalt(II) nitrate hexahydrate was used instead of zinc(II) nitrate hexahydrate. The two MOFs are isostructural. They both crystallize in the triclinic space group $P\bar{1}$ with one deprotonated DCT, one zinc(II) cation, one DMF molecule, half a molecule of L2 and one water molecule in the ASU (Fig 3.9 and Fig 3.10). The metal center in both MOFs is coordinated to six ligands and it exhibits a metal paddle wheel coordination environment composed of two nitrogen atoms and four oxygen atoms. The packing diagrams for **RMMOF 2** (Fig 3.11) and **RMMOF 3** (Fig 3.12) show channels occupied by DMF molecules. **RMMOF 2** has potential solvent accessible volume of 17% (Fig 3.13). The DMF as well as the *S* atoms in **RMMOF 3** are disordered over two positions with 65:35% and 55:45% occupancies, respectively.

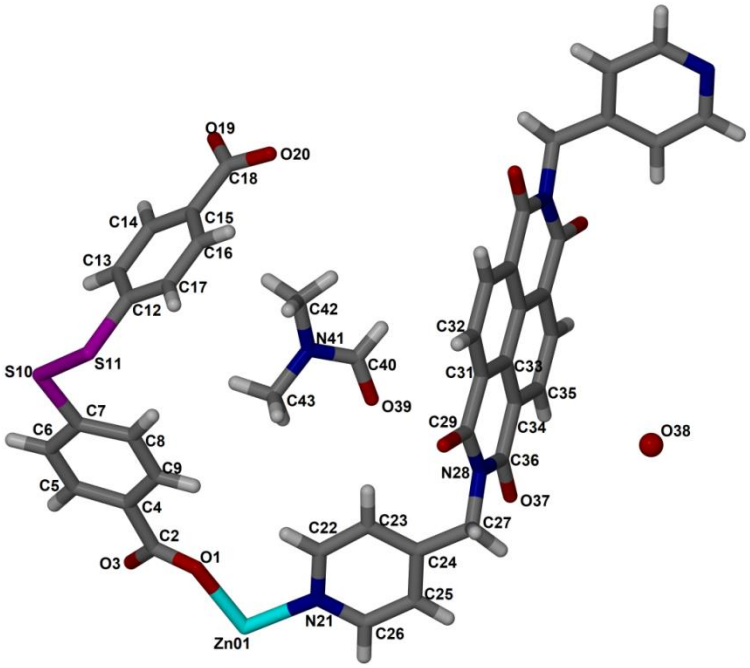

Fig 3. 9 The molecular structure of **RMMOF 2** showing crystallographic labelling scheme for the asymmetric unit.

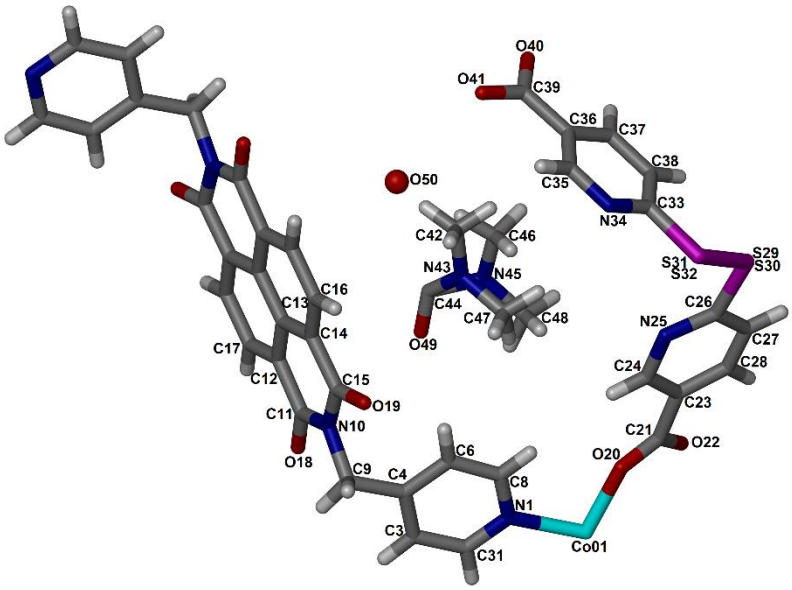

Fig 3. 10 The molecular structure of **RMMOF 3** showing crystallographic labelling scheme for the asymmetric unit.

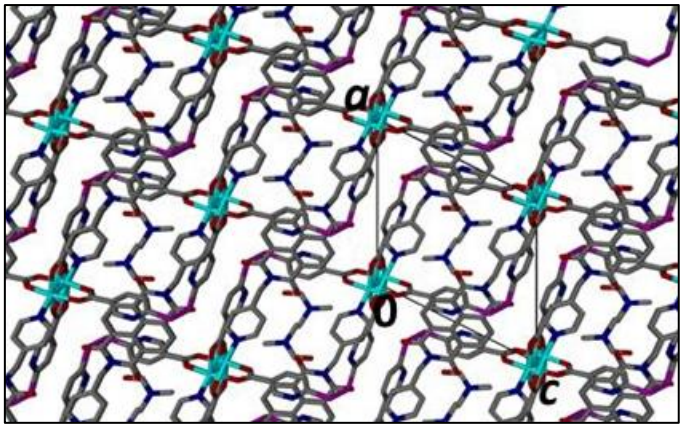

Fig 3. 11 The packing diagram of **RMMOF 2** viewed in the ac plane. The DMF molecules are located in channels running along the *b* axis.

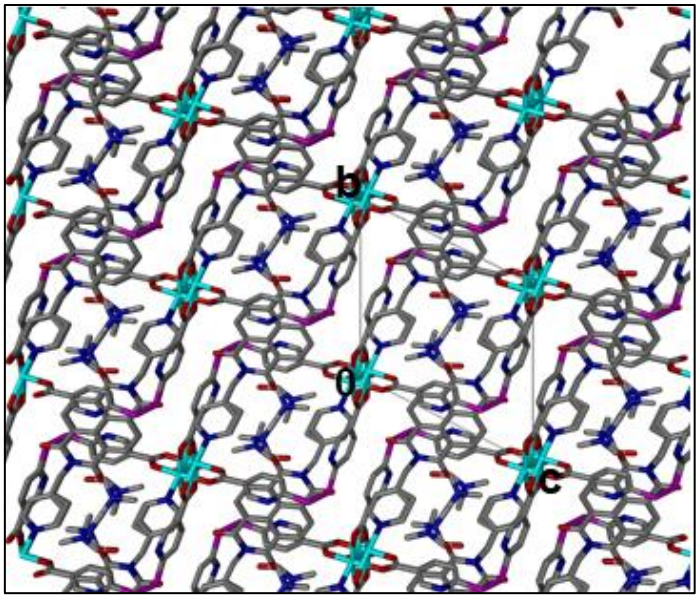

Fig 3. 12 The packing diagram of **RMMOF 3** viewed in the *bc* plane. The DMF molecules are located in channels running along the *a* axis.

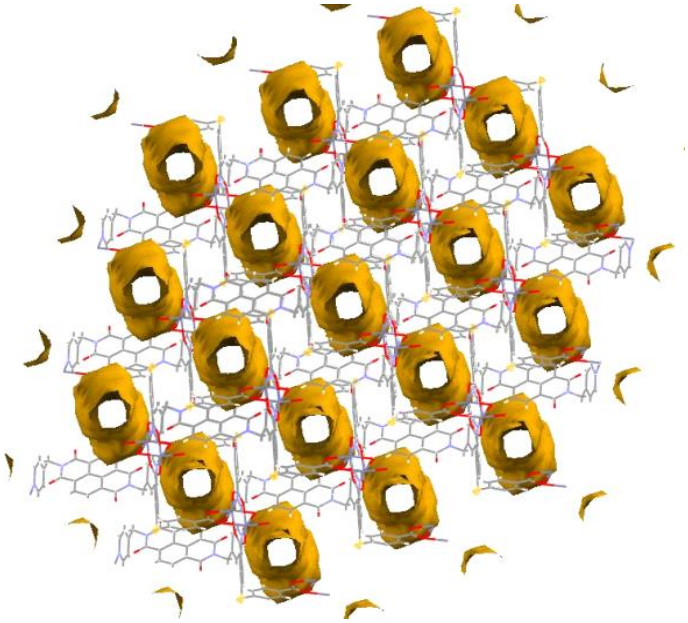

Fig 3. 13 A plot of solvent accessible volume in **RMMOF 2** generated using the Mercury program. The structure possesses 1D channels along the *b* axis.

3.2.2 Thermogravimetric analysis (TGA)

The thermal profile of the as-synthesized **RMMOF 2** shows a weight loss of 12.25% (calculated 12.93%) in the temperature range of 90 °C to 270 °C (Fig 3.14). This is attributed to loss of one DMF molecule and one water molecule. The framework remains stable until 307 °C after which decomposition commences. The desolvated phase of **RMMOF 2** was prepared by heating the as-synthesized crystals in an oven under vacuum at 100 °C for twenty-four (24) hours. The process of desolvation was confirmed using TGA (Fig 3.14). Desolvated **RMMOF 2** remains stable during the desolvation process and its framework decomposes at 307 °C. The TGA of the as-synthesized **RMMOF 3** shown in Fig 3.15 indicates one step weight loss (10.23%) from 60 °C to 250 °C which is attributed to the loss of one DMF molecule and one water molecule (calculated 12.58%). The **RMMOF 3** framework is stable until 322 °C after which decomposition commences.

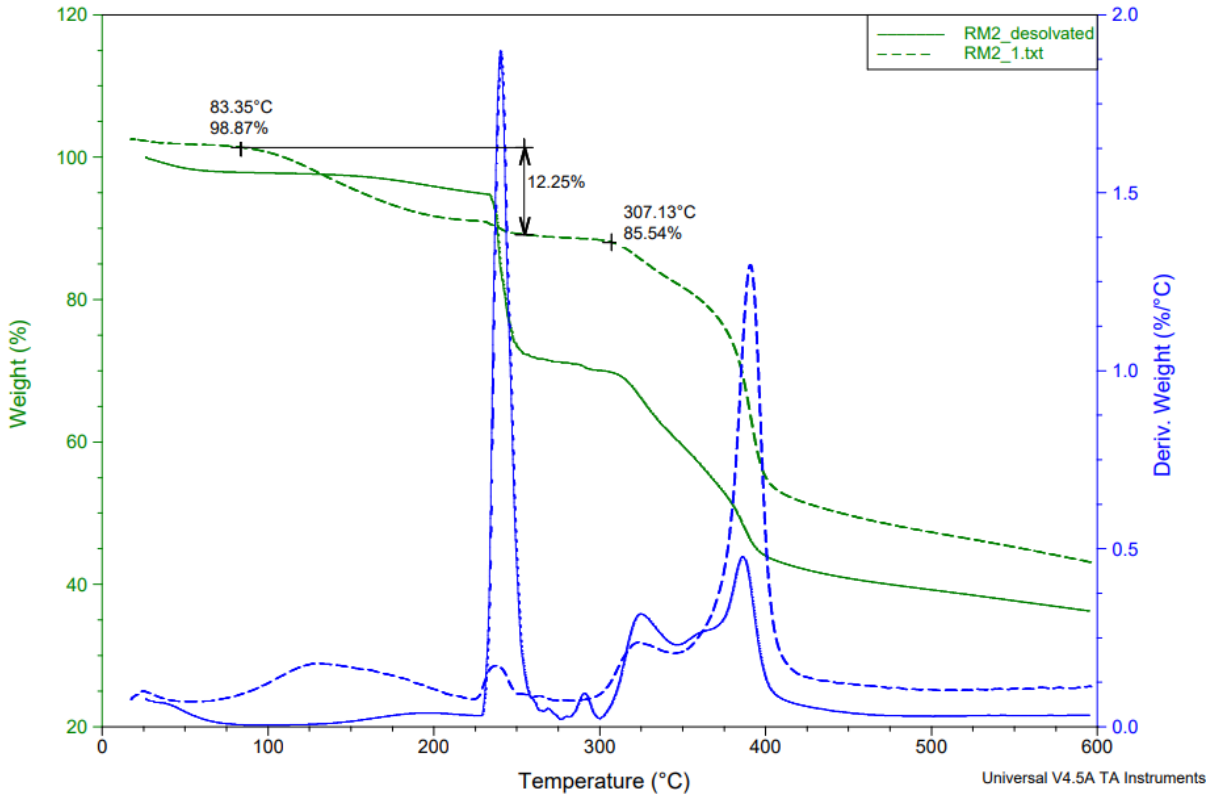

Fig 3. 14 TGA profiles of as-synthesized **RMMOF 2** (dashed green) and desolvated **RMMOF 2** (solid green) as well as the first derivatives; as-synthesized (dashed blue) and desolvated (solid blue).

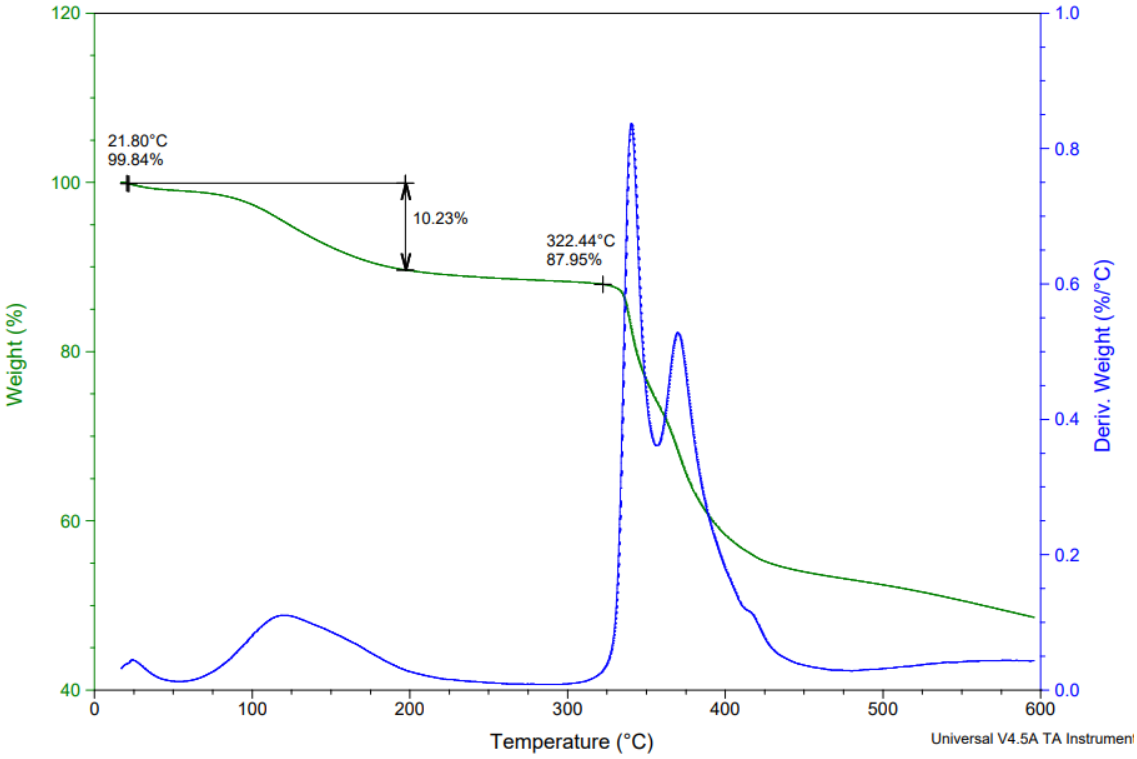

Fig 3. 15 TGA profile of as-synthesized **RMMOF 3** (solid green) as well as its first derivative (solid blue).3.2.3 Powder X-ray diffraction (PXRD)

The purity of **RMMOF 2** and **RMMOF 3** was confirmed by PXRD (Fig 3.16 and Fig 3.17). Both compounds remain crystalline after desolvation.

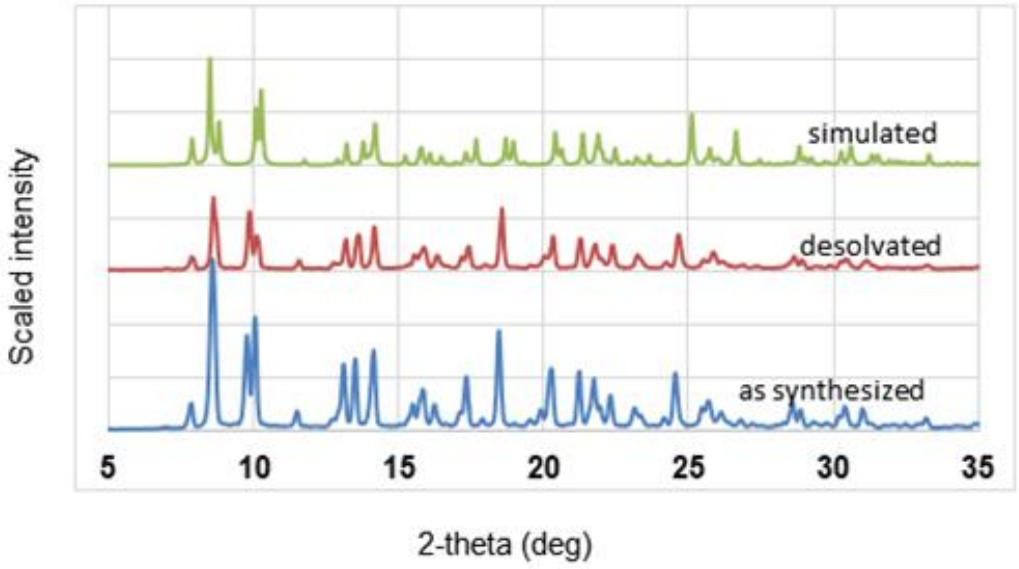

Fig 3. 16 PXRD patterns of as-synthesized **RMMOF 2** (blue), desolvated **RMMOF 2** (red) and simulated **RMMOF 2** (green).

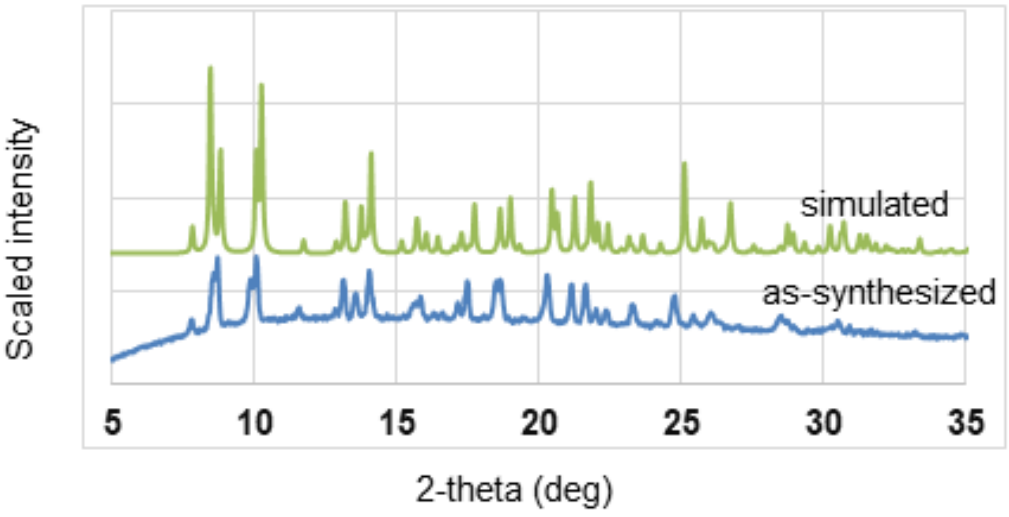

Fig 3. 17 PXRD patterns of as-synthesized **RMMOF 3** (blue) and simulated **RMMOF 3** (green).

3.2.4 Post-synthetic modification of RMMOF 2

The desolvated phase of **RMMOF 2** was soaked in a DMF solution of $CuCl_2$ for 3 weeks. The resulting green powder was filtered and dried in an oven at 100 °C for 24 hours. The green powder was analysed using TGA, PXRD and BET analysis. Thermal profile indicates that **RMMOF 2-Cu** decomposition commences at 280 °C. PXRD (Fig 3.19) shows that the compound maintains crystallinity during the post synthetic modification process.

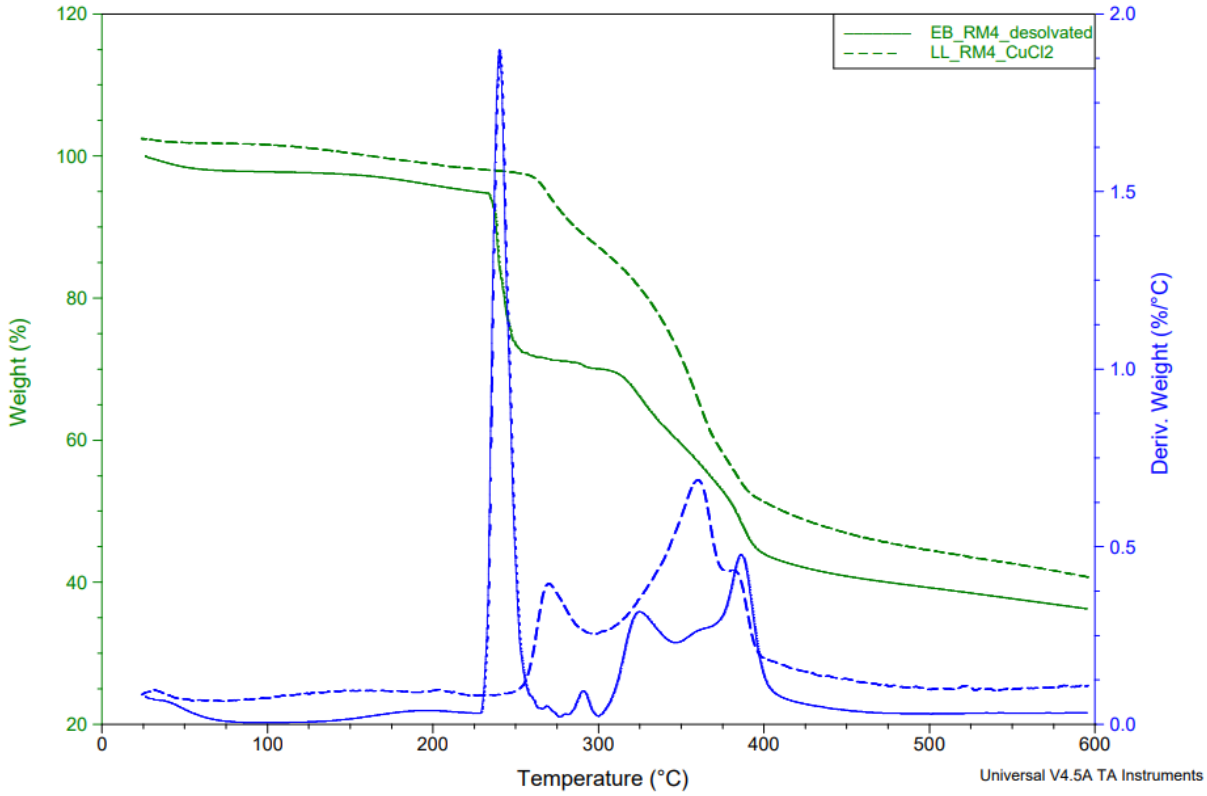

Fig 3. 18 TGA profiles of desolvated **RMMOF 2** (solid green) and desolvated **RMMOF 2**-Cu (dashed green) as well as the first derivatives; desolvated **RMMOF 2** (solid blue) and desolvated **RMMOF 2**-Cu (dashed blue).

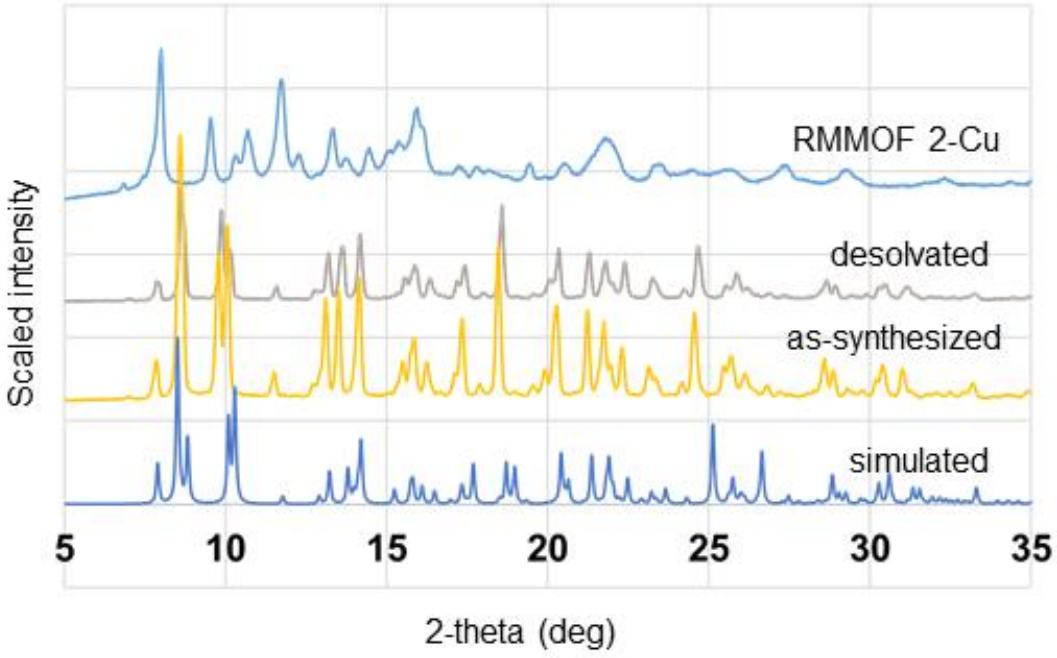

Fig 3. 19 PXRD patterns of simulated **RMMOF 2** (blue), as-synthesized **RMMOF 2** (orange), desolvated **RMMOF 2** (purple) and desolvated **RMMOF 2**-Cu (blue).3.2.5 Brunauer-Emmet-Teller (BET) analysis

BET measurements for **RMMOF 2** and **RMMOF 2-Cu** were performed using N_2 at 77 K (Fig 3.20). The BET surface area of **RMMOF 2** and **RMMOF 2-Cu** were 0.3584 $m^2\ g^{-1}$ and 6.1073 $m^2\ g^{-1}$ respectively. The quantity of gas adsorbed by pure **RMMOF 2** was found to be 15.95 $cm^3\ g^{-1}$ (STP) and the amount adsorbed by **RMMOF 2**-**Cu** was found to be 0.29 $cm^3\ g^{-1}$ (STP).

3.2.6. Challenges encountered with the PSM experiments.

The reagent used for synthesis of L1 and L2; 1,4,5,8-Naphthalenetetracarboxylic dianhydride was discontinued by the suppliers in 2019 and 2020 due to shortage of raw materials. Therefore, some of the studies which were planned for this work could not be completed. These include determining the amount of adsorbed $CuCl_2$ by **RMMOF 1** and **RMMOF 2** as well as determining the adsorption mechanism.

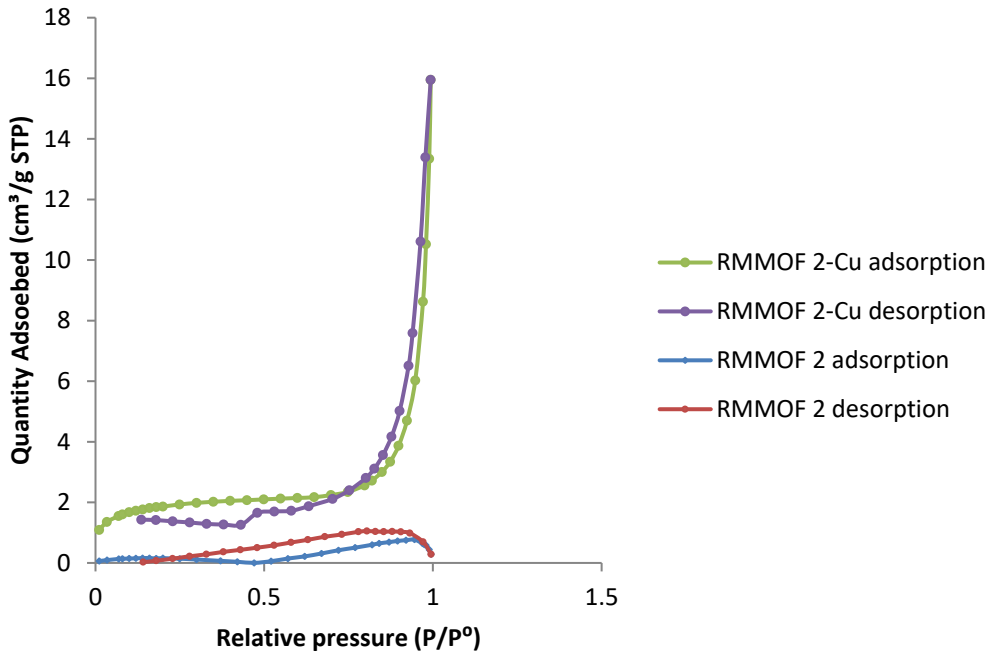

Fig 3. 20 BET analysis for pure **RMMOF 2** and **RMMOF 2**-Cu measured at 77 K.

3.3 RMMOF 4

3.3.1 Single crystal X-ray diffraction (SCXRD)

RMMOF 4 was synthesized by heating a mixture of 2,2'-bis(pyridin-2-ylmethyl)-[5,5'-biisoindoline]-1,1'-3,3'-tetraone (L3), 4,4'-oxybis(benzoic acid) and zinc(ll) nitrate hexahydrate under solvothermal conditions (100 °C, 7 days). **RMMOF 4** crystallizes in the orthorhombic space group *Pbca*. The asymmetric unit (Fig 3.21) consists of two DMF molecules, three deprotonated 4,4'-oxybis(benzoic acid) and five zinc(II) cations. The ligand L3 did not coordinate to the metal centre. The packing diagram (Fig 3.22) shows continuous channels occupied by uncoordinated DMF molecules. The compound has potential solvent accessible volume of 22% and contains 3D channels (Fig 3.23). The DMF molecules in the channels are disordered and could not be modelled. The number of uncoordinated DMF molecules inside the channels were determined from TGA.

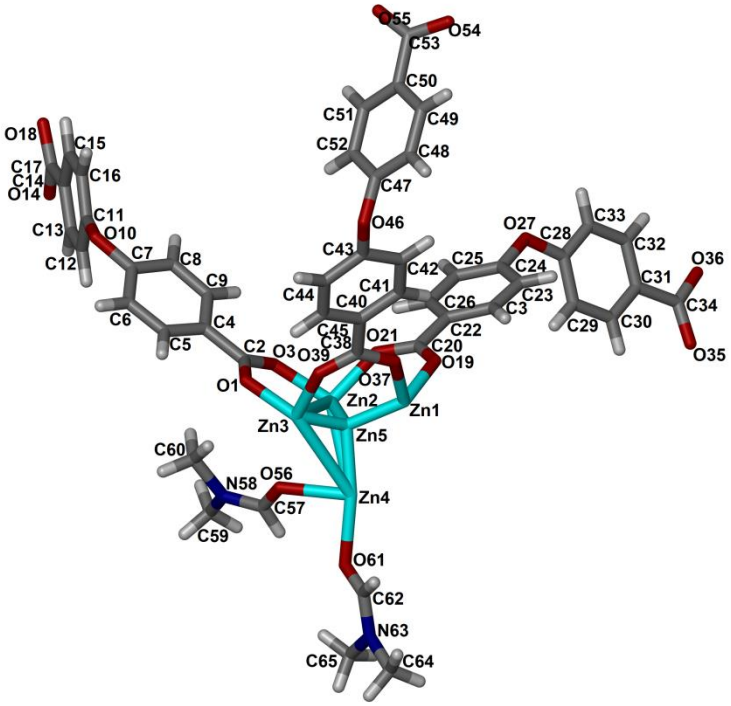

Fig 3. 21 The molecular structure of **RMMOF 4** showing crystallographic labelling scheme for the asymmetric unit.

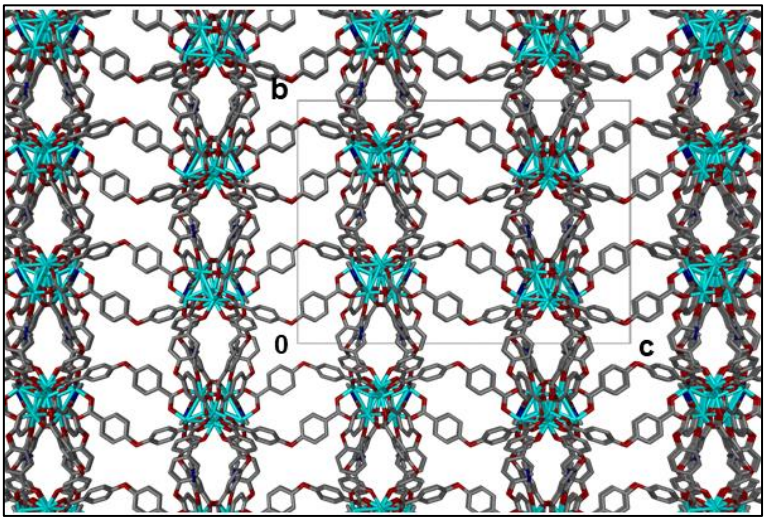

Fig 3. 22 The packing diagram of **RMMOF 4** viewed in the *bc* plane. The DMF molecules are located in channels running along the a axis.

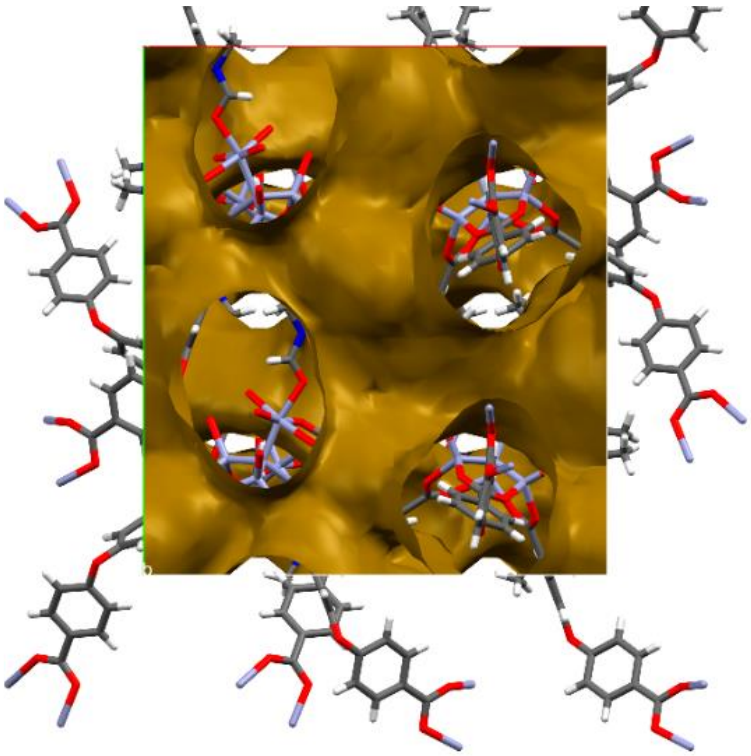

Fig 3. 23 A plot of solvent accessible volume in **RMMOF 4**. The structure possesses channels extending in three dimensions.

3.3.2 Thermogravimetric analysis (TGA)

The thermal profile (Fig 3.24) of **RMMOF 4** shows 35.27% (calculated 35.29%) weight loss in the temperature range of 20 °C to 200 °C. This is attributed to the loss of six (6) DMF molecules; two (2) coordinated DMF molecules (calculated 11.76%) and four (4) uncoordinated DMF molecules (calculated 23.53%). The framework remains stable from 200 °C to 392 °C after which decomposition commences. Desolvated **RMMOF 4** was prepared by heating the as-synthesized crystals in an oven under vacuum at 100 °C for 24 hours. The thermal profile of desolvated **RMMOF 4** indicates weight loss around 250 °C attributed to the remaining of DMF molecules. The decomposition of the framework commences at 392 °C.

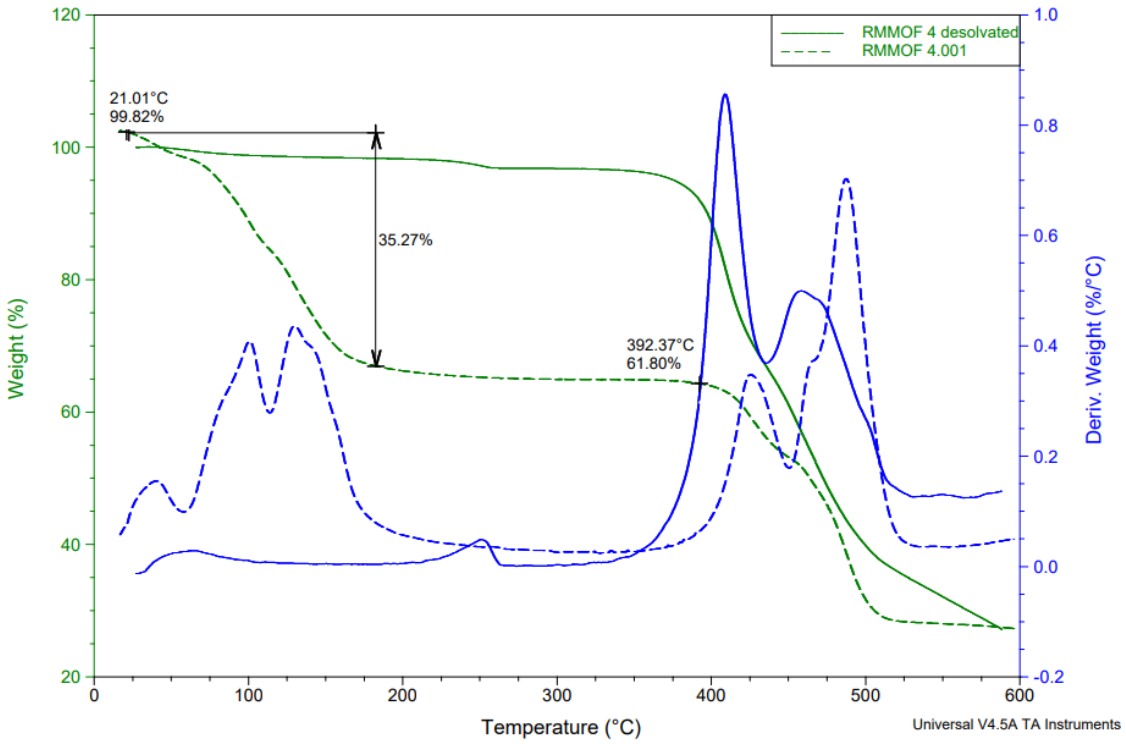

Fig 3. 24 TGA of as-synthesized **RMMOF 4** and desolvated **RMMOF 4** (solid and dashed line, respectively). The first derivatives of the weight % graph are shown in blue; as-synthesized and desolvated represented by (solid and dashed line).

3.3.3 Variable-temperature powder X-ray diffraction (VT-PXRD)

To determine the stability of the compound at different temperatures, PXRD patterns (Fig 3.25) were recorded at 25 °C intervals from 25 °C to 200 °C. The PXRD patterns show that desolvation begins at room temperature as evidenced by the changes in the PXRD pattern at 25 °C. As the temperature increases the structure loses its crystallinity and becomes amorphous.

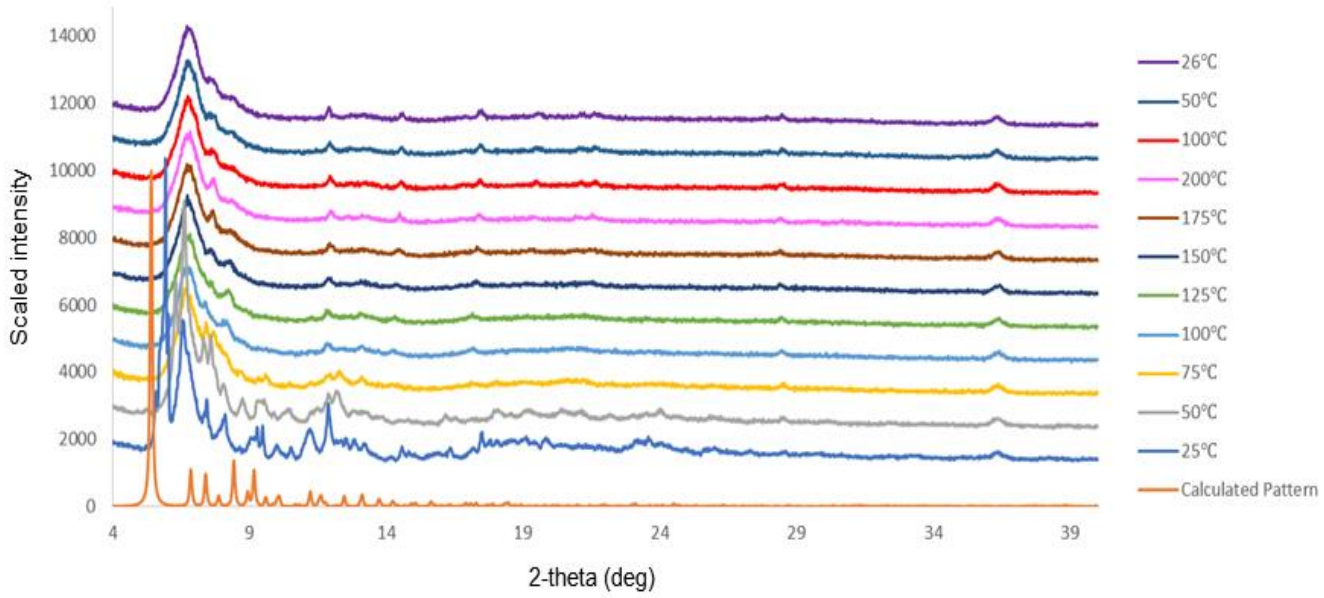

Fig 3. 25 Simulated PXRD pattern for **RMMOF 4** as well as the PXRD patterns for the as-synthesized **RMMOF 4** at different temperatures.

3.3.4 CO_2 sorption

To test the porosity of desolvated **RMMOF 4**, the sorption capacity of desolvated **RMMOF 4** was investigated at 273 K using CO_2 as a test gas (Fig 3.26). The **RMMOF 4** sorption isotherm display reversible Type-I behaviour with a small degree of hysteresis. The compound adsorbs approximately 12 cm^3 g^{-1} (STP) CO_2.

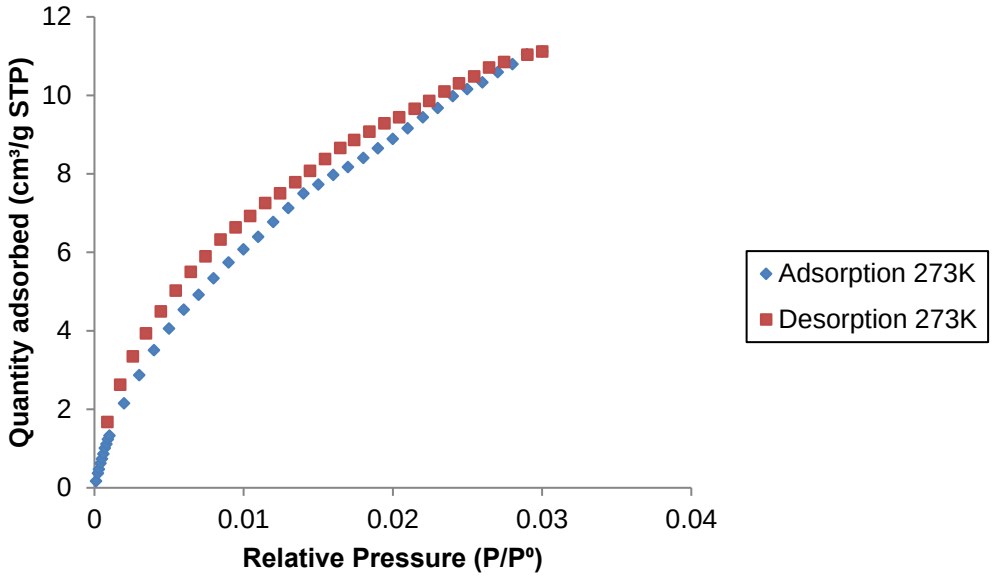

Fig 3. 26 CO2 adsorption and desorption isotherms of desolvated **RMMOF 4** at 273 K.

3.4 RMMOF 5

3.4.1 Single crystal X-ray diffraction (SCXRD)

RMMOF 5 was synthesized by heating a mixture of 2,6-naphthalenedicarboxylic acid, 2,2'-bis(pyridin-4-ylmethyl)-[5,5'-biisoindoline]-1,1'-3,3'-tetraone (L4) and cadmium(II) nitrate tetrahydrate at 100 °C for 48 hours. **RMMOF 5** crystallizes in the triclinic space group $P\bar{1}$. The asymmetric unit consist of two L4 ligands, two independent halves of deprotonated 2,6-naphthalenedicarboxylic acid, one cadmium(II) cation and DMF molecules (Fig 3.27). The metal centre is coordinated to four oxygen atoms and two nitrogen atoms. The DMF molecules are disordered and could not be modelled. The packing diagram indicates continuous 1D channels running along the *a* axis (Fig 3.28). The structure contains 1D channels and contains 27% potential solvent accessible space (Fig 3.29).

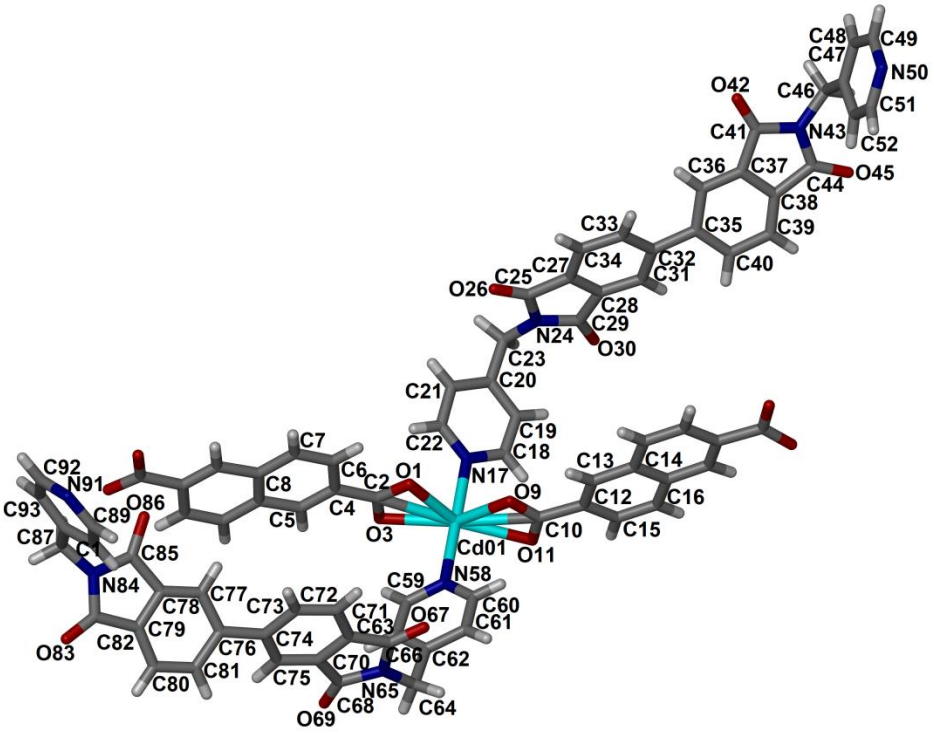

Fig 3. 27 The molecular structure of **RMMOF 5** showing crystallographic labelling scheme for the ASU. DMF molecules are disordered and could not be modelled.

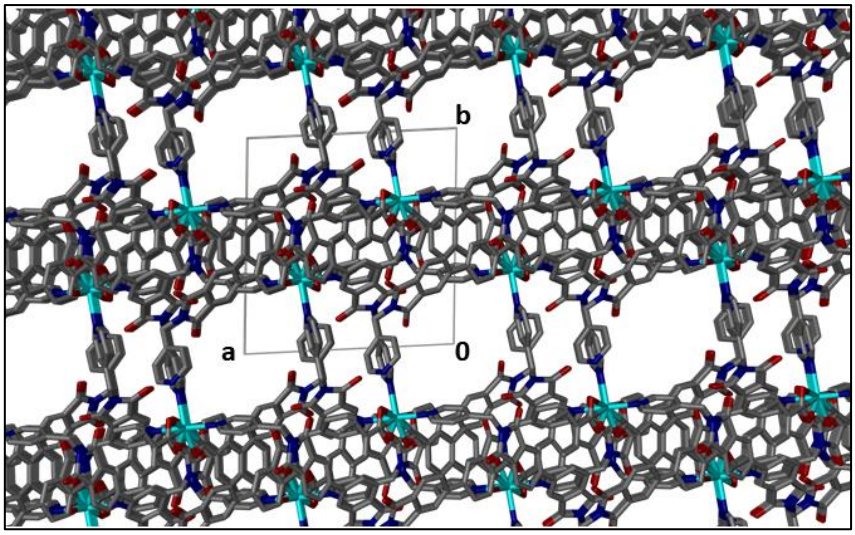

Fig 3. 28 The packing diagram of **RMMOF 5** viewed in the *bc* plane. The DMF molecule are located in channels running along the *a* axis.

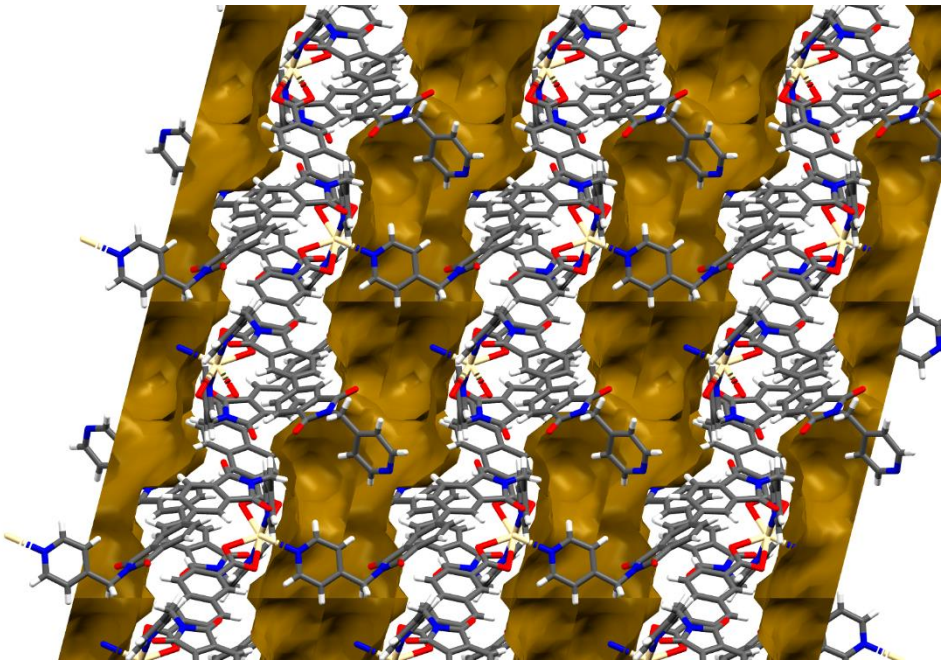

Fig 3. 29 One-dimensional channels showing 27% potential solvent accessible volume in **RMMOF 5** viewed in the *bc* plane.

3.4.2. Thermogravimetric analysis (TGA)

The thermal profile of **RMMOF 5** is shown in Fig 3.30. The thermogram shows a weight loss of 14.94% (calculated 14.56%) in the temperature range 80 °C to 200 °C which is attributed to the loss of three (3) DMF molecules. From 200 °C, no weight loss is observed until the temperature reaches 354 °C after which decomposition of the framework commences. **RMMOF 5** desolvated phase was prepared by heating the as-synthesized crystals in an oven

under vacuum at 100 °C for 24 hours. The framework is stable from 200 °C to 354 °C and the decomposition commences at 354 °C (Fig 3.30).

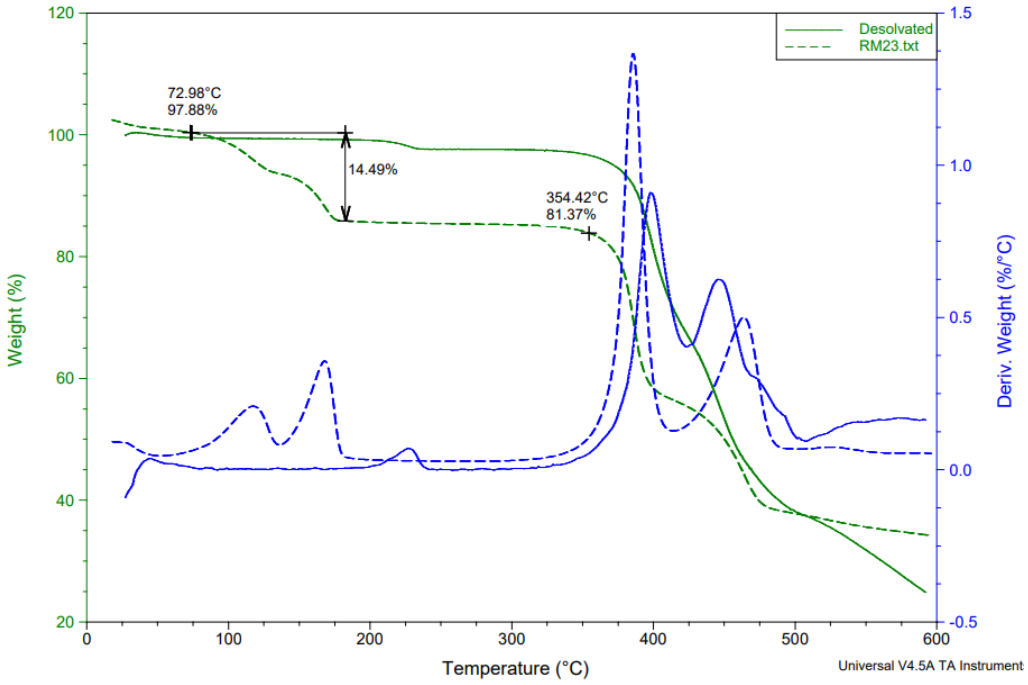

Fig 3. 30 TGA profile of as-synthesized **RMMOF 5** (dashed green) and desolvated **RMMOF 5** (solid green) as well as the first derivatives of as-synthesized (dashed blue) and desolvated (solid blue).

3.4.3 Powder X-ray diffraction (PXRD)

PXRD data were collected at different temperatures (heating from 25–200 °C and cooling from 200–25 °C) to test the stability of **RMMOF 5** (Fig 3.31). The variable-temperature PXRD patterns suggest that the **RMMOF 5** framework maintains crystallinity during desolvation. From 25 °C to 75 °C the as-synthesized PXRD pattern is similar to the simulated PXRD pattern. From 125 °C, the diffraction peak at about 10° 2θ undergoes reduction in size due to the loss of solvent.

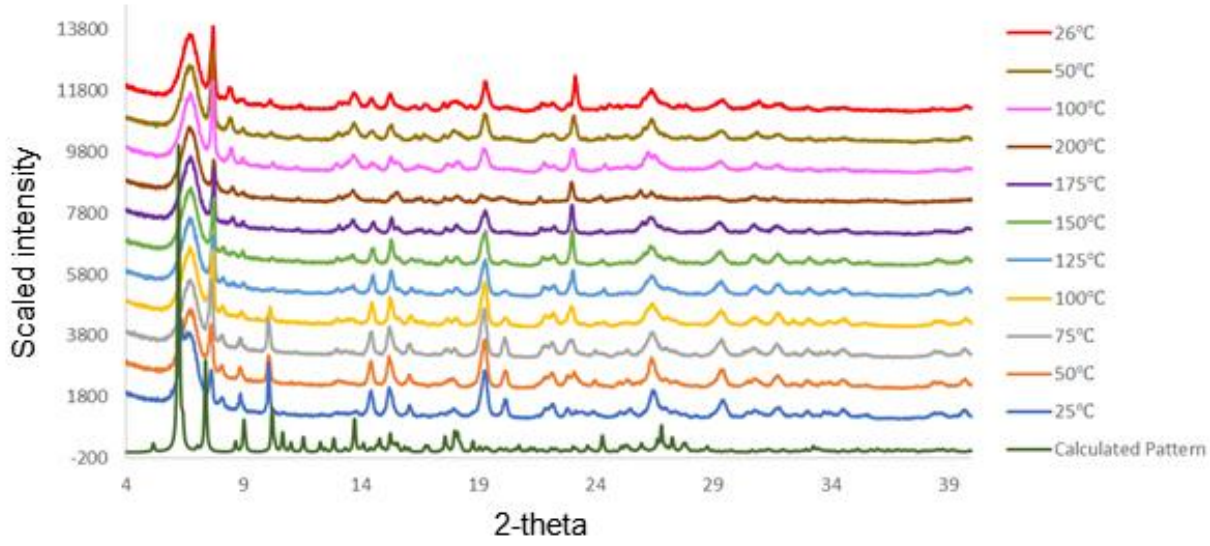

Fig 3. 31 Variable temperature PXRD patterns of simulated **RMMOF 5** and the as-synthesized **RMMOF 5** at different temperatures.

3.4.4 CO_2 sorption

To test for porosity, the sorption capacity of the desolvated phase of **RMMOF 5** was investigated using CO_2 as the test gas (Fig 3.32). **RMMOF 5** adsorbs approximately 6 $cm^3\ g^{-1}$ (STP) of CO_2 at 273 K. The sorption isotherms display reversible Type-I behaviour and shows a slight hysteresis on the desorption curve.

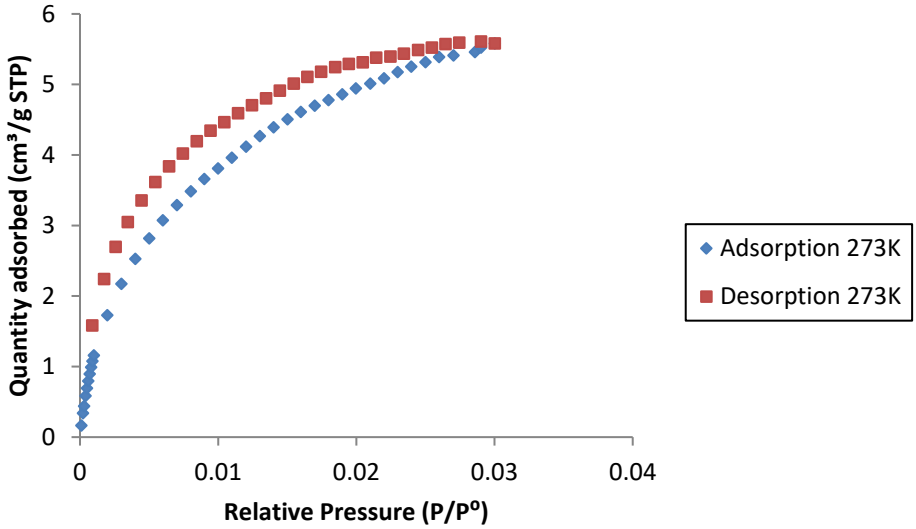

Fig 3. 32 CO2 adsorption and desorption isotherms of desolvated **RMMOF 5** at 273 K.

3.5 RMMOF 6

3.5.1 Single crystal X-ray diffraction (SCXRD)

RMMOF 6 was synthesized by reacting 2,6-naphthalenedicarboxylic acid, 2,2'-bis(pyridin-4-ylmethyl)-[5,5'-biisoindoline]-1,1',3,3'-tetraone (L4) and zinc(II) nitrate hexahydrate at 100 °C for 48 hours. **RMMOF 6** crystallizes in the monoclinic space group *C*2/*c*. The asymmetric unit consists of half an L4 molecule, half a Zn(II) cation and half a molecule of deprotonated 2,6-naphthalenedicarboxylic acid disordered over two positions (Fig 3.33). The zinc metal centre is coordinated to four oxygen atoms of the carboxylate ions and two nitrogen atoms of the pyridyl ring. The packing diagram viewed in the *bc* plane reveals large channels running along the *a* axis occupied by DMF molecules (Fig 3.34). The DMF molecules are disordered and could not be modelled. The compound has 22% solvent accessible space (Fig 3.35).

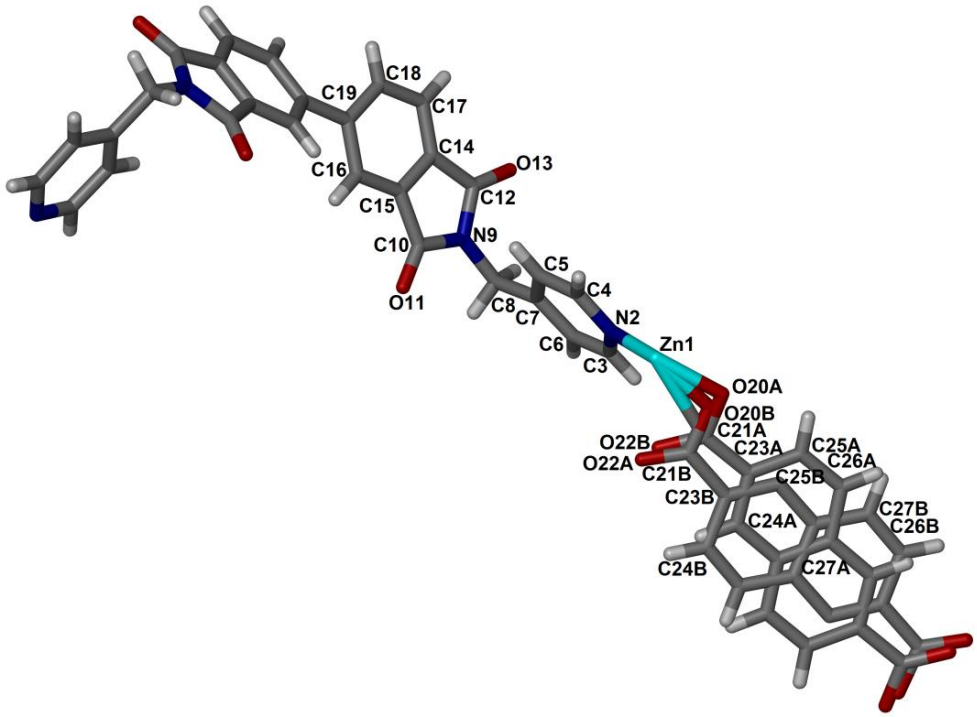

Fig 3. 33 The molecular structure of **RMMOF 6** showing crystallographic labelling scheme for the asymmetric unit.

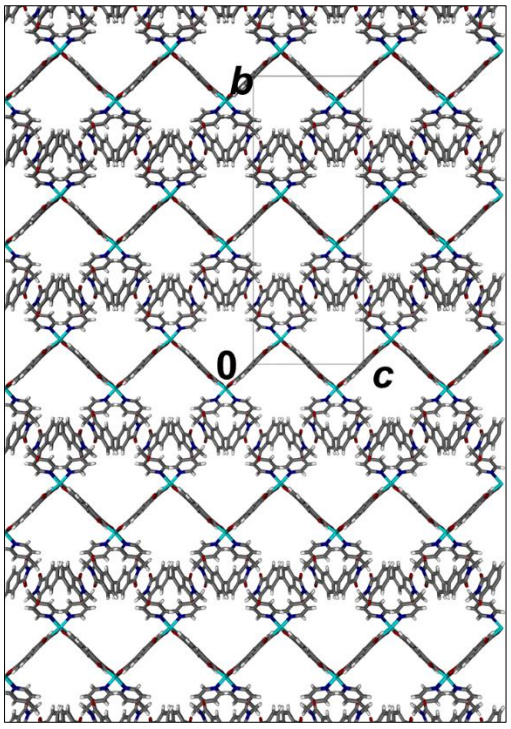

Fig 3. 34 The packing diagram of **RMMOF 6** viewed in the *bc* plane. The DMF molecules are located in channels running along the *a* axis.

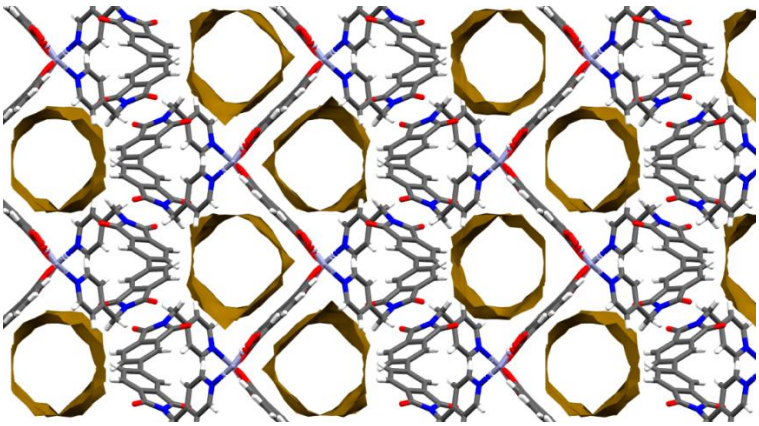

Fig 3. 35 A plot of solvent accessible volume in **RMMOF 6**. The structure has one-dimensional channels amounting to 22% solvent accessible voids.

3.5.2 Hot Stage Microscopy (HSM)

Hot Stage Microscopy (HSM) was conducted to investigate the temperature at which the solvents are removed, the temperature at which the crystal starts to lose its monocrystallinity as well as the temperature at which decomposition of the framework commences. The HSM of **RMMOF 6** (Fig 3.36) does not show any solvent loss. **RMMOF 6** crystals become opaque at 255 °C which indicates the loss of monocrystallinity due to desolvation. Opacification of

crystals is complete at 310 °C. At 410 °C, crystals begin to turn brown which indicates the decomposition of the framework. The decomposition process is complete at 445 °C.

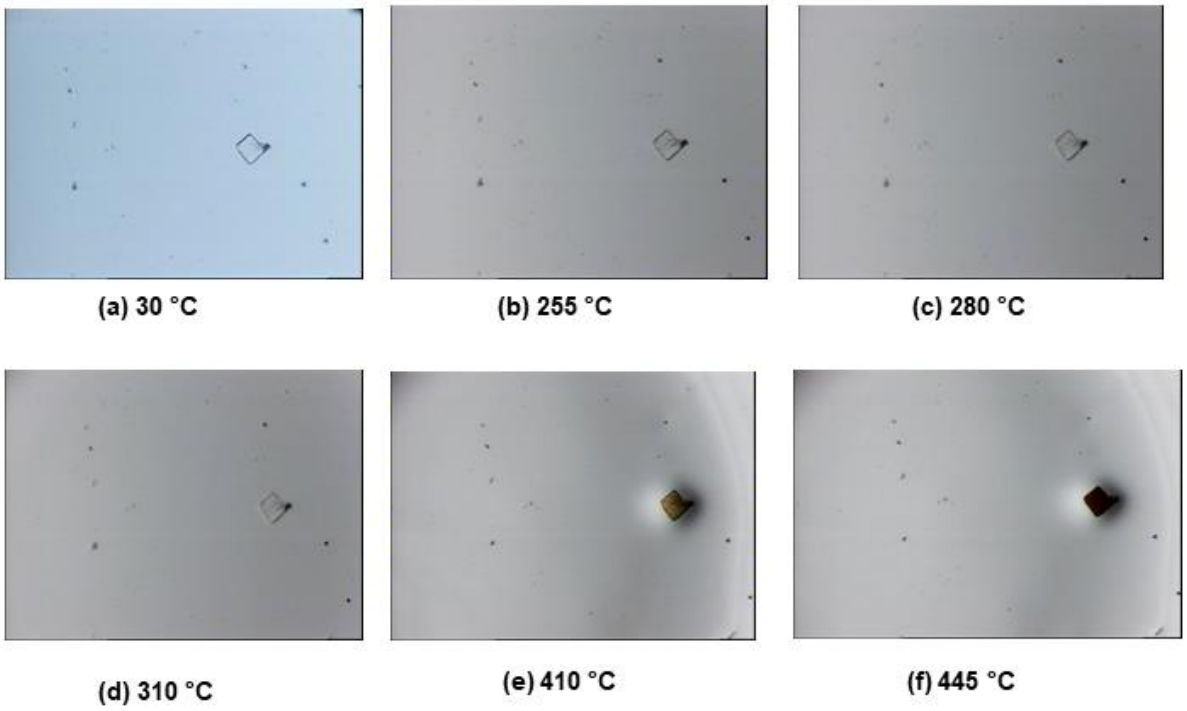

Fig 3. 36 Hot stage microscope photographs of **RMMOF 6** under silicone oil at different temperatures: (a) 30 °C, (b) 255 °C, (c) 280 °C, (d) 310 °C, (e) 410 °C and (f) 445 °C.

3.5.3 Thermogravimetric analysis (TGA)

The TGA profile of the as-synthesized **RMMOF 6** is shown in Fig 3.37. The TGA profile indicates a weight loss of 27.68% in the temperature range of 30 °C to 300 °C which is attributed to the loss of two DMF molecules (calculated 27.96%). The framework is stable until 351°C after which decomposition commences. The desolvated phase of **RMMOF 6** was prepared by heating the crystals at 100 °C under vacuum for 24 hours. Desolvated **RMMOF 6** decomposes at 351 °C.

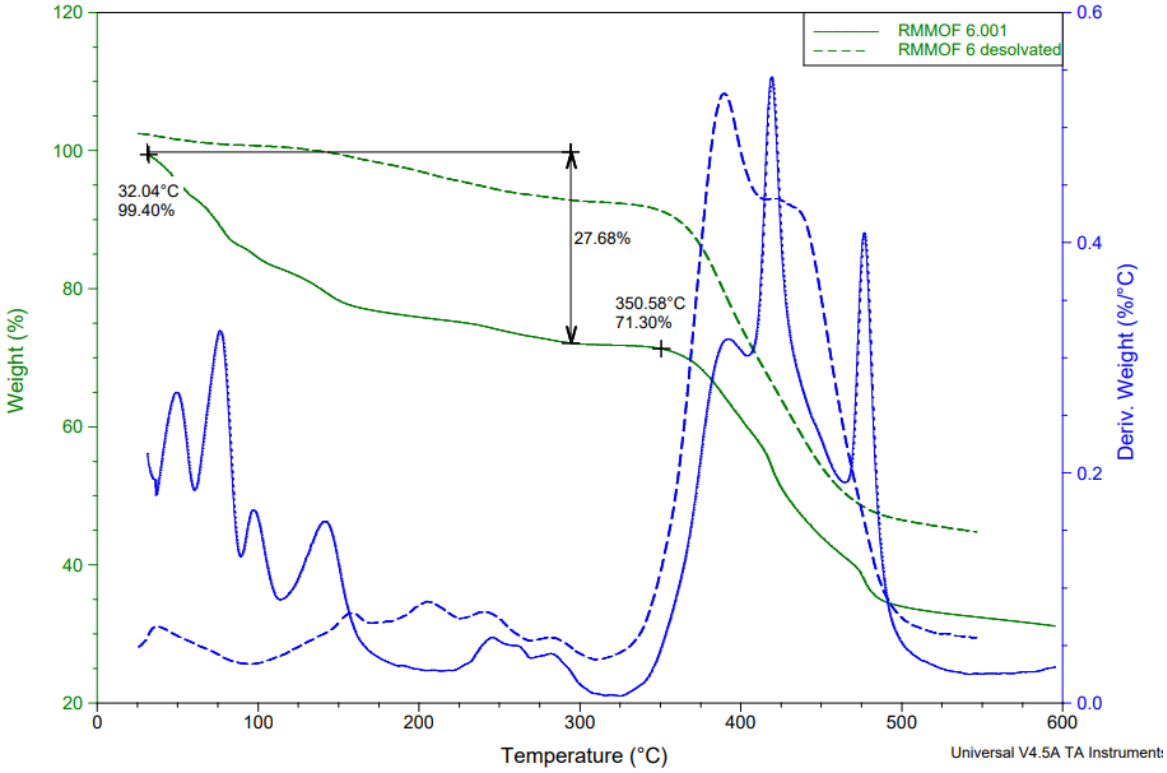

Fig 3. 37 TGA profile of as-synthesized **RMMOF 6** (green, solid) and desolvated **RMMOF 6** (green, dashed) as well as the first derivatives as-synthesized (blue, solid) and desolvated (blue, dash).

3.5.4 Powder X-ray diffraction (PXRD)

PXRD was used to confirm bulk phase purity of **RMMOF 6** as well as to confirm stability of the MOF after desolvation (Fig 3.38).

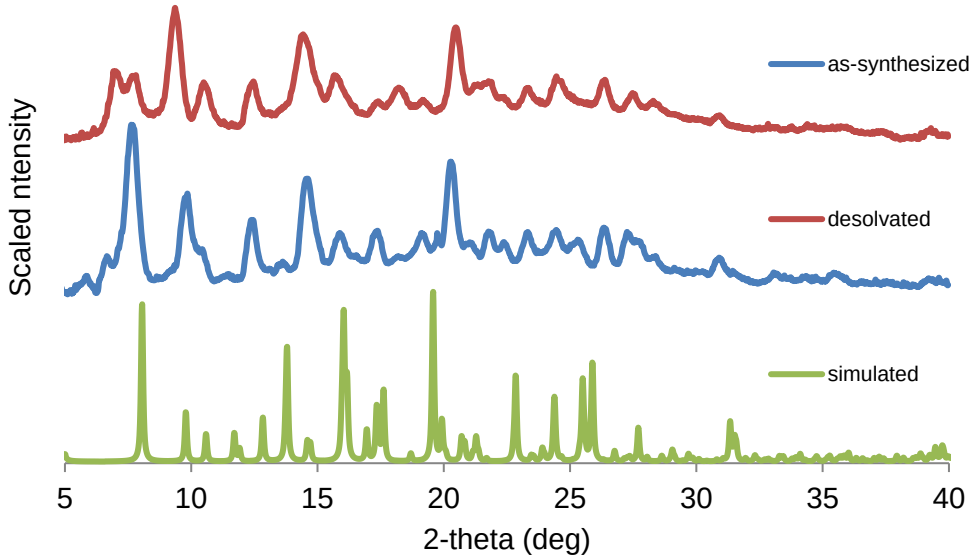

Fig 3. 38 PXRD patterns of as-synthesized **RMMOF 6** (blue), desolvated **RMMOF 6** (red) and simulated (green).

3.5.5 CO_2 sorption

The porosity of the desolvated **RMMOF 6** was investigated at 195 K and 273 K using CO_2 as the test gas (Fig 3.39). The sorption isotherms at both 273 K and 195 K displays Type-I sorption behaviour. At 273 K the quantity of CO_2 adsorbed by **RMMOF 6** is 35 cm^3 g^{-1} (STP) while at 195 K the compound adsorbs 80 cm^3 g^{-1} (STP). Sorption isotherms at 273 K indicate no hysteresis while at 195 K there is some hysteresis on the adsorption curve.

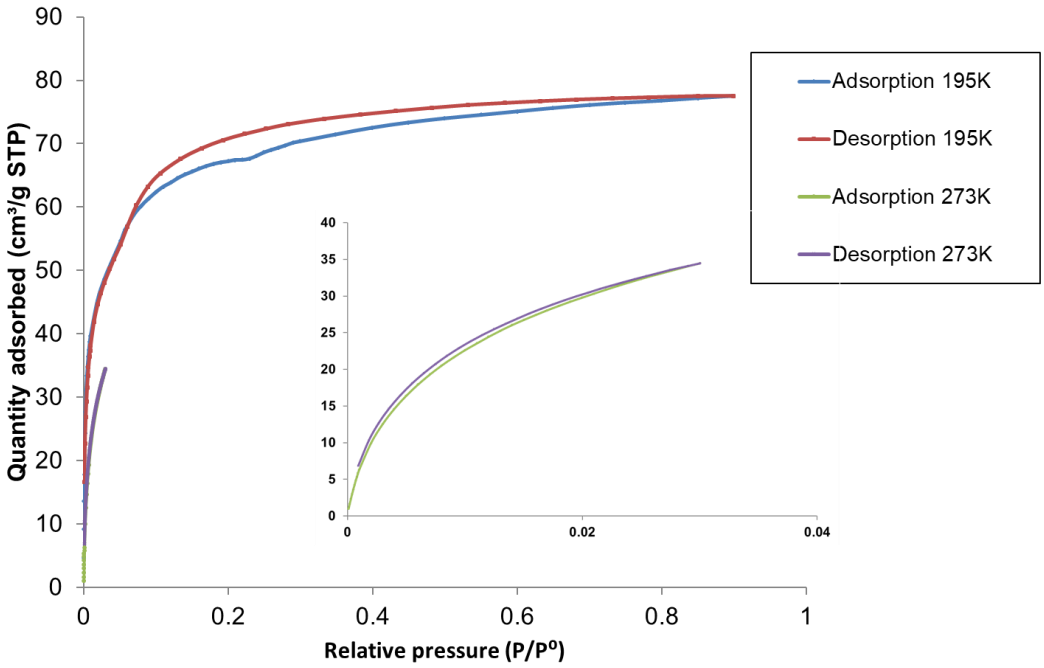

Fig 3. 39 Adsorption and desorption isotherms of desolvated **RMMOF 6** for CO2 at 195 K and 273 K.

3.6 RMMOF 7

3.6.1 Single crystal X-ray diffraction (SCXRD)

Crystals of **RMMOF 7** were grown from the solvothermal reaction of copper(II) chloride, 5,5'-carbonylbis(2-(pyridin-3-ylmethyl)isoindoline-1,3-dione) (L5) and 2,6-naphthalene dicarboxylic acid (Fig 3.40). The mixture was heated in an oven at 100 °C for 72 hours. **RMMOF 7** crystallizes in the monoclinic space group *C2/c*. The asymmetric unit consists of one copper cation, one deprotonated 2,6-naphthalenedicarboxylic acid anion, half a molecule of ligand L5. The ligand L5 is disordered over two positions with a 43:57% and 52:48% occupancy. The framework contains the paddle wheel $[Zn_2(COO)_4]$ units and is two-fold interpenetrated. The packing diagram (Fig 3.41) reveals continuous channels running along

the *c* axis. The DMF molecules are located in continuous channels occupying a potential solvent accessible area of 33% (Fig 3.43).

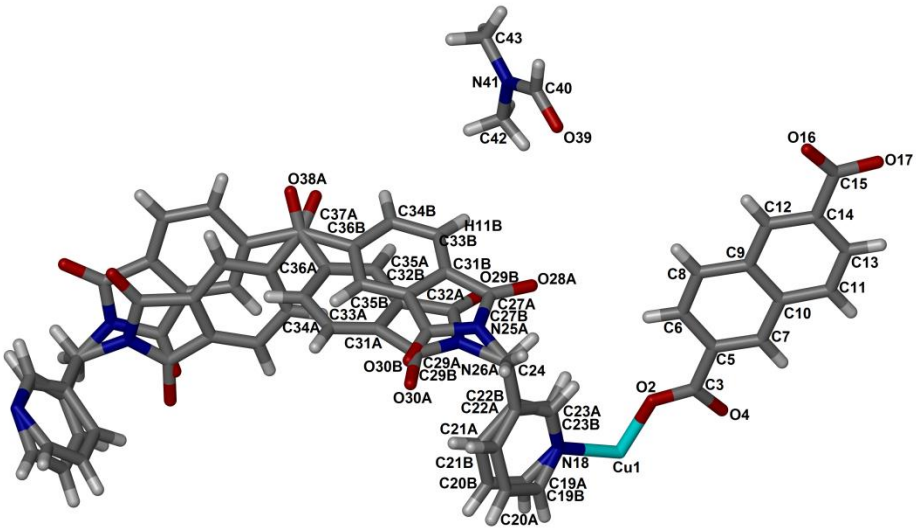

Fig 3. 40 The molecular structure of **RMMOF 7** showing crystallographic labelling scheme for the asymmetric unit.

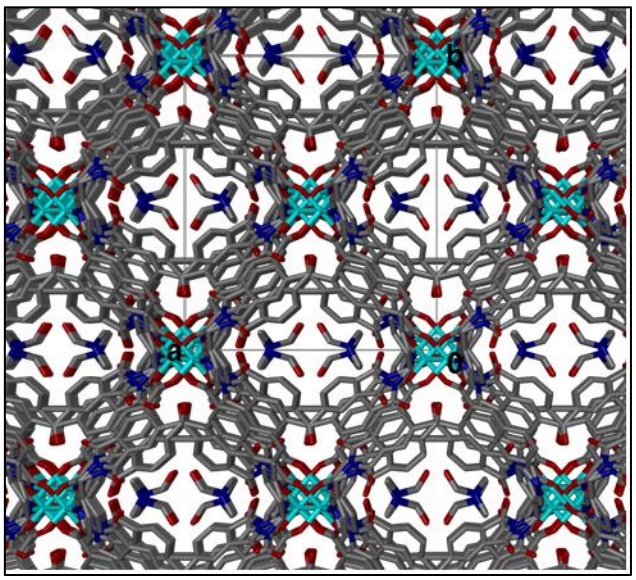

Fig 3. 41 The packing diagram of **RMMOF 7** viewed in the *ac* plane. The DMF molecules are located in channels running along the *a* axis.

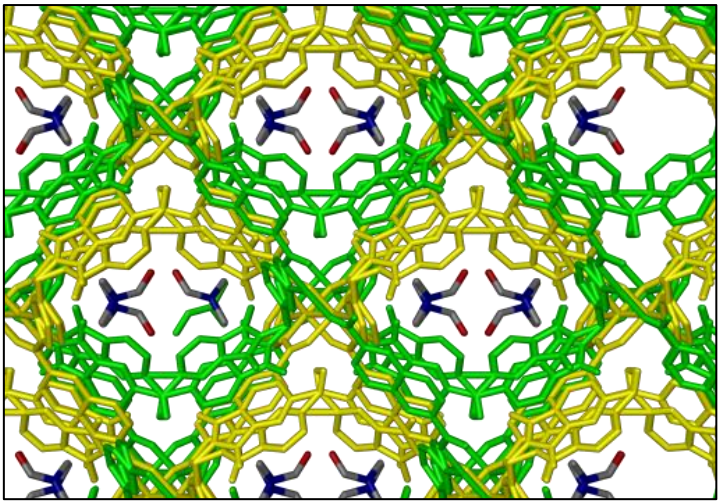

Fig 3. 42 The packing diagram of **RMMOF 7** showing two-fold interpenetration.

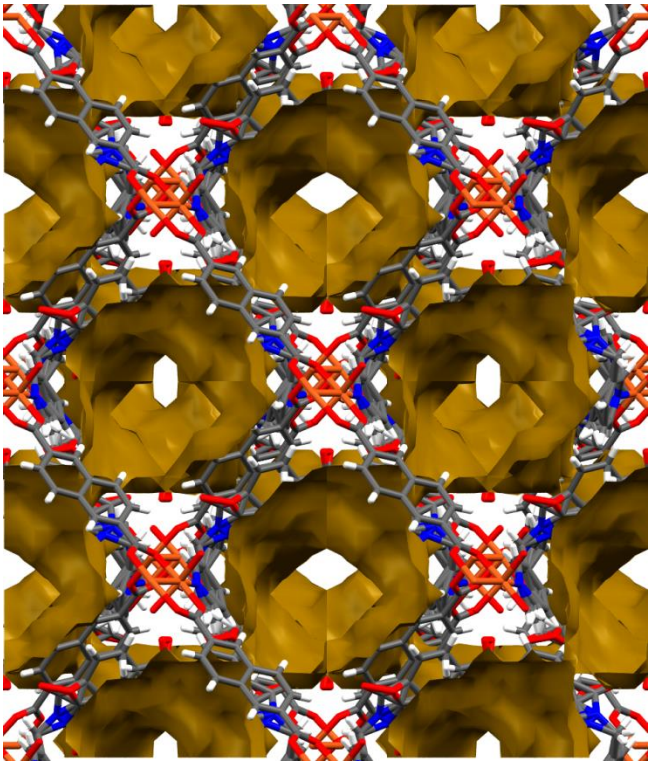

Fig 3. 43 A plot of solvent accessible volume in **RMMOF 7** generated using the Mercury program. The structure contains 33% solvent accessible voids.

3.6.2 Hot Stage Microscopy (HSM)

HSM of **RMMOF 7** (Fig 3.44) display bubbles at 325 °C indicating the loss of solvent. The decomposition of the framework commences at 335 °C.

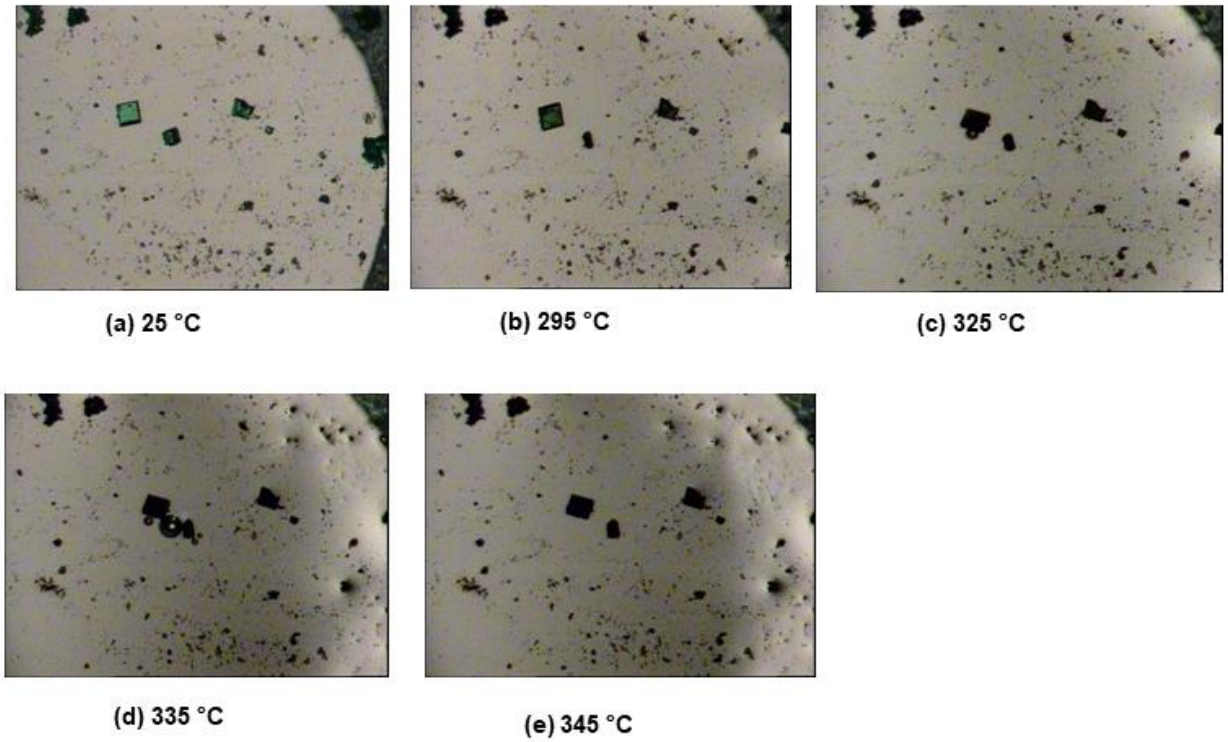

Fig 3. 44 Hot stage microscope photographs of **RMMOF 7** under silicone oil at different temperatures: (a) 25 °C, (b) 295 °C, (c) 325 °C, (d) 335 °C and (e) 345 °C.

3.6.3 Thermogravimetric analysis (TGA)

The thermal profile of **RMMOF 7** shown in Fig 3.45 indicates a weight loss of 27.35% (calculated 28.20%) occurring in the temperature range of 20 °C to 200 °C which corresponds to three DMF molecules. The decomposition of the framework commences at 273 °C. Desolvated **RMMOF 7** was prepared by heating the as-synthesized crystals at 100 °C under vacuum for 24 hours. Desolvated **RMMOF 7** decomposes at 272 °C.

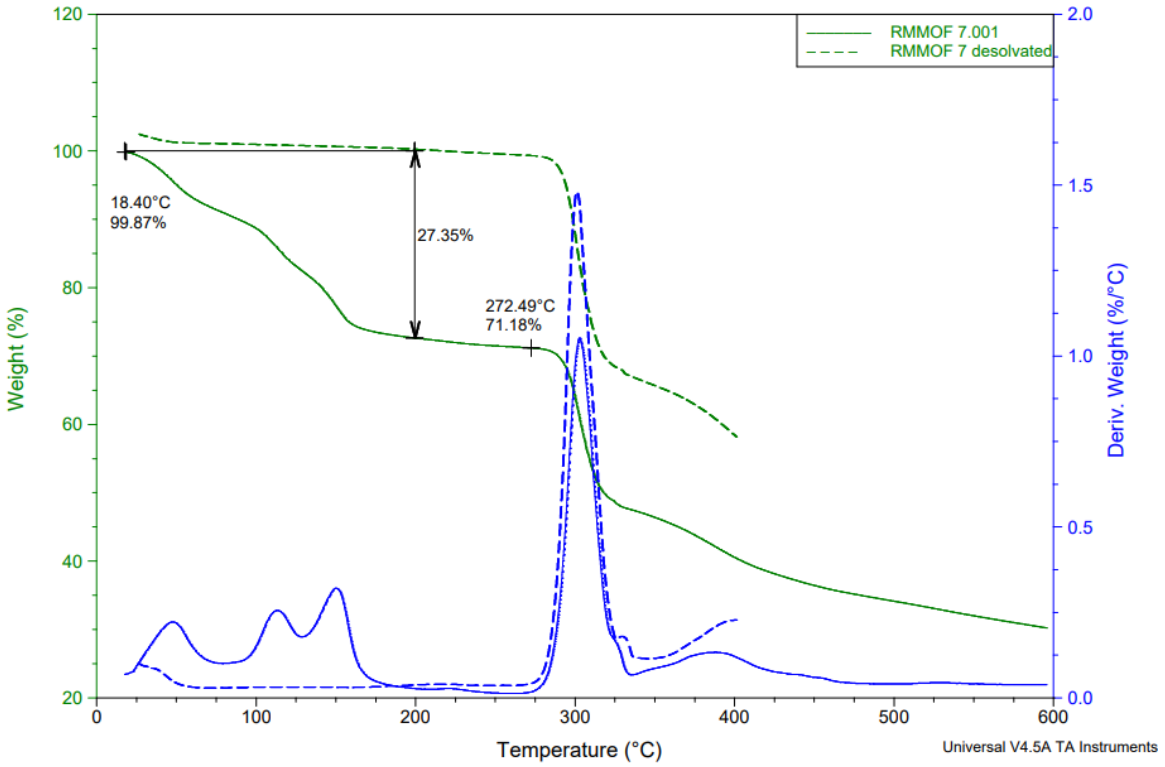

Fig 3. 45 TGA profile of as-synthesized **RMMOF 7** (green, solid) and desolvated **RMMOF 7** (green, dash) as well as the first derivatives of as-synthesized (solid, blue) and desolvated (dashed blue).

3.6.4 Variable-temperature powder X-ray diffraction (VT-PXRD)

The VT-PXRD patterns of **RMMOF 7** (Fig 3.46) were conducted from 298 K to 473 K. The patterns indicate that the structure remain stable and crystalline until it reaches 323 °C.

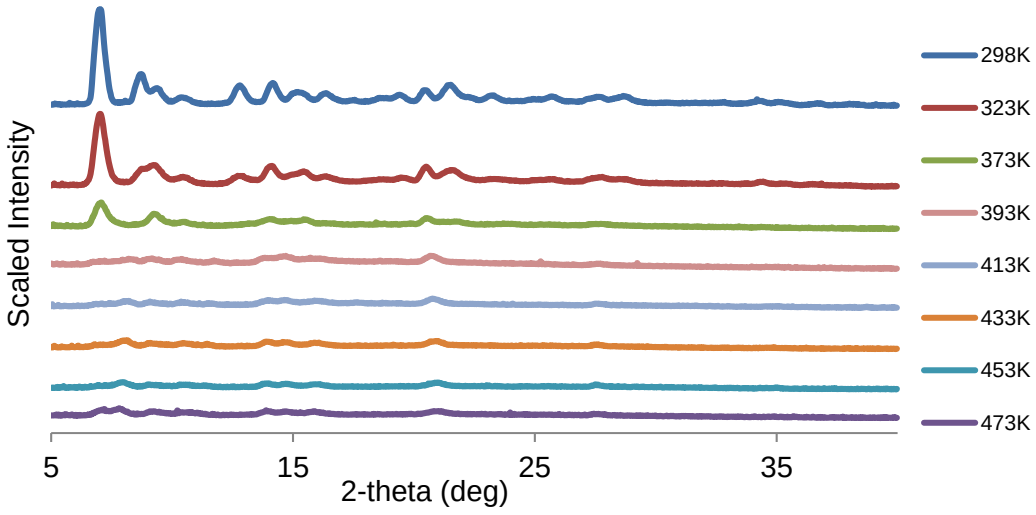

Fig 3. 46 VT-PXRD patterns of as-synthesized **RMMOF 7** at different temperatures.

3.6.5 CO_2 sorption

CO_2 sorption isotherms of **RMMOF 7** were measured at 195 K and 273 K (Fig 3.47). **RMMOF 7** adsorbs 30 cm^3 g^{-1} (STP) at 195 K and 11 cm^3 g^{-1} (STP) at 273 K. Both isotherms display Type-I behaviour. There is some hysteresis on the desorption isotherm at 195 K and but no hysteresis at 273 K.

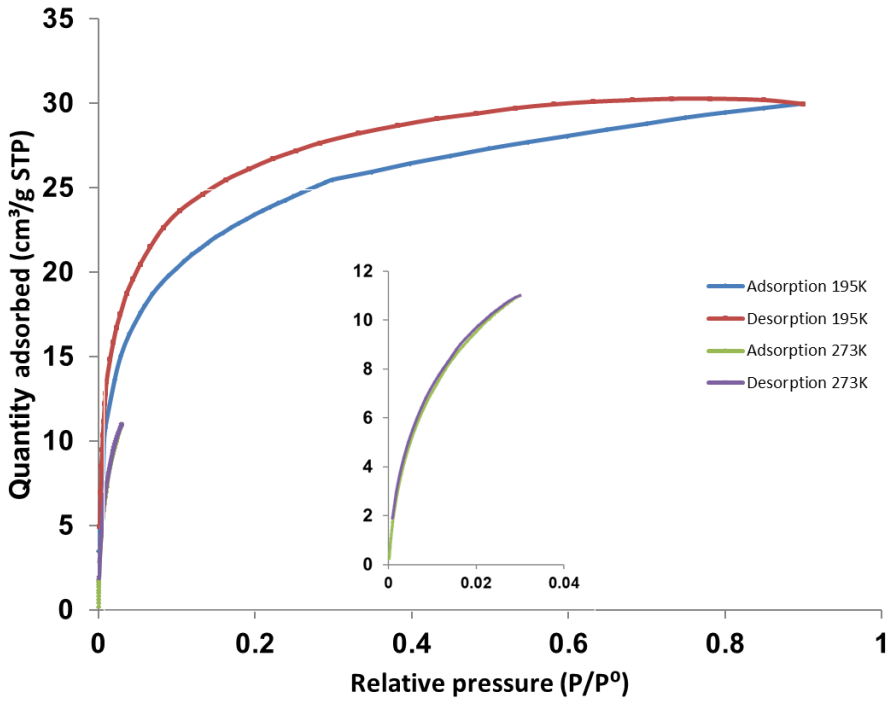

Fig 3. 47 Adsorption and desorption isotherms of desolvated compound **RMMOF 7** for CO2 at 195 K and 273 K.

3.7 SUMMARY

Seven (7) new MOFs were successfully synthesized and characterized using SCXRD, TGA and PXRD. The thermal stability of the MOFs was determined using TGA. TGA revealed that **RMMOF 5** is the most thermally stable (decomposes at 354 °C) whereas **RMMOF 7** is the least thermally stable (decomposes at 272 °C). All the MOFs except **RMMOF 4** maintain crystallinity during desolvation. **RMMOF 4** loses crystallinity at 75 °C and becomes amorphous. **RMMOF 4** contains 3D channels while all the other MOFs contain 1D channels. **RMMOF 7** possesses the largest amount of solvent accessible space accounting for 33% of the unit cell volume. Doping **RMMOF 1** and **RMMOF 2** with $CuCl_2$ yielded **RMMOF 1-Cu** and **RMMOF 2-Cu** which possess higher surface areas than the parent MOFs. Gas sorption experiments conducted at 195 K revealed that **RMMOF 6** adsorbs the largest amount of CO_2 gas (80 cm^3 g^{-1} (STP)) while **RMMOF 5** adsorbs least amount of CO_2 gas (6 cm^3 g^{-1} (STP)). Compared to other MOFs reported in the literature, the MOFs reported here possess very

small surface areas and have very low adsorption capacities. The sorption capabilities of **RMMOF 4** – **RMMOF 7** may be improved by metal doping.

3.8 CRYSTALLOGRAPHIC DATA

Crystal data for RMMOF 1: $C_{29}H_{19}N_5O_7S_2Zn$, M = 678.98, 0.12 × 0.10 × 0.05 mm^3, triclinic, space group P-1 (No. 2), a = 10.4935(6), b = 10.9862(6), c = 13.8461(7) Å, α = 67.843(2), β = 69.241(2), γ = 79.441(2)°, V = 1380.11(13) Å^3, Z = 2, D_c = 1.634 g/cm^3, F_{000} = 692, MoKα radiation, λ = 0.71073 Å, T = 173(2)K, 2θ_{max} = 54.3º, 34675 reflections collected, 6121 unique (R_{int} = 0.0316). The structure was solved and refined using the programs SHELXS-97 (Sheldrick, 1990) and SHELXL-97 (Sheldrick, 1997) respectively. The program X-Seed (Barbour, 1999) was used as an interface to the SHELX programs, and to prepare the figures. Final *GooF* = 1.043, *R1* = 0.0447, *wR2* = 0.1127, *R* indices based on 5468 reflections with I >2sigma(I) (refinement on F^2), 388 parameters, 0 restraints. Lp and absorption corrections applied, μ = 1.101 mm^{-1}.

Crystal data for RMMOF 2: $C_{28}H_{23}N_5O_8S_2Zn$, M = 687.00, 0.25 × 0.11 × 0.09 mm^3, triclinic, space group P-1 (No. 2), a = 10.6721(12), b = 11.9911(13), c = 12.6303(14) Å, α = 113.680(2), β = 96.988(2), γ = 104.127(2)°, V = 1390.8(3) Å^3, Z = 2, D_c = 1.640 g/cm^3, F_{000} = 704, MoKα radiation, λ = 0.71073 Å, T = 173(2)K, 2θ_{max} = 54.3º, 25969 reflections collected, 6164 unique (R_{int} = 0.0332). The structure was solved and refined using the programs SHELXS-97 (Sheldrick, 1990) and SHELXL-97 (Sheldrick, 1997) respectively. The program X-Seed (Barbour, 1999) was used as an interface to the SHELX programs, and to prepare the figures. Final *GooF* = 1.045, *R1* = 0.0466, *wR2* = 0.1256, *R* indices based on 5328 reflections with I >2sigma(I) (refinement on F^2), 392 parameters, 0 restraints. Lp and absorption corrections applied, μ = 1.096 mm^{-1}.

Crystal data for RMMOF 3: $C_{28}H_{23}CoN_5O_8S_2$, M = 680.56, 0.20 × 0.14 × 0.10 mm^3, triclinic, space group P-1 (No. 2), a = 10.6213(16), b = 12.0105(18), c = 12.6758(18) Å, α = 113.809(2), β = 96.934(2), γ = 104.114(2)°, V = 1390.3(4) Å^3, Z = 2, D_c = 1.626 g/cm^3, F_{000} = 698, MoKα radiation, λ = 0.71073 Å, T = 173(2)K, 2θ_{max} = 54.3º, 30143 reflections collected, 6135 unique (R_{int} = 0.0336). The structure was solved and refined using the programs SHELXS-97 (Sheldrick, 1990) and SHELXL-97 (Sheldrick, 1997) respectively. The program X-Seed (Barbour, 1999) was used as an interface to the SHELX programs, and to prepare the figures. Final *GooF* = 1.067, *R1* = 0.0485, *wR2* = 0.1334, *R* indices based on 5151 reflections with I >2sigma(I) (refinement on F^2), 396 parameters, 0 restraints. Lp and absorption corrections applied, μ = 0.830 mm^{-1}.

Crystal data for RMMOF 4: $C_{48}H_{38}N_2O_{17}Zn_5$, M = 1241.65, 0.26 × 0.13 × 0.05 mm^3, orthorhombic, space group *Pbca* (No. 61), a = 20.9907(13), b = 23.9080(16), c = 32.705(2) Å, V = 16412.9(19) Å^3, Z = 8, D_c = 1.005 g/cm^3, F_{000} = 5008, MoKα radiation, λ = 0.71073 Å, T = 173(2)K, 2θ_{max} = 50.4º, 440488 reflections collected, 14584 unique (R_{int} = 0.0876). The structure was solved and refined using the programs SHELXS-97 (Sheldrick, 1990) and SHELXL-97 (Sheldrick, 1997) respectively. The program X-Seed (Barbour, 1999) was used as an interface to the SHELX programs, and to prepare the figures. Final *GooF* = 1.097, *R1* = 0.0926, *wR2* = 0.2915, *R* indices based on 11363 reflections with I >2sigma(I) (refinement on F^2), 653 parameters, 0 restraints. Lp and absorption corrections applied, μ = 1.485 mm^{-1}.

Crystal data for RMMOF 5: $C_{68}H_{49}CdN_9O_{13}$, M = 1275.51, 0.45 × 0.25 × 0.07 mm^3, triclinic, space group P-1 (No. 2), a = 14.0598(8), b = 14.6288(9), c = 17.9911(11) Å, α = 103.920(2), β = 101.065(2), γ = 90.753(2)°, V = 3518.1(4) Å^3, Z = 2, D_c = 1.204 g/cm^3, F_{000} = 1380, MoKα radiation, λ = 0.71073 Å, T = 173(2)K, 2θ_{max} = 54.5º, 128550 reflections collected, 15693 unique (R_{int} = 0.0559). The structure was solved and refined using the programs SHELXS-97 (Sheldrick, 1990) and SHELXL-97 (Sheldrick, 1997) respectively. The program X-Seed (Barbour, 1999) was used as an interface to the SHELX programs, and to prepare the figures. Final *GooF* = 1.543, *R1* = 0.1043, *wR2* = 0.3319, *R* indices based

on 12746 reflections with I >2sigma(I) (refinement on F^2), 797 parameters, 0 restraints. Lp and absorption corrections applied, μ = 0.377 mm^{-1}.

Crystal data for **RMMOF 6**: $C_{40}H_{24}N_4O_8Zn$, M = 754.02, 0.10 × 0.10 × 0.10 mm^3, monoclinic, space group $C2/c$ (No. 15), a = 8.5971(8), b = 36.044(3), c = 13.8200(13) Å, β = 94.919(2)°, V = 4266.6(7) $Å^3$, Z = 4, D_c = 1.174 g/cm^3, F_{000} = 1552, MoKα radiation, λ = 0.71073 Å, T = 173(2)K, $2\theta_{max}$ = 55.1º, 48495 reflections collected, 4921 unique (R_{int} = 0.0593). The structure was solved and refined using the programs SHELXS-97 (Sheldrick, 1990) and SHELXL-97 (Sheldrick, 1997) respectively. The program X-Seed (Barbour, 1999) was used as an interface to the SHELX programs, and to prepare the figures. Final *GooF* = 1.884, *R1* = 0.1270, *wR2* = 0.4093, *R* indices based on 3949 reflections with I >2sigma(I) (refinement on F^2), 316 parameters, 0 restraints. Lp and absorption corrections applied, μ = 0.626 mm^{-1}.

Crystal data for **RMMOF 7**: The structure proved to be challenging to solve. $C_{42}H_{30}N_4O_{10}Cu$, M = 820.24, 0.060 x 0.120 x 0.130 mm^3, monoclinic, space group $C2/c$ (No. 15), a = 17.8775(6), b = 18.9796(6)), c = 21.6123(7) Å, β = 114.5107(10)°, V = 6672.4(6) $Å^3$, Z = 8, D_c = 1.177 g/cm^3, F_{000} = 3376, MoKα radiation, λ = 0.71073 Å, T = 173(2)K, $2\theta_{max}$ = 56.6º, 184096 reflections collected, 8314 unique (R_{int} = 0.0344). The structure was solved and refined using the programs SHELXS-97 (Sheldrick, 1990) and SHELXL-97 (Sheldrick, 1997) respectively. The program X-Seed (Barbour, 1999) was used as an interface to the SHELX programs, and to prepare the figures. Final *GooF* = 5.628, *R1* = 0.240, *wR2* = 0.5568, *R* indices based on 9776 reflections with I >2sigma(I) (refinement on F^2), 297 parameters, 0 restraints. Lp and absorption corrections applied, μ = 0.946 mm^{-1}.

CHAPTER 4

CONCLUSION AND FUTURE WORK

4.1 CONCLUSION

In conclusion five (5) pyridyl donor diimide ligands were successfully synthesized and characterized using NMR. Seven (7) new MOFs namely **RMMOF 1**, **RMMOF 2**, **RMMOF 3**, **RMMOF 4**, **RMMOF 5**, **RMMOF 6** and **RMMOF 7** were prepared using the solvothermal method. The MOFs were characterized using SCXRD, TGA and PXRD. SCXRD reveals that all the structures possess channels of varying sizes occupied by solvent molecules (DMF and/or water). The solvent accessible space was estimated using the Mercury program. It was found that **RMMOF 7** has the largest solvent accessible voids accounting for 33% of the total volume. **RMMOF 1** and **RMMOF 2** were post-synthetically modified by doping with $CuCl_2$. The BET analysis revealed an increase of surface area for **RMMOF 1-Cu** (16.3475 $m^2.g^{-1}$) and **RMMOF 2-Cu** (6.1073 $m^2.g^{-1}$) compared to the surface area of **RMMOF 1** (2.6814 $m^2.g^{-1}$) and **RMMOF 2** (0.3584 $m^2.g^{-1}$). Gas adsorption capacities for **RMMOF 4** – **RMMOF 7** were tested using carbon dioxide gas. The MOFs show very low adsorption capacities at 273 K and 195 K with **RMMOF 6** showing the highest loadings of 35 $cm^3\ g^{-1}$ (STP) at 273 K and 80 $cm^3\ g^{-1}$ (STP)at 195 K.

4.2 FUTURE WORK

Due to challenges associated with COVID19 some of the characterization work could not be completed. Therefore, future work planned for this project includes CO_2 sorption measurements for **RMMOF 4** and **RMMOF 5** at 195 K. Future work also includes adsorption kinetics experiments for **RMMOF 1-Cu** and **RMMOF 2-Cu**.

REFERENCES

1. D. V. Soldatov and I. S. Terekhova, *J.Struct. Chem.*, 2005, **46**, S1.
2. J. M. Lehn, *Supramol. Chem.,* 1993, **260**, 1762.
3. P. Thuery, *Inorg chem.,* 2010, **49**, 9078.
4. E. H. Witlicki, S. W. Hansen, M. Christensen, S. D. Nygaard and A. H. Flood, *J. Phys. Chem*., 2009, **34**, 9450.
5. C. G. Wermuth, C. R. Ganellin, P. Lindberg and L. A. Mitscher, *Pure Appl. Chem.*, 1998, **66**, 1077.
6. K. Takemoto, N. Sonoda, J. L. Atwood, J. E. D. Davies and D. D. MacNicol, *Inclusion Compounds*, London: Academic Press, 1984.
7. C. B. Aakeröy, *Acta Cryst. B.,* 1997, **53**, 569.
8. H. Margenau, D. Terhaad and N. R. Kestner, *Theory of Intermolecular Forces*, Burlington MA: Elsevier Science, 1971.
9. G. R. Desiraju, D. D. MacNichol, F. Toda and R. Bishop, *Review of General Principles,* Oxford: Pergamon, 1996.
10. F. London, *Z. Physik*., 1930, **63**, 245.
11. S. L. Childs, L. Chyall, J. T. Dunlap, B. C. Stahly and V. N. Smolenskaya., *J. Am. Chem. Soc*., 2004, **126**, 1335.
12. G. R. Desiraju, J. W. Steed and M. Dekker*, Hydrogen bonding*, New York: Basel, 2004.
13. D. J. Millen, *J. mol. Struct.*, 1990, **237**, 15.
14. G. A. Jeffrey, *An introduction to hydrogen bonding*, New York: Oxford university press. 1997.
15. G. C. Pimentel and A. L. McClellan, *The Hydrogen Bond*, Freeman San Francisco, 1960.
16. V. P. Gupta, *Principles and applications of Quantum Chemistry*, Academic Press, 2016.
17. E. Kryachko and S. Scheiner, *J. Phys. Chem*., 2004, **108**, 2527.
18. A. Nangia, *J. Chem. Sci*., 2010, **122**, 295.
19. M. Hosseini, *Coord. Chem. Rev.,* 2003, **240**, 157.
20. A. Petitjean, A. Khoury, R. G. Kyritsakas and J. M. Lehn, *J. Am. Chem. Soc*., 2004, **126**, 6637.
21. K. E. Riley and P. Hobza, *Acc. Chem. Res*., 2013, **46**, 927.
22. N. J. Silva, F.B. Machado, H. Lischka and A. J. Aquino, *Phys. Chem. Chem. Phys*., 2016. **18**, 22300.
23. V. A. Parsegian, *Van der Waals forces,* Cambridge University Press, 2005.
24. C. J. Van Oss, M. K. Chaudhury and R. J. Good, *Chem. Rev*., 1988, **88**, 927.

25. S. Zuluaga, P. Canepa, K. Tan, Y. J. Chabal and T. Thonhauser, *J. Phys. Phys, Condens. Matter*., 2014, **26**, 133002.
26. G. R. Desiraju, *Angew. Chem. Int. Ed*., 2007, **46**, 8342.
27. J. W. Steed and J. L. Atwood, *Supramol. Chem*., 2000, **9**, 4.
28. G. R. Desiraju, *J. Mol. Struct*., 2003, **656**, 5.
29. Z. Hasan, J. Jeon and S. H. Jhung, *Rev. J. Hazard. Mater*., 2013, **244**, 444.
30. E. Batisai, M. Lusi, T. Jacobs and L. J. Barbour, *Chem. Commun.*, 2012, **48**, 12171.
31. H. W. Langmi, J. Ren, B. North, M. Mathe and D. Bessarabov, *Electrochimica. Acta.,* 2014, **128**, 368.
32. K. Sumida, D. L. Rogow, J. A. Mason and J. R. Long, *Chem. Rev*., 2011, **112**, 724.
33. M. D. Allendorf, C. A. Bauer, R. K. Bhakta and R. J. T. Houk, *Chem. Soc. Rev*., 2009, **38**, 1330.
34. V. I. Isaeva and L. M. Kustov, *Pet. Chem.,* 2010, **50**, 167.
35. L. R. Mingabudinova, V. V. Vinogradov and V. A. Milichko, *Chem. Soc. Rev.,* 2016, **45**, 5408.
36. G. Ferey, *Chem. Soc. Rev*., 2008, **37**, 191.
37. S. Kitagawa, R. Kitaura and S. I. Noro, *Angew. Chem. Int. Ed*., 2004, **43**, 2334.
38. M. Hirscher, *Angew. Chem, Int. Ed*., 2011, **50**, 58.
39. R. Seetharaj, P. V. Vandana, P. Arya and S. Mathew, *Arab. J. Chem.*, 2019, **3**, 295.
40. Y. F. Song and L. Cronin, *Ang. Chem., Int. Ed*, 2008, **47**, 4635.
41. O. K. Farha, A. M. Shultz, A. A. Sarjeant, S. T. Nguyen, and J. T. J. Hupp, *J. Am. Chem. Soc*., 2011, **133**, 5652.
42. Z. Wang and S. M. J. Cohen, *J. Am. Chem. Soc*., 2007, **129**, 12368.
43. P. V. Dau and S. M. Cohen, *Chem. Commun*., 2013, **49**, 6128.
44. S. M. Cohen, *Chem. rev*., 2012, **112**, 970.
45. J. P. Hobson, *J. Phys. Chem*., 1969, **73**, 2720.
46. S. Brunauer, L. S Deming, W. E. Deming and E. Teller, *J. Am. Chem. Soc.*, 1940, **62**, 1723.
47. C. De Smedt, F. Ferrer, K. Leus and P. Spanoghe, *Adsorp Sci Technol.*, 2015, **33**. 462.
48. S. Lowell and J. E. Shields, *J. Colloid Interface Sci*., 1985, **103**, 226.
49. K. S. W. Sing and S. J. Gregg, *Adsorption, Surface Area and Porosity*, Academic Press, London, 1984.
50. S. Brunauer, L. S. Deming, W. S. Deming and E. Teller, *J. Am. Chem. Soc*., 1940, **62**, 1723.
51. R. J. Kuppler, D. J. Timmons, Q. Fang, J. Li, T. A. Makal and M. D. Young, *Coord. Chem. Rev*., 2009, **253**, 3042.

52. N. L. Rosi, J. Eckert, M. Eddaoudi, D. T. Vodak, J. Kim and M. O'Keeffe, *Science*., 2003, **300**, 1127.
53. R. B. Lin, W. Zhou, Z. Zhang, S. Xiang, and B. Chen, *EnergyChem.,* 2019, **1**, 100006.
54. S. Kaye, A. Daily, O. Yaghi and J. Long, *J. Am. Chem. Soc*., 2007, **129**, 14176.
55. K. Koh, A. Wong-Foy and A. Matzger, *J. Am. Chem. Soc*., 2009, **131**, 4184.
56. Y. Yan, X. Lin, S. Yang, A. J. Blake, A. Daily, N. R. Champness, P. Hubberstey and M. Schroder, *Chem. Commun*., 2009, **9**, 1025.
57. H. Furukawa, N. Ko, Y. B. Go, N. Aratani, S. B. Choi, E. Choi, A. O. Yazaydin, R. Q. Snurr, M. O'Keeffe and J. Kim, *Science*., 2010, **329**, 424.
58. M. Kondo, T. Yoshitomi, H. Matsuzaka and S. Seki, *Angew. Chem. Int. Ed*., 1997, **36**, 1725.
59. Y. Peng, V. Krungleviciute, I. Eryazici, J. T. Hupp, O. K. Farha and T. Yildirim, *J. Am. Chem. Soc*., 2013, **135**, 11887.
60. Y. He, W. Zhou, T. Yildirim and B. Chen, *Energy Environ. Sci*., 2013, **6**, 2735.
61. A. Millward and O. Yaghi, *J. Am. Chem. Soc*., 2005, **127**, 17998.
62. H. Y. Deng, J. R. He, M. Pan, L. Li and C. Y Su, CrystEngComm., 2009,**11**, 909.
63. Paratone N oil, (Exxon Chemical Co., Tx, USA).
64. APEX2, Version 1.0-27, Bruker AXS Inc., Madison, Wisconsin, USA.
65. Bruker (2007), Bruker AXS Inc., Madison, Wisconsin USA, 2007.
66. Sheldrick, G.M. SADABS, Bruker AXS Inc., Madison, Wisconsin USA, 2001.
67. L. J. Barbour, J. Supramol. Chem., 2001, **1**, 189.
68. G. M. Sheldrick, SHELXS-97, Program for Crystal Structure Solution, University of Gottingen, Germany, 1997.
69. G. M. Sheldrick, SHELXL-97, Program for Crystal Structure Solution, University of Gottingen, Germany, 1997.
70. POV-RayTM, Version 3.6. 2004 Williamstone, Persistence of Vision Raytracer Pty. Ltd.
71. F. Allen, *Acta Crystallogr*, Sect. B., 2002, **58**, 380.
72. Soft Imaging System GmbH: Digital Solutions for Imaging and Microscopy, Version 3.1 for Windows, © 1987-2000.